A NOVEL ACTUATOR FOR HIGH-TORQUE LOW-SPEED APPLICATIONS

by

Mahmoud Nouri

A thesis submitted to the Department of Electrical and Computer Engineering

In conformity with the requirements for

the degree of Master of Applied Science

Queen's University

Kingston, Ontario, Canada

(August, 2018)

Abstract

There are many applications where there is a demand for high torque at low speed. One application in the robotics area is haptics where a user kinesthetically gets in touch with a virtual object by means of a hand-held electromechanical interface known as haptic device. A haptic device requires a motor with high torque at low speed (~ zero). A geared actuation mechanism, therefore, is conventionally used in the haptic devices available in the market. Geared solutions, introduce backlash, decrease back-drivability and transparency. Thus, a direct drive solution is a tiny move with a big gain in haptic technology that has been proposed in this thesis.

Series motor known also as universal motor has the highest torque density and highest torque per ampere amongst all types of motors due to its inherent characteristic. That's simply because its torque varies with the square of current making it very popular in high-torque demanding applications as industrial/commercial drills, vacuum cleaners, washing machines, and Traction vehicles. However, it only rotates in one direction, i.e., it cannot generate negative torque (brake torque). If by any means series motor could generate brake torque, it will be a top candidate motor for direct drive high torque demanding applications at low speed including haptic technology. Also, the negative torque capability can be used in electrical dynamic braking of universal motors.

In this thesis, two novel methods have been proposed to convert a unidirectional series motor into a bidirectional series motor. The first one is referred to as "diode-method" which includes a new topology and a conventional PI-controller for the toque control of the motor. The second method, "active-bridge-method" uses a new topology along with a new switching/control approach to control the torque. Diode-method only works for DC drive applications whereas active-bridge method works for both DC and AC drive applications. Due to the practical simplicity and faster response, diode-method is the preferred solution for DC drive applications. While the active-bridge method is the only solution for the AC drive applications. It can also be applied for electrical dynamic braking of universal motors.

Matlab/Simulink simulations have been carried out to verify functionality of both methods. Also, we built a prototype setup in ePOWER Lab, only for diode-method, to ensure practical feasibility.

Acknowledgements

Queen's is a great university for sure, but it was not only a school for me to learn and do research but also a place to grow, a community to relate, a society to connect, an attitude to believe and a home to belong to. I appreciate years of my life that have been passed here in beautiful Kingston being a member of Queen's grand family. Here, I want to take the advantage and use this space to thank God for his non-stop energies and vibes supporting me throughout my life and here at Queen's. I also offer my deepest gratitude to my supervisors Dr. Keyvan Hashtrudi-Zaad, Dr. Alireza Bakhshai, and Dr. Yan-Fei Liu for their kind support throughout my program. I would like to appreciate Dr. James Reynolds' help to facilitate my defense exam and approvals. Special thanks to Dr. Suzan Eren and Dr. Majid Pahlevani for their valuable effort to examine my thesis. I would like to thank my friends in and outside of Queen's University including Hamidreza, Meraj, Mostafa, Mahdi, Mohsen, Agha Maysam, Omid and Mojtaba for their generous support and encouragement. I would take the chance to gratefully acknowledge the financial support provided by Queen's University, Queen's University Graduate Awards and Queen's University Teaching Assistantships.

Finally, I would like to thank my family for their encouragement and unwavering support throughout my life.

Table of Contents

List of Figures

List of Tables

Chapter 1

Introduction

1.1 Introduction

Many applications exist in which actuation requires to be provided at high torque and low speed including drill motors, oil well drills, elevators, milling machines, etc. In many of these applications there is a need for gearbox to increase the torque and decrease the speed. Haptic technology is another application requiring high torque low speed actuation which is the main case driving us to research on high torque actuator.

Haptic technology allows a user to kinesthetically get in touch with a virtual object through a hand-held electromechanical device known as haptic interface [1-2]. The goal of the design of a haptic system is to maintain system stability [3]. Figure 1-1 shows an example of a haptic manipulation in which the operator uses a HD2 haptic interface from Quanser to work on the simulated model of the spine in the computer for the purpose of medical haptic training.

A haptic interface can possibly make sensitive tasks feasible provided that it has been properly designed for such an application. In case of surgery, the haptic device senses the position of the surgeon's hand (device handle) and based on the penetration depth of the handle into the organ, which is proportional to the handle displacement, a corresponding reaction force is calculated within the computer model of organ. and then it is fed back to the surgeon's hand by means of the actuator [5-6]. Applications of this technology include a large variety of human activities such as training, education, entertainment, healthcare, scientific visualization, telecommunication, design, manufacturing, and marketing [7-10].

A force-feedback haptic interface can be viewed as a block consisting of four subset blocks. These subset blocks include electronics and drive, mechanical structure, computer graphics and control [11]. Performance of each of these blocks contributes to the overall haptic device performance [12]. In order to have a haptic device working properly, each block has to address the requirements that a given application necessitates. Therefore, based on the

application, different design specifications will be required and the importance of any of these properties can vary from one to another [13].

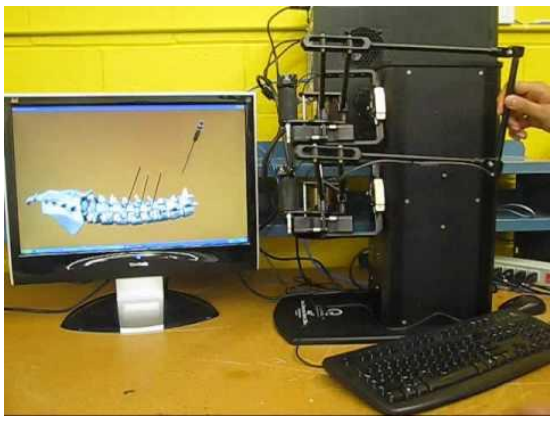

Figure 1-1 Medical training haptic device - HD2 haptic device from Quanser [11]

Most of the available in the market haptic devices are run by electric actuators in particular, permanent magnet DC motors due to their ease of control. For instance, HD2 from Quanser (Figure 1-1) uses a coreless permanent magnet dc motor from Faulhaber. Phantom Premium 1.5, shown in Figure 1-2, also uses a corelss permanent magnet dc motor from Maxon Motor.

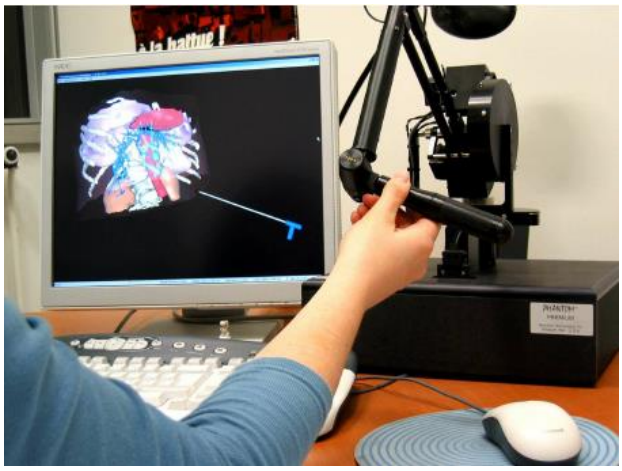

Figure 1-2 Phantom Premium 1.5 haptic device from 3D Systems [11]

Omega.6 from Force Dimension a Swiss product, uses a permanent magnet dc motor as the actuator, Figure 1-3.

Figure 1-3 Omega.6 haptic device from Force Dimension [12]

Most of haptic appliactions require user to manipulate the virtual task (dynamic object) by interacting with the haptic interface. This requires the haptic interface to output high amount of torque at low speed. Therefore, the motor that is used as the electric actuator of the haptic device has to generate high amount of torque at low speed. Beside the toque speed characteric, other specifications including Maximum Excertable Force, Maximum Continuous Force, Inertia, Noise and EMC, Thermal Time Constant, Stiffness, Dynamic Range Position Resolution, should all be considered in a haptic interface design.

1.2 Motivation of This research

We are seeking to develop a haptic actuator that is able to generate sufficient amount of torque at low speed that would allow to manipulate hard virtual objects. The actuators of the available in the market haptic devices are electric motors that have not been specifically made for those conditions. Figure1-1 to Figure 1-3 are examples in which a permanent magnet DC motor has been used as the electric actuator. These motors cannot address the high torque

requirement of the application, therefore, a gearbox or a cable mechanism has been integrated in them to increase the torque generated by the motor and decrease the speed. However, adding a gearbox mechanism will degrade system specifications such as backlash, back-drivability and transparency. It also adds to inertia, cost, loss and complexity of the overall system. Therefore, it is very beneficial to eliminate the gearbox and come up with a high toque direct-drive mechanism.

Series motors (also known as universal motors) have the highest torque at low speed (~ zero) amongst all types of motors. Based on their inherent torque ampere characteristic, series motors electromagnetic torque varies with the square of the motor current making them high torque motors at low speed. The major drawback of the series motor is that it cannot generate torque in both forward and backward directions. In other words, series motors are inherently unidirectional which can only rotate in one direction. However, a bidirectional motor that can rotate in both directions is an essential requirement for a haptic actuator.

That said, if we could devise a method to convert unidirectional series motor to electrically bidirectional series motor then we have solved the issue of high torque at low speed for a haptic device. We accomplish this through design of power electronics switching circuitry in-line with armature and field coil. Therefore, without any change in the mechanical and structural design in the series motor, by only adding a power electronics circuitry a series motor will be converted to a bidirectional series motor capable of generating high torque at low speed in both forward and backward rotation.

1.3 Contributions

In this thesis contributions are as follows:

- Review of different types of motors available in the market and comparing them in terms of haptic device design specifications

- Proposal of a novel bidirectional actuator based on the series motor for high torque demanding applications such as haptic technology
- Proposal of a topology referred to as “Diode-method” to convert unidirectional series motor into a bidirectional series motor
- Proposal of “Active-bridge method” as a generalized topology to covert unidirectional series motor into a bidirectional series motor addressing wider range of applications
- Proposal of a novel control strategy for “Active-bridge method”
- Computer simulation of both “Diode-method” and “Active-bridge method”
- Design of a laboratory prototype from scratch for practical implementation of “Diode-method”

1.4 Thesis Outline

This thesis is outlined in 5 chapters. The first chapter introduces the topic and motivation of the research and explains the current issue in high torque demanding application focusing on haptic technology as the targeted application. Chapter 2 is devoted to study of haptic device and motors in which a comparison of motors available in the market has been presented in terms of haptic device design specifications. Chapter 3 proposes the first novel method referred to as “Diode-method”. Simulation and experimental results of “Diode-method” is presented at the end of this chapter. Chapter 4 explains the second novel method referred to as “Active-bridge method”. A comparative analysis of the simulation results of both methods has been carried out at the end of chapter 4. Finally, chapter 5 concludes the thesis and presents possible future work.

Chapter 2

Study of Haptic Device and Motors

2.1 Introduction

So far from chapter 1, it is known that we aim to develop a bidirectional high torque low speed actuator that could address high torque demanding applications. Also it was mentioned that one of main applications that is targeted in this thesis is haptic technology which requires a bidirectional high torque low speed actuator. A haptic actuator plays a fundamental role in a haptic device and it determines many of the design specifications of the haptic device [1-8]. Haptic actuators can come in the form of motors and also magnetic actuators [9-11]. Therefore, study of the motors is very crucial when it comes to haptic interface design.

In this chapter, first haptics as a science and technology will be discovered and the important design specifications of a haptic interface will be explained. Then the study of different types of motors will be presented.

2.2 Haptics - Haptic Interface

Haptics is the science that deals with information acquisition and object manipulation through the sense of touch. Generally, the haptics can be subdivided into three categories [12]. First is human haptics which involves with the study of human sensing and manipulation via the sense of touch. Second is computer haptics which deals with models and force reflecting behavior of virtual objects and also rendering algorithms for real-time computation of feedback force display [13]. Third is machine haptics or haptic technology which deals with the design of haptic interfaces which employ mechanical, programmed physical devices that can be utilized for human-computer communication by means of the human sense of touch [14-18]. What we are dealing with in this work is related to haptic technology.

Haptic interfaces are devices composed of mechanical components in physical contact with the human body for the purpose of exchanging information with the human nervous system [19]. Haptic interfaces are generally categorized as passive and active haptic interfaces. Passive haptic interface only receives inputs and no output force or quantity is generated in them.

Keyboard, mouse and trackball are three well-known examples of passive haptic interfaces. However, active haptic devices, which will be referred to as haptic devices in this report, generate a feedback to the user. Force-feedback haptic device as an example of active haptic device, reacts to the user's hand by applying a feedback force aiming to recreate the sense of touch for the operator or to convey information to the operator [20]. In the next section force-feedback haptic device will be elaborated.

2.3 Force-Feedback Haptic Device

A Force-feedback haptic interface is composed of mechanical and electrical components that has been programmed so to provide a feeling of sensation of an object to the operator's hand [21]. It has actually two basic functions, first to measure the positions and contact forces of the user's hand (and/or other body parts) and second is to display contact forces and positions to the user. At present, most of the force-reflecting haptic interfaces sense position of their end-effector and display forces to the human user [22]. Applications of this technology include a large variety of human activities such as training, education, entertainment, health care, scientific visualization, telecommunication, design, manufacturing and marketing. Specifically, in medicine, aids for the disabled such as haptic interfaces for the blind; manipulating micro and macro robots for minimally invasive surgery; remote diagnosis for telemedicine are the applications. video games and simulators that enable the user to feel and manipulate virtual solids, fluids, tools, and avatars makes the device good for entertainment [23-25]. Furthermore, for the purpose of education this force-feedback device can be used to let the students feel the phenomena at nano, macro, and astronomical scales. Integration of haptics into CAD systems so that the designer can manipulate different parts of the mechanical structure makes this device suitable for industry applications. Force-feedback device can also be beneficial to the applications such as graphic arts. In this way, virtual art exhibits, concert rooms, and museums in which the user can login remotely to play the musical instruments, and to touch and feel the

haptic attributes of the displays; individual or co-operative virtual sculpturing across the internet.

A force-feedback haptic device can be viewed as a block consisting four subset blocks, see **Figure 2-2**. These subset blocks include: electronics and drive, mechanical structure, computer graphics and control [26]. Performance of each of the above blocks contribute to the overall haptic device performance. Figure 2-2 clearly depicts an example of haptic interface which is a 6 degree of freedom (DOF) Delta haptic device [27]. As it can be seen from this figure, the delta haptic interface has a mechanical structure which is composed of parallelogram linkages, handle tip (nacelle) and the accessories. The mechanical structure has been designed such that the friction and inertia will be efficiently low and ignorable. DC motors and encoders as two other components of the delta haptic device can be seen in the picture. Any position change in the nacelle will be translated to a rotor angular disposition through the linkages. The encoder, thereafter, senses the angle of the rotor and as it is shown in Figure 2-2, sensed data goes to digital signal processor (DSP) as the main controller chip passing through signal conditioning and amplification circuit. The information regarding to the rotor position is sent to computer program by DSP and then the reaction force (torque) correspondent to the position change of the nacelle will be computed by means of any real-time haptic rendering technique in the computer. Then the calculated force is generated by the motor (actuator) and will be applied back to the operator's hand [28, 29].

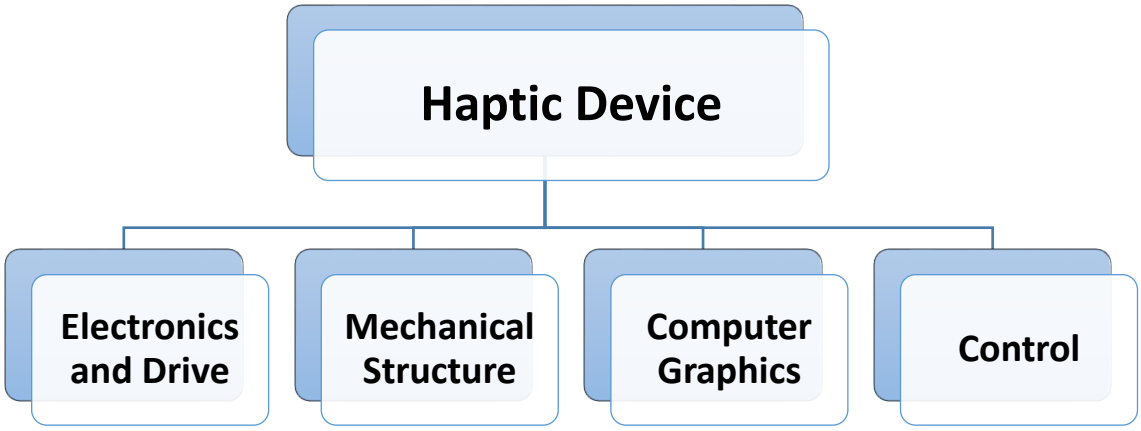

Figure 2-1 Delta force-feedback haptic device [13]

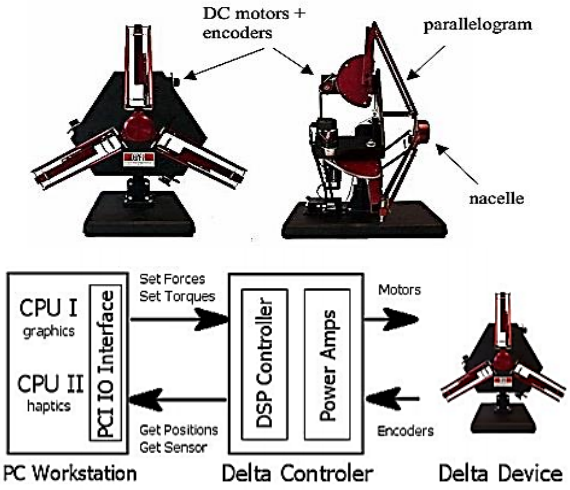

Figure 2-2 Haptic device elements [13]

Electronics and drive block is composed of motor, encoder, sensor, micro-controller, signal conditioning circuit and power electronics converter [30]. The motor acts as the actuator of the haptic interface and generates the amount of torque that is needed according to the computer graphic calculations. Detailed information about motors will be provided later in this chapter.

The encoder is used to sense the position of the rotor that is proportional to translational disposition of the device handle (nacelle) [31]. Depending on the type of the encoder, it can track linear or rotary motion, they can have optical or magnetic technology and they can be

incremental or absolute. Beside encoders, hall-effect sensors are the other options for position/speed measurements [32].

The heart of the haptic interface is the micro-controller or the digital signal processor (DSP). The measured and sensed data will be converted to digital values inside the DSP by means of analog to digital converter (ADC). On the other hand, the information regarding to the virtual model of the objects is on the computer which communicates with the master controller in the DSP through any communication protocol (Serial, USB, CAN, etc.). All of the control and communication tasks are carried out within the DSP which includes torque/speed control of the motor (drive), Kinematic, protection tasks, and communications with motor and computer [33].

The mechanical design and structure of the input device plays an important role in stability, performance, and efficiency of the haptic device. A proper design should have low friction, low inertia, high stiffness, backdrivability, and no back-lash.

2.4 Haptic Interface Design Specifications

A force-feedback haptic interface with a proper design should address a number of requirements based on the application. The design specifications for a haptic interface include: Inertia, friction/damping, backlash, backdrivability, maximum/continuous/minimum force, dynamic range, stiffness, position resolution, system latency, device latency, update rate, bandwidth, maximum acceleration, precision and repeatability, fidelity, and workspace. A brief description of each of these important parameters is given as follows [3, 34-44]:

Inertia: This is a measure of the mass of an object. For stability of interaction and transferring the feel of manipulation to the user, the mechanical impedance that user feels should be close to that of the virtual object. This makes the dynamic of haptic device transparent. Therefore, it is important that the haptic device have the lowest inertia possible in order to increase the

transparency of the device. In other words, a haptic device needs to communicate between the real and virtual world without introducing extra forces. Translational inertia can be measured in grams, while rotational inertia is expressed as mass times a distance squared (g·cm2).

Backdrivability: The ability to move the end-effector in the workspace without opposition. The device should ideally produce no forces on the user's hand when there is no interaction with an object in the virtual world. A device's backdrivability is usually characterized by backdrive friction (N). There are certain elements that reduce backdrivability, such as gears and friction in the motors and their transmissions. It is possible to have different values for each degree of freedom, especially in rotation and translation motions.

Friction / Damping: Kinetic friction comes in two varieties – Coulomb friction, which is independent of velocity, and viscous friction (or damping) which is proportional to velocity. If sufficiently high, they will degrade the force transferred to the user. Coulomb Friction is measured in N, but damping is usually reported as a coefficient in N·s/m or kg/s.

Maximum Exertable Force: The maximum force that the actuators can exert. It may be over a time period of several milliseconds, allowing a momentary tap or touch on a hard object.

Maximum Continuous Force: The maximum amount of force that the hand controller can exert for an extended period of time.

Minimum Displayed Force: The ability of a hand controller to display slight forces is a result of its low friction and its precise motor control.

Stiffness: The ability of the hand controller to mimic a solid virtual wall. It has been reported that stiffness needs to be 25 N/mm in order to feel stiff to a user when vision is obscured (Tan et al., 1994).

Position Resolution: The smallest amount of movement over which the sensors can detect a change of position. Good position resolution is one factor in displaying stiff virtual walls without vibration.

Thermal Time Constant: The amount of time in which the actuator (motor) reaches to its upper bound thermal limit due to the excess of current through its windings.

Electromagnetic Compatibility (EMC): The capability of haptic device to operate properly under noisy environment (noise immunity), and also not generating emissions to other sensitive equipment working nearby.

System Latency/ Update Rate: The total time lag of the components in the hand-controller (device handle) –computer system. The inverse, the update rate in Hertz, is more often used. The complete loop consists of position from the device, computation of force in the simulation, force sent to the device, and the next device position read. It may be characterized by the time delay between successive commands sent to the hand controller. This time will vary according to the speed and quality of the computer.

Device Latency: The time delay between sending a command to a device and receiving a response from that device. This would normally include geometrical computations (the forward and inverse kinematics), some of which may take place in the computer.

Bandwidth: The frequency ranges over which the hand-controller provides feedback. The range needed will depend on the operation being performed. Generally, small, precise movements will require a higher frequency feedback than large, more powerful movements. For example, tactile sensing requires the highest frequency (100-1000 Hz), while kinesthetic and proprioceptive sensing requires a bandwidth of 20 to 30 Hz. The response bandwidth required

by the hand and fingers to exert force is much lower, being between 5 and 10 Hz. (Burdea, 1996)

Update Rate: The speed at which the feedback loop can be completed, measured in Hz.

Backlash: This is characterized by moving the end-effector without a corresponding position being sensed. It feels like a dead-zone or void in space that occurs when you move the end effector in one direction against an opposing force, then switch to another direction where no force opposes the motion. It is often associated with gear systems where it is defined as the excess space between the interfacing teeth.

Maximum Acceleration: Important for emulating stiff walls. This may be measures by accelerometers attached to the hand controller.

Fidelity: The ability of the simulator to simulate real-world interactions. A high-fidelity device has high sensor resolution, good actuator performance, low computer latency and near ideal transparency in the transmission of the forces.

Workspace: The volume (or area) that the hand controller can reach is reported as the workspace. The workspace should be chosen according to the intended range of motion of the user's hand. With some devices, handle rotation may be restricted towards the limits of the translational workspace. Translational workspace is the volume traversed in Cartesian coordinates. Rotational workspace is the angle range in pitch, yaw and roll.

Based on the application the significance of any of these properties can vary from one to another. In the case of actuator design where only motor and the accessories are in the circuit, only some of the specific characteristics and properties will appear to be pivotal. Therefore, as long as it is concerned with actuator design for force-feedback haptic device, the more important design specifications and properties can be summarized as in Table 2-1.

Table 2-1 List of important specifications for design of haptic interface actuator

Specification	Description
Inertia (g.cm^2)	It effects dynamic response of the system. Lighter rotor with smaller diameter will have a lower inertia.
Maximum Exertable force (N)	When application needs high torque.
Continuous Force (N)	The same as maximum force and even more important as it also has to do with thermal consideration of the actuator.
Noise and EMC	Switching motor drives generate noises that can deteriorate performance of the system.
Thermal Time Constant	Motor has to have a long operation cycle which will cause overheating issues.
Minimum Displayed Force	To generate very small feedback forces motor has to pass this spec.
Position Resolution	The accuracy of the applied feedback force is dependent upon resolution.

2.5 Motors

The role of actuators is very critical in the design of force-feedback haptic interfaces [45]. In fact, some of the specifications of the haptic devices are directly related to the motor properties and parameters [46-49]. For instance, thermal limitation of a haptic interface is determined by the motor and the driver circuit. Also when it comes to design a haptic interface with a specific requirement for maximum and/or continuous exertable force, it should be addressed by the motor and its driver [50-55].

Depending on the application of the haptic device and the properties of the objects intended for haptic manipulation torque-speed requirements of the actuator may vary. For example, if it is intended to manipulate a stiff wall then the motor has to generate higher torques at low speed. For selection of motors specifically for haptic devices, no distinctive work has been done, so far. However, a comparative study of electric motor drive selection has been carried out for hybrid electric vehicles (HEVs) [65]. Other common specifications for motor drive system that should be considered in selection procedure, are cost, efficiency, noise (electromagnetic and acoustic), thermal thresholds. In a general view, out of all several types of motors that exist in industry, there are five categories of motors that can possibly be a solution to a specific drive application depending on its specification requirements. These motor types include DC brushed motors, permanent magnet synchronous motors (PMSMs), induction motors (IMs), and switch reluctance motors (SRMs) [66-70]. These motors have been widely used as major types of

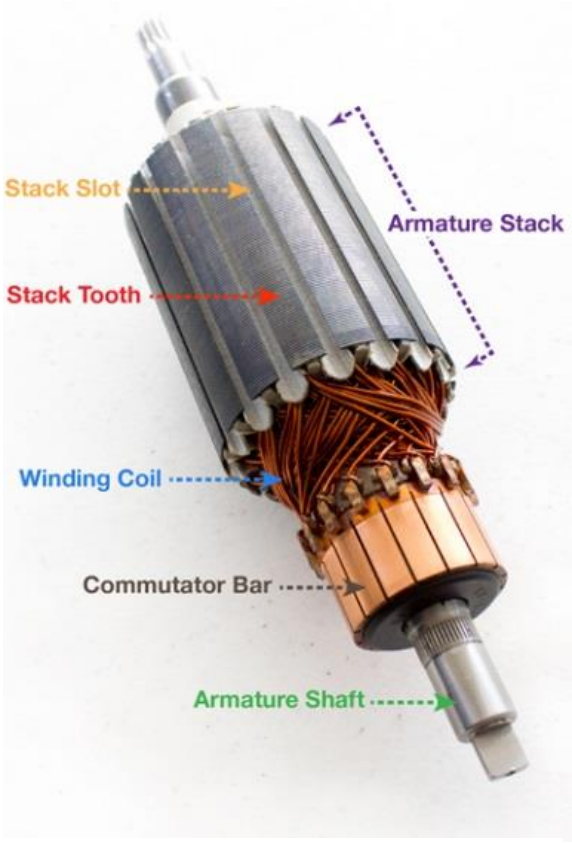

Figure 2-3 Rotor structure of a brushed DC motor

electric motors in HEVs as well as EVs as drives. Information and analysis regarding each of these motor types along with specialty motors which widely used in motion control and automation industry is provided in the following sections.

2.5.1 DC Brushed Motors

DC motors have been popular in electric propulsion due to the suitable torque–speed characteristics they have and their speed control which is very simple [56]. They are also very cheap and the manufacturing technology is mature. However, dc motor drives have a bulky construction, low efficiency, low reliability, and higher need of maintenance, mainly due to the presence of the mechanical commutator (brush) [59-60]. In high power ratings issues regarding to dc brushed motors appear to be more challenging then in low power applications [61]. For high power applications, ac brushless competitors are more interesting and there high reliability and maintenance-free operation are prime considerations. But in low power drive applications DC drives are still more than an alternative. Here four types of DC brushed motors are discussed.

Figure 2-3 shows the rotor of a typical dc motor structure in which the commutator can be seen clearly. Structure of different types of dc motors may vary in terms of windings connections and the overall structure remains the same.

2.5.1.1 Separately Exited Motor

Decoupled torque/flux characteristic makes separately excited DC motor excellent for precise position, speed, and torque control applications including trains and traction systems and variable speed drives [62]. The equivalent circuit along with its typical torque-speed characteristic have been shown in Figure 2-4.

A specific type of this motor that has been used as an actuator in a haptic knob is a coreless Maxon model RE25 (graphite brushes, 18 V) that features a very small inertia due to the elimination of core. Also another instance of this type of motor used in again a haptic knob is a wound Pittman model 8693 (19 V) [1].

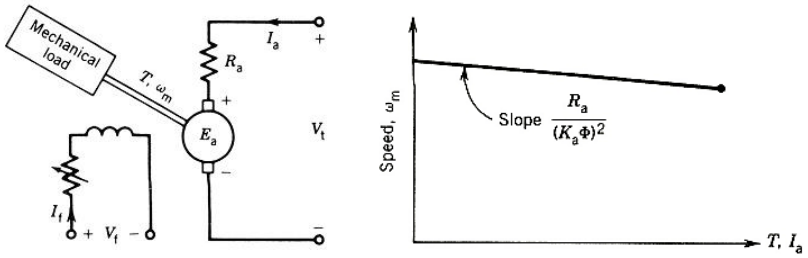

Figure 2-4 Separately excited DC motor: Circuit (Left), Torque-speed characteristic (Right) [60]

2.5.1.2 Series (Universal) Motor

Figure 2-5 shows the steady state equivalent circuit of a series DC motor as well as its torque-speed characteristic for various values of R_{ae}. In a series motor, electromagnetic torque varies with the square of armature current. This inherent feature of series motor results in two unique characteristics which are high starting torque and unidirectional rotation. The former makes the series motor first choice in applications requiring high torque at low speed such as subway cars, automobile starters, cranes, blenders, etc. The latter, on the other hand, makes the series motor work both on AC or DC supply. That is why series motors are also known as universal motors. However, universal motors that are supplied by AC source have a slightly different structural design. For minimizing the core loss in universal motors, the stator and rotor cores are laminated whereas in a DC fed series motor there is no need for core lamination. Nonetheless, most of the series motors used and available in the market are in the form of universal motor. Figure 2-6 shows a drill in which a series (universal) motor has been used.

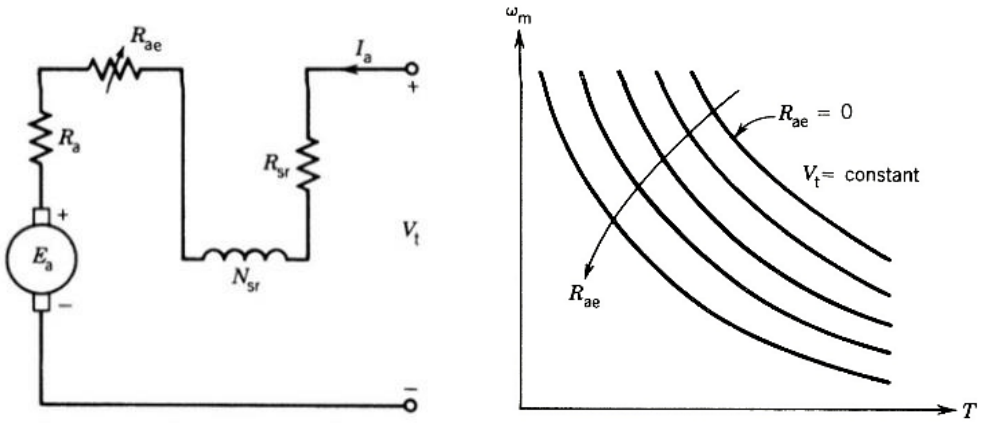

Figure 2-5 Series DC motor: Circuit (Left), Torque-speed characteristic (Right) [60]

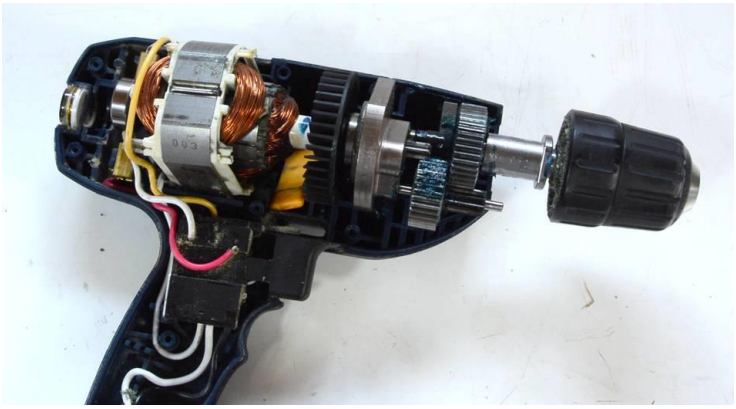

Figure 2-6 Universal motor – Drill [72]

The inherent unidirectional characteristics of the series motor, however, is a significant disadvantage in servo drive and motion control applications. Because the torque generated by this motor is always positive, it cannot generate brake torque which is big barrier for series motor to be used in drive and torque control applications. In this thesis, with the aid of power electronics switching circuitries presented in chapters 3 and 4, and without any change in mechanical and structural design, any series (universal) motor will be capable of bidirectional rotation and generating accelerating or decelerating (brake) torque.

2.5.1.3 Shunt Motor

A shunt dc motor along with its schematic diagram are shown in Figure 2-7. The armature circuit and the shunt field circuit are connected across a dc source of fixed voltage V_t. An external field variable resistor (R_{fc}) can be used in the field circuit to control the speed of the motor. Its torque-speed characteristics appears to be the same as that of the separately excited motor as illustrated in Figure 2-4. As to mention some example applications of DC shunt motor, it can be used where constant speed is required and starting conditions are not severe. The various applications of DC shunt motor are in Lathe Machines, Centrifugal Pumps, Fans, Blowers, Conveyors, Lifts, Weaving Machine, Spinning machines, etc [64].

2.5.1.4 Compound Motor

Figure 2-8 shows compound wound motor that includes both shunt and series windings. In cumulative compound motor series and shunt fluxes aid each other while in differential compound motor they oppose each other. Torque-speed characteristics of different DC motors that have been mentioned so far, has been depicted in Figure 2-9. Amongst all, series motor can generate the highest torque at low speed and after that is cumulative compound filed dc motor. Cumulative compound wound motors are virtually suitable for almost all applications such as business machines, machine tools, agitators and mixers etc. Compound motors are used to drive loads such as shears, presses and reciprocating machines, rolling mills and other loads requiring large momentary torques [66].

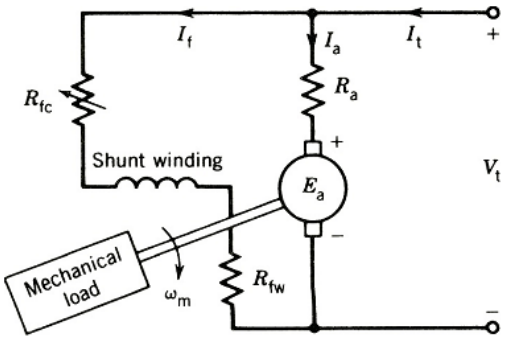

Figure 2-7 Shunt DC motor [60]

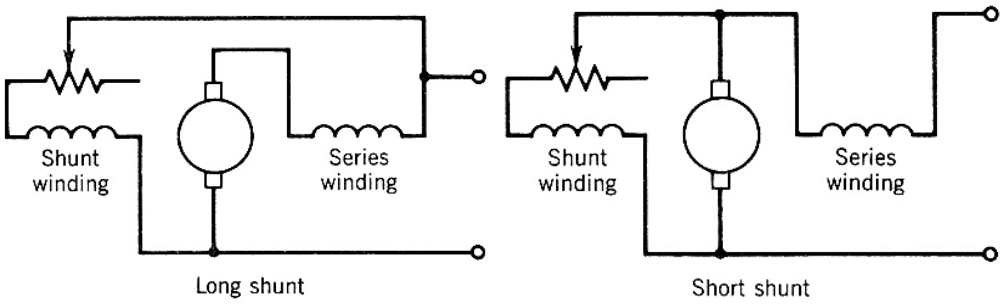

Figure 2-8 Compound wound motor winding connections [60]

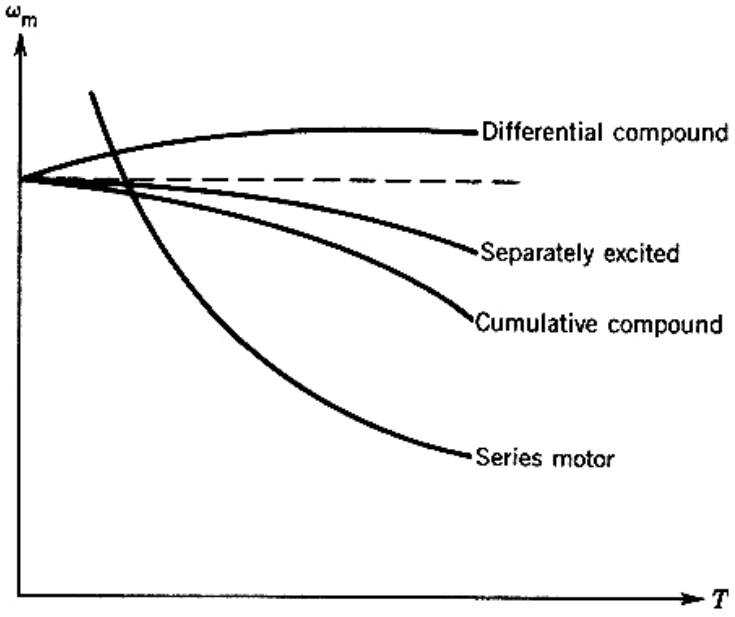

Figure 2-9 Torque-speed characteristics of different dc motors [60]

2.5.2 Permanent Magnet Synchronous Motors (PMSMS)

A PM BL (permanent magnet brush less) motor has a permanent magnet rotor and a wound field stator, which is connected to a power electronic switching circuit. The definite advantages of PM BL drives are their inherently high efficiency, high power density, and high reliability [67]. The key problem is their relatively high cost due to PM materials.

In a general classification based on the operating current and no-load electromotive-force (EMF) waveforms, PM BL motors are divided into two PM BL ac (BLAC) and PM BL dc (BLDC) categories. For the PM BLAC drives, they operate with sinusoidal current and sinusoidal airgap flux so that they need a high resolution position signal for closed-loop control, hence desiring a costly position encoder or resolver. On the other hand, for the PM BLDC drives, they operate with a rectangular current and a trapezoidal airgap flux so that they just need a low-cost sensor for phase-current commutation. Theoretical current/flux waveforms of PM BL operation have been shown in Figure 2-10. Also torque-speed characteristics of the PM BL drives both with and without control can be seen in Figure 2-11. It can be seen that the BLAC drive offers higher torque and power capabilities than the BLDC drive [68]. Today more and more applications rely on BLDC including medical equipment, home appliances, building controls and industrial automation such as actuators, CNC machines, industrial robots, and extruder drivers.

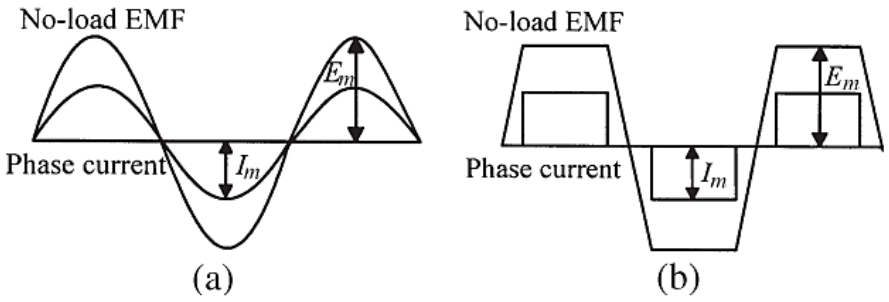

Figure 2-10 Theoretical waveforms of PM BL operations.
(a) BLAC. (b) BLDC [63]

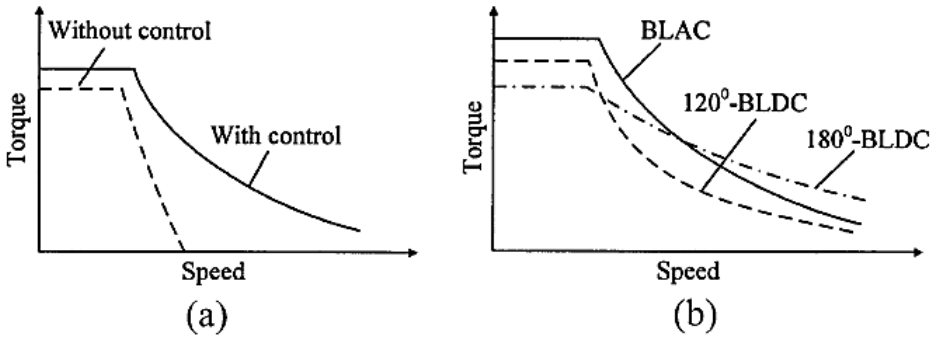

Figure 2-11 Torque-speed characteristics of the PM BL drives. (a) With and without control. (b) BLAC versus BLDC [63]

2.5.3 Induction Motor

Induction motors (IMs) are broadly used in ac drive applications and they are widely accepted as the most potential candidate for the electric propulsion of HEVs, owing to their reliability, ruggedness, low maintenance, low cost, and ability to operate in hostile environments. Based on the rotor type, induction motors are either wound rotor or squirrel cage rotor, see Figure 2-12. Today, an IM drive is the most mature technology among various commutator-less motor drives [67]. They can be used in so many applications including conveyors, cranes, pumps, elevators and compressors.

Figure 2-12 Induction motor, squirrel cage rotor [27]

Torque-speed characteristics of an IM dive has been shown in Figure 2-13. Basic converter topology which is used to drive an IM (3-phase IM) is a 3-leg inverter. With the aid of vector control coupled torque/flux behavior of the induction motor is not a big issue. FOC[1] can decouple the torque control from the flux control. However, limited starting torque (torque at low speed) is an issue with them that is solved by addition of gearbox in electric vehicles and traction applications. Other drawbacks that are concerned with IMs are mainly high loss, low efficiency, low power factor.

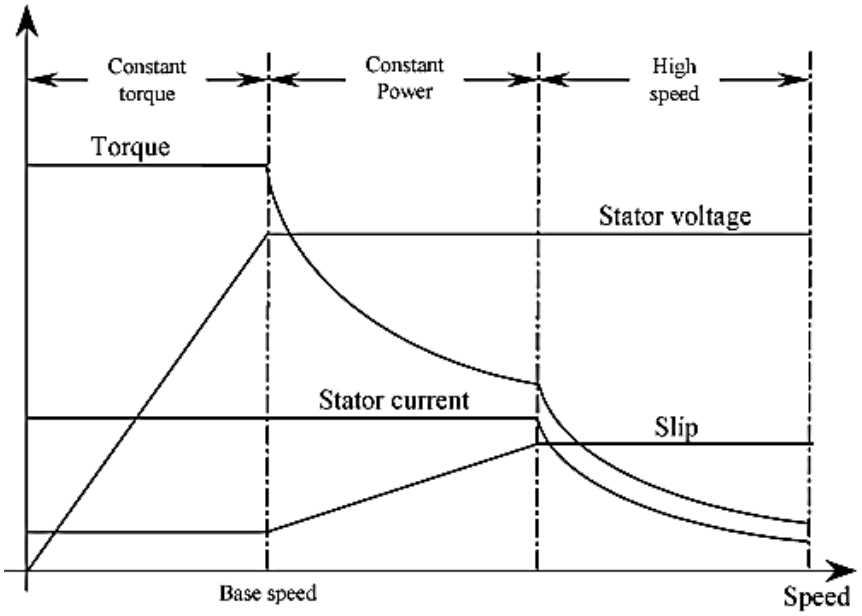

Figure 2-13 IM Torque-speed [27]

2.5.4 Switch Reluctance Motor

Switched reluctance machines (SRMs) have salient stator and rotor poles with concentrated windings on the stator and no winding on the rotor. A 12/8 SRM (12 stator poles and 8 rotor poles) has been shown in Figure 2-15. SRMs are cheap, easy to manufacture and they have rugged structure and withstand high temperatures [74].

[1] Field Oriented Control

Figure 2-15 Switched reluctance motor (12/8) [28]

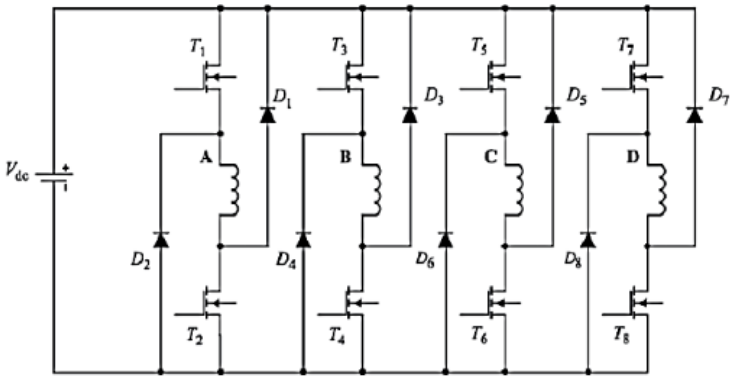

Figure 2-14 Two-switch-per-phase converter for an 8/6 SRM drive [74]

The SRM machines are well suited for high-speed operations and tend to have higher efficiency at high speeds. The classic SRM drive as a system with converter involves two switches and a winding in series that has been shown in Figure 2-14. High torque ripples along with high noise levels are the main issues that can limit applications of SRMs for haptic applications. They are not suitable to work at very low speeds as they are for high speed. Traction drives in automotive industry, high speed pumps and compressors, household appliances, fans, windscreen wiper, are examples of applications of this type of motor.

2.5.5 Specialty Motors

Besides the major types of motors discussed above, there are a number of other motors used in specific applications that are usually referred to as specialty motors. In this section,

outrunner brushless dc motor, universal motor, pancake motor and torque motor will be covered as they can be a candidate for haptic interface design.

2.5.5.1 Outrunner BLDC Motor

In a different perspective, mostly common in UAV (unmanned aerial vehicle) and remote controlled (RC) airplane industry, miniature dc motor drives are divided into two groups of inrunner dc motors and outrunner dc motors. Inrunner motors are essentially the conventional dc brushed motors with permanent magnets. Inrunner motors spin their central part that is wrapped with copper windings. The magnets are on the outer casing that is stationary. Since the electrical windings spin, conductive electrical brushes must be used to make the electrical connection. The brushes cause drag that lowers the efficiency of the motors. The bigger problem with inrunner motors is that they have a relatively high motor constant (Kv) value. What this means is that they tend to spin at high RPM with little torque. Therefore, for the applications requiring high torques at low speed gearbox should be used to increase motor torque which adds to the cost and complexity of overall drive system. Moreover, the gearbox introduces friction and loss, degrades backdrivability, decreases efficiency, and adds system weight [65].

In contrast, outrunner motors still have the copper windings on the inside, but now the magnets on the outside casing spin around. This arrangement avoids the need for brushes. Since the larger diameter outside is the rotary part, outrunner motors naturally develop more torque

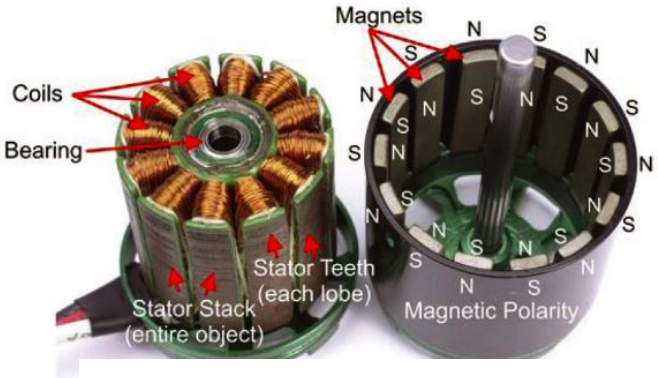

Figure 2-16 Outrunner BLDC components [66]

than inrunner motors. This feature is interesting in haptic interface actuator design. Specifically, force-feedback sensation recreation of stiff walls needs an actuator motor that can run at low speed but generating high torques. So, this type could be a candidate for the aforementioned application. Figure 2-16 shows different components of an outrunner BLDC motor [65, 67]. Torque speed characteristics of Outrunner BLDC motors are similar to that of BLDC motors shown in Figure 2-11b with the difference that Outrunner motors generate higher amount of torque at low speed compared to BLDC motors.

2.5.5.2 Pancake Motor

Pancake motors, also referred to as Flat motors and ServoDisc motors, are compact sized motors that benefit from their iron-less disc armature design. Figure 2-17 shows Pancake motors. The thin, low-inertia iron-loss armature design leads to exceptional torque-to-inertia ratios. Briefly, it includes advantages such as smooth rotation, long brush life, high speed capability, instantaneous torque, full torque in all speed ranges, and extra momentary torques.

Most ServoDisc motors are rated for peak current of 10 times the continuous rating. This capability of pancake motor to generate higher than normal torques at demand is an interesting characteristic in haptic device design. However, they are comparatively expensive.

Figure 2-17 Pancake motor [72]

2.5.5.3 Torque Motor

Torque motors are designed to provide high starting torque and sloping characteristics (torque is highest at zero speed and decreases steadily with increasing speed), and operate over a wide speed range. Figure 2-18 shows a sample torque motor from Allied Motion [75]. They also provide stable operation, especially in the low speed range or under a locked rotor condition. Torque motors have a high starting torque and sloping characteristics, allowing easy speed control simply by changing the voltage supplied to the motor. (The motor torque varies in proportion to the square of the voltage, see Figure 2-19).

Torque motors are essentially permanent magnet synchronous motors that have a different structural design. They are constructed with a large diameter and higher number of magnetic poles. Therefore they can generate high torque while operating at low speed. Therefore, torque motors can be a candidate for haptic technology. However, they are expensive due to their specific design and integrated water cooling system.

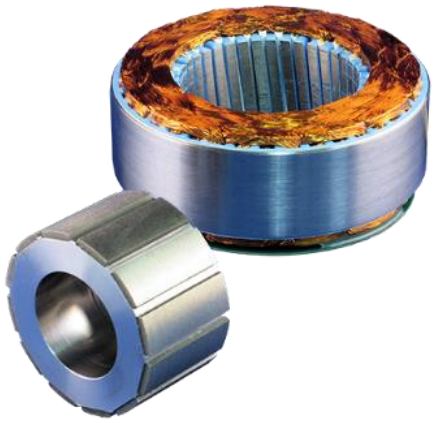

Figure 2-18 Torque motor from Allied Motion [75]

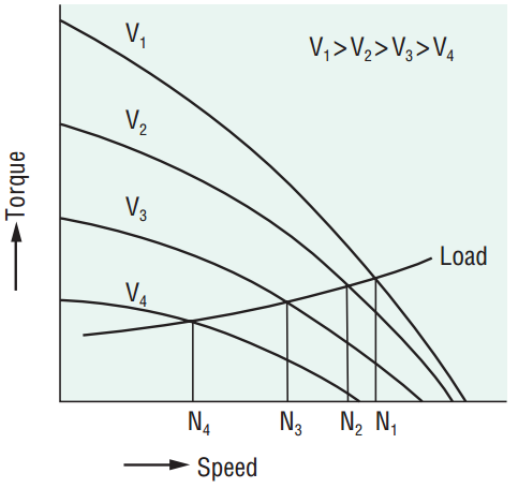

Figure 2-19 Torque-speed characteristics of a Torque motor [75]

2.5.6 Comparison of Motors Based On Haptic Interface Design Requirements

So far a number of motors with different types and characteristics have been concisely reviewed. There are several different applications for these motors ranging from very low power to high power ratings and from precision micro-drives to high power elevators. However, as the actuator of a haptic device the motor needs to satisfy application-specific design requirements which were discussed in the second chapter of this document.

As mentioned earlier, a haptic device is of our interest that is intended for virtual manipulation of stiff or relatively stiff objects. In term of the actuator properties, the motor should be capable of generating high torques at very low speeds close to zero consistently. Due to the nature of haptic manipulation which is relatively slow and also the longevity of the manipulation, the motor needs to generate torques for a relatively long time. This can cause overheating issues especially when the speed is around zero it will not even have the natural cooling and that worsens the thermal issues.

Properties of the virtual object that is intended to be virtually manipulated by the haptic device plays an important role in the characteristic requirements of the motor as the actuator. If

it has a hard surface or if it is a stiff wall, then the motor should run at low-speed high-torque operating point. But if the object is very soft or when free movement in the air is the case, then the motor should generate low torque at high speed. Therefore, the design of a haptic device is such that it covers all ranges of speeds and torques is significantly challenging task to fulfill.

Other important characteristics that the motor should have is that it should be capable of having intermittent work cycles. This is because the nature of manipulation is so that so many movements of the hand when manipulating or touching an object will be turned into several different torque set-points for the motor and these set-points can possibly vary in a discontinuous way depending on the application. Sudden movements of the hand-controller can be translated into applying step torque changes to the motor.

One other point is that in a haptic device torque control is the target and unlike several applications that are concerned with position or speed control, which have more limited and definite options of motors as an appropriate candidate, a wider range of motor types could be used as the actuator. For position/speed control applications more research has been done and as mentioned earlier there are couple of studies that have been dedicated to the selection of motors as in traction applications in HEVs and EVs for instance. However, many motor types that are not considered as candidates of position/speed control applications could be possibly a candidate for torque control in a haptic device. This is actually why this study also covers the very basic motor topologies as they might turn to be suitable for this specific application.

Furthermore, among existing published works on the topic of haptic devices, only a few types of motors have been reported for use as a haptic device actuator. Wound rotor brushed dc motor, coreless dc motor and permanent magnet brushless dc motor are only three types that have been used and reported. Table 2-2 provides more detail about these three cases. At the end, to put all the information together in a comparative way, Table 2-3 gives an overall idea of

comparison among different motor types with the perspective of haptic interface design requirements.

Table 2-2 Three motor types used as actuator in haptic device in references [1] and [10]

Motor Type	Motor Model	Manufacturing Company	Application
Wound rotor brushed DC motor	**8693**	**Pittman**	**Haptic Knob [1]**
Coreless brushed DC motor	**RE25**	**Maxon Motor**	**Haptic Knob [1]**
BLDC motor	**EC Φ45**	**Maxon Motor**	**1 D.O.F Haptic Interface [10]**

Table 2-3 Comparative analysis of different motors

Features / Motors	TLS	I	TT	E	CC	DC	VSO	C	TM	CT*
Separately Excited DC	M	H	L	M	L	L	H	L	H	M
Series (Universal)	VH	H	L	M	L	L	H	L	H	M
Shunt DC	M	H	L	M	L	L	L	L	H	M
Compound wound	M	H	L	M	L	L	M^{+}	L	H	M
Coreless DC	M	VL	M	H	L	H	H	L	M	Zero
Pancake (flat)	H	L	H	H	M	M	H	H	M	Zero
Induction	M	M	M	M	H	M	H	L	H	M
Switched reluctance	M	L	H	H	H	H	H	L	H	L
BLDC	M	L	H	H	H	M	H	M	M	MH
Torque	H	VH	H	L	H	M	M	H	L	MH
Outrunner BLDC	H	H	H	H	H	M	H	H	M	MH

Table 2-3 Legend:

TLS: Torque at low speed, I: Inertia, TT: Thermal threshold, E: Efficiency, CC: Control complexity, DC: Driver complexity, VSO: Variable speed operation, C: Cost, TM: Technological maturity, CT: Cogging torque*.

VL: Very Low, L: Low, M: Medium, MH: Moderately High, H: High, VH: Very High.

***** Cogging torque is defined as the attraction/interaction of the magnetic poles to the teeth (steel structure) of the laminations within an un-energized motor. The motor with less cogging torque will have a smoother operation.

+ Depending on the type of compound motor this characteristic can vary from L to H.

As can be seen in Table 2-3, series (universal) motor, pancake motor, torque motor, and outrunner BLDC motor all can generate high torque at low speed where the series motor has the highest starting torque per ampere amongst all due the fact that its torque varies with the square of the current.

However, unidirectional rotation of the series motor does not leave any chance for this motor to be a candidate for high torque low speed application, specifically, for a haptic device. In next chapters, therefore, power electronics based methods will be presented to solve the issue of unidirectional rotation of series motor to benefit from its very high starting torque.

Chapter 3

Novel Bidirectional Series Wound Motor Diode-Method

3.1 Introduction

As mentioned before, in a haptic device the actuator motor should generate high torque at low speed (~ zero). Therefore, amongst the existing motors in the market outrunner BLDC motors, Permanent magnet synchronous torque motors, and Pancake motors can be candidates to address requirement of high torque at low speed in haptic simulations (Table 2-3, Chapter 2).

Outrunner BLDC and torque motors are essentially permanent magnet synchronous motors (PMSM) in which the torque varies linearly with motor speed as well as current [79]. They relatively generate higher torque at low speed compared to a typical PMSM due to their different mechanical and structural design. In fact, outrunner BLDC is a radial flux PMSM in which the rotor surrounds the stator. Therefore, due to the larger rotor diameter outrunner BLDC motors generate high torque low speed motors but only compared to inrunner or typical PMSMs.

Permanent magnet torque motors are also different with typical PSMSs in their mechanical design. They have higher number of poles to work at low speed and the rotor and stator diameter is larger than that of a typical PMSM with same power rating. Due to their large rotor diameter they can generate higher torque and work at lower speed.

Pancake motors, known also as flat or armature printed motors, are DC brushed axial flux motors with constant field magnets on the stator. The armature coil is printed on rotor disc. As a result the inertia of this motor is very low. Again due to their mechanical and structural design Pancake motors are generate high torque at low speed. However, the relation between torque, speed and current in them is still a linear. Moreover, they are significantly expensive.

Series motors (universal motors), however, generate torque that is related to square of current. Due to this inherent nonlinear characteristic series motors' torque increase exponentially as the speed closes to zero. Therefore, they have the highest torque per ampere (torque density) amongst all type of motors. However, as mentioned before, series motors can

only rotate in one direction. Thus, it is not considered as a candidate motor for high torque low speed applications where bidirectional rotation is required, i.e., four-quadrant T-ω. Moreover, due to their unidirectional rotation (torque), universal motors do not benefit from electrical braking. Therefore, series motors (universal motors) would be a significant high torque low speed candidate if they could run in both directions. The other significant benefit of bidirectional operation of universal motors would be generating electrical brake.

There are quite a few patents in which a circuit has been proposed for dynamic braking of the DC series motor [76, 77]. Dynamic braking aims to bring the universal motor to standstill when the motor is disconnected from the AC source. In all of these patents, an auxiliary circuitry is connected to the motor and dissipates the energy stored in the field and armature winding.

Figure 3-1 shows the circuit proposed in [76]. While the AC source is connected to the universal motor switches are in RUN mode, see Figure 3-1a. In the RUN mode, the field winding (shown by 18 on Figure 3-1) is in series with armature (12). The branch consisting of the capacitor (26), resistor (28) and diode (24) is in parallel with AC source. Diode (24) rectifies the current. Therefore, the capacitor will charge to the peak voltage of the AC source and the current through it will go to zero. In STOP mode field winding (18) will become parallel with armature. It also will be in parallel with the capacitor (26) and resistor (28). The capacitor (26) will discharge in field winding (18) and brings the universal motor to standstill. Likewise other patents the circuit of Figure 3-1 can only bring the motor to stop when the motor is disconnected from the source. Therefore, a bidirectional universal motor capable of generating negative torque will be very useful for fast dynamic braking of universal motors with minimal added circuitry.

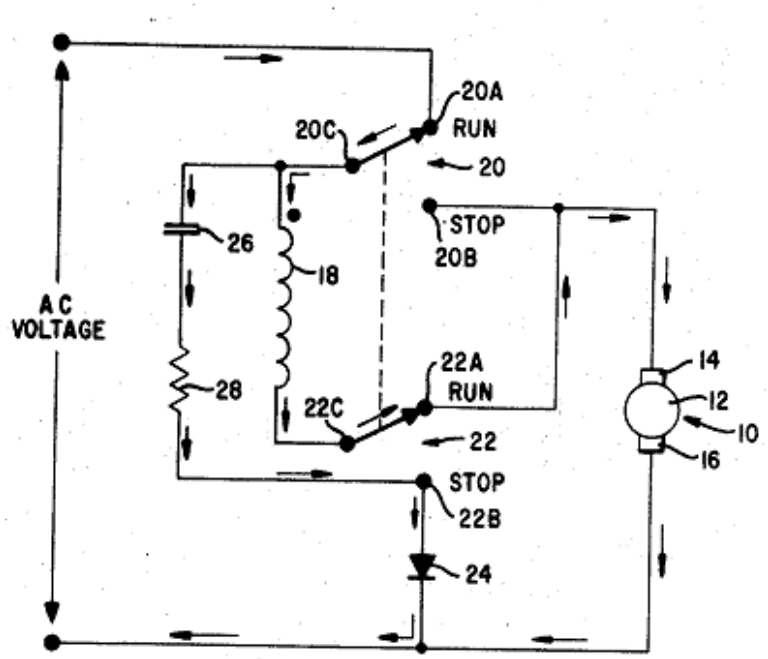

(a)

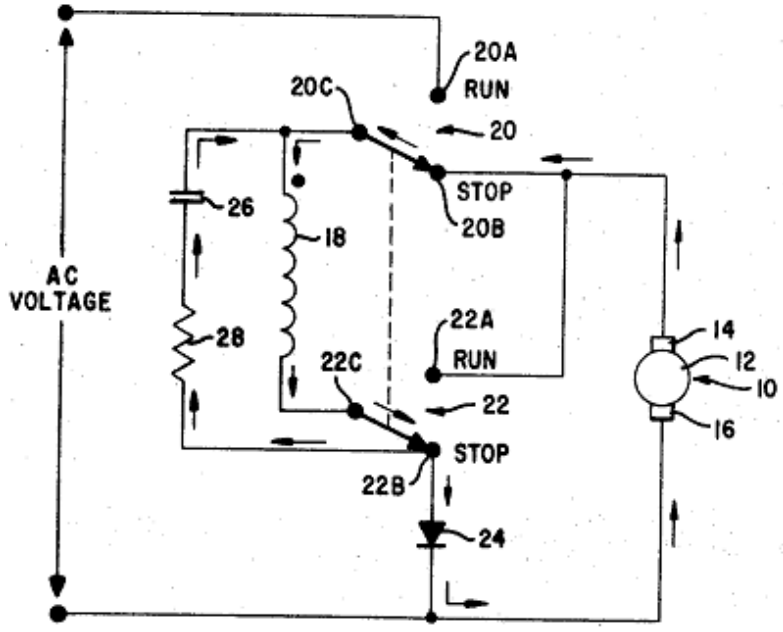

(b)

Figure 3-1 Dynamic braking of universal motor [76].
(a) Motor mode (RUN)
(b) Brake mode (STOP)

For any type of motors to rotate in both directions, they require to generate positive (forward) and negative (reverse) torque. In all type of motors except series (universal) motor, the electronmagnetic torque has a linear relationship with motor current. Therefore, in all of them, by changing the polarity of supply voltage, hence the current direction, a negative torque is generated. Series motors torque, however, varies with the product of two equal currents, i.e., square of armature (or field) current. Therefore, by changing (reversing) the polarity of the supply voltage the armature and field current equally change direction and as a result the torque polarity will remain constant.

The armature current and filed current are equal in a series motor due the series connection of field and armature windings. Now, suppose that we add switches in line with field and armature windings as shown in Figure 3-2. Therefore, with a positive supply voltage (V_t) the field current (i_f) and the armature current (i_a) will be in the same direction if the switches S1 and S2 will be in position 1, see Figure 3-2 (a). This will generate a positive torque which results in forward rotation of series motor. Otherwise, with a negative supply voltage ($-V_t$) the field current (i_f) and the armature current (i_a) will be in the opposing directions if the switches S1 and S2 switch to position 2, a negative torque will be generated and motor will rotate in backward direction, see Figure 3-2 (b).

However, with the circuit of Figure 3-2 which uses double-pole switch to reverse the connection of field winding, a huge voltage spike will be generated at the moment of switching from forward bias (Figure 3-2 (a)) to reverse bias (Figure 3-2 (b)). Voltage spikes are generated due to the commutation of inductive current. In this thesis, we have introduced two different topologies that can do this transition smoothly. The first is known as “diode-method” is explained in this Chapter and the second, referred to as, “active-bridge method” is presented in Chapter 4.

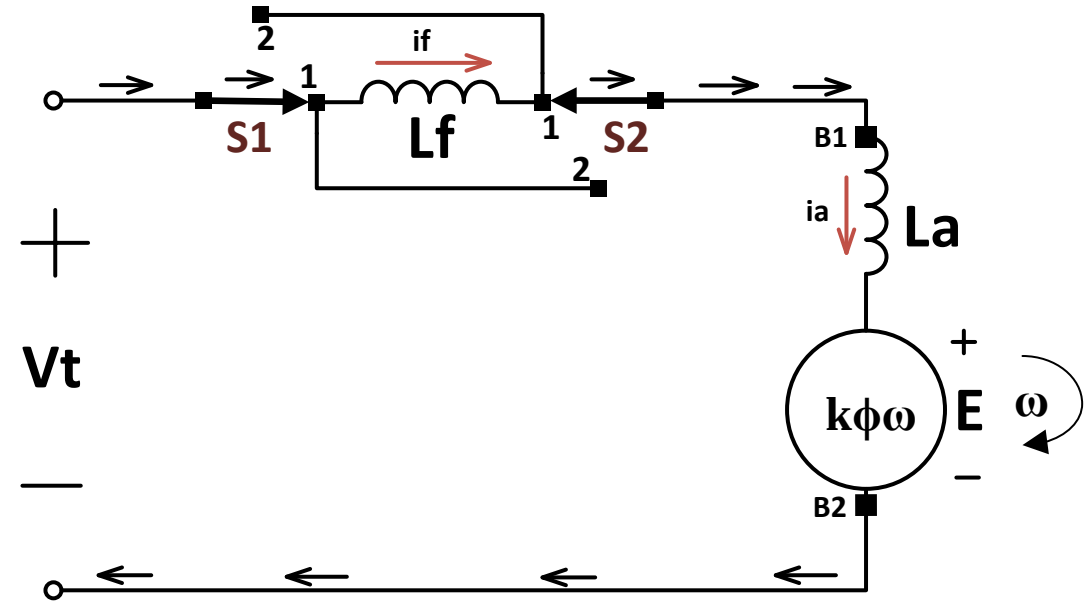

(a)

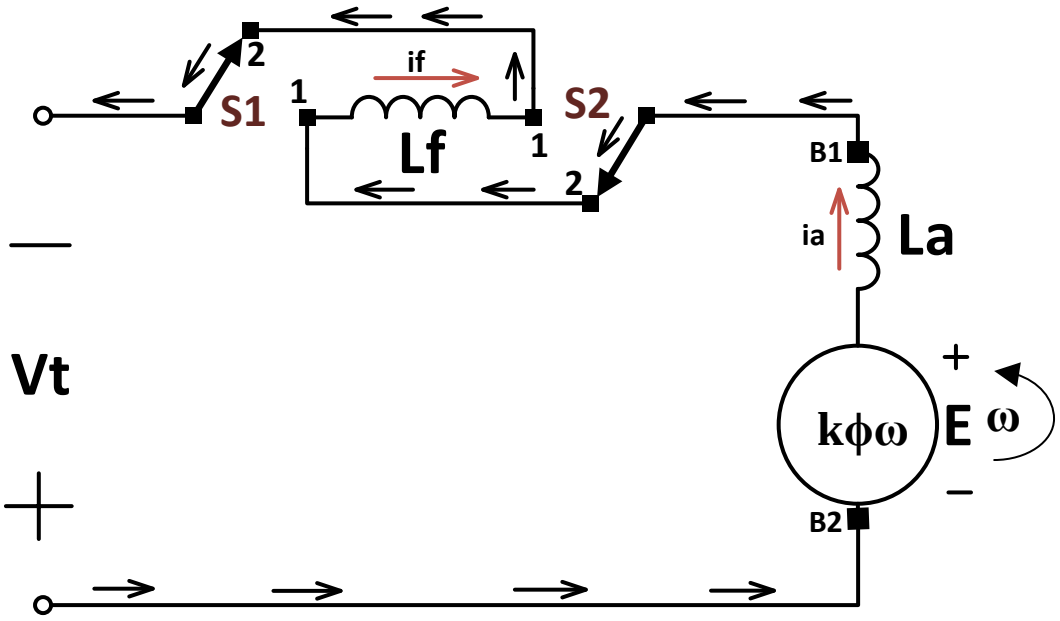

(b)

Figure 3-2 Series motor with reversal switches
(a) Forward bias
(b) Reverse bias

3.2 Proposed Topology for Diode-Method

3.2.1 Topology

We came up with the idea that if we could keep the direction of field current constant and let the armature current reverse upon the command for direction change then the reverse torque can be generated by DC series motor letting it rotate in the opposite direction. Therefore, with this perspective, efficiently using 4 diodes as a bridge rectifier, armature current can be rectified to be forced to go through the field winding only in one direction. This modification will also preserve the fundamental characteristics of the series motor which is the series connection of the two windings. Thus, with the added circuitry, the magnitude of the current in both field and armature windings still remains equal. Also, no passive element is added to the circuit and the solution does not add loss to the structure except the negligible diode loss. The proposed topology with full four-quadrant torque control for the series wound dc motor is shown in the following Figure 3-3.

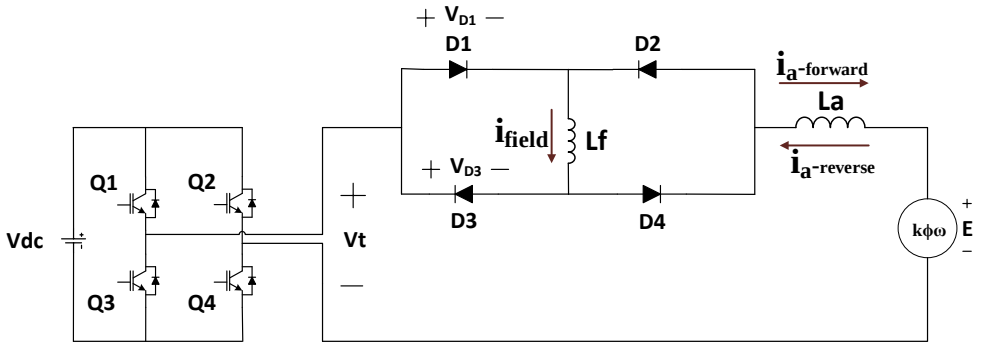

Figure 3-3 Proposed Topology – Diode Method

When the switches Q1 and Q4 are ON and switches Q2 and Q3 are off respectively, then a positive voltage (+Vdc) will be applied to the terminals of the bi-directional series wound motor and Vt will be equal to +Vdc. Consequently, Diodes D1 and D4 will be forward biased and conduct and motor starts to rotate in the forward direction (clockwise as shown in the Figure 3-4).

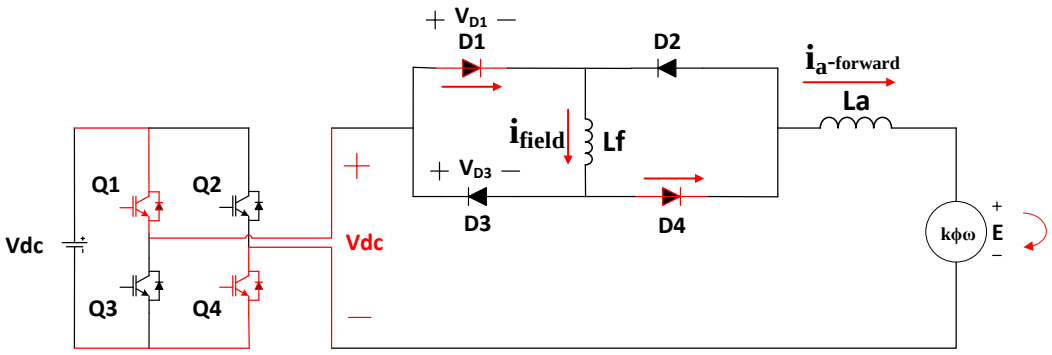

Figure 3-4 Forward bias – Diode method

When the control command dictates the motor to rotate in the opposite direction, switches Q2 and Q3 turn ON and switches Q1 and Q4 turn OFF. Consequently, a negative voltage (-Vdc) will be applied across the terminals Vt. Thus, diodes D1 and D4 will be reversed biased and diodes D2 and D3 will conduct as shown in the Figure 3-5. It should be added that if the armature current has a non-zero value at the time of direction change command, then diodes D1 and D4 still continue to conduct till the applied negative voltage brings the current to zero and then diodes D1 and D4 turn OFF and diodes D2 and D3 turn ON to let the the armature current build up in the opposite direction ($i_{a\text{-reverse}}$ shown in the Figure 3-5). As shown in the Figure 3-5, armature current i_a changes direction but the direction of field current i_{field} remains the same in both conditions which is the whole point of the diode-method to generate negative torque in the series wound dc motor.

In a series wound motor the electromagnetic torque (Te) generated by motor is calculated by the following equation:

$$T_e = k\phi i_a \qquad (3\text{-}1)$$

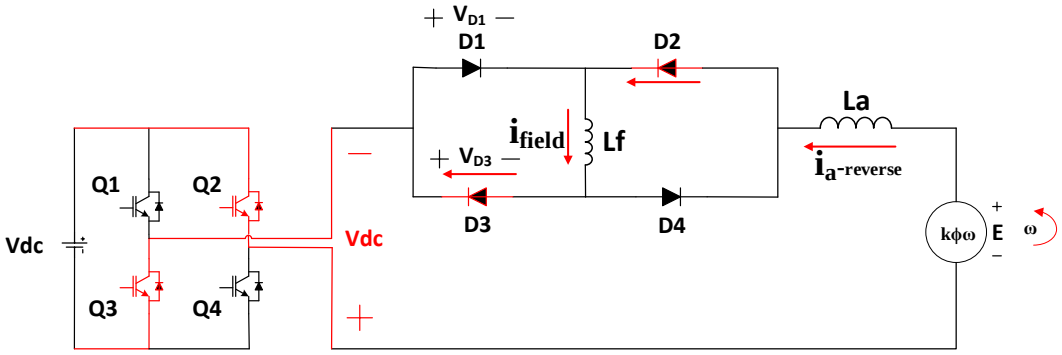

Figure 3-5 Reverse bias – Diode method

where k is the armature constant, ϕ is magnetic flux and i_a is the armature current. Armature constant is calculated based on the construction of the armature winding and is given in equation (3-2).

$$k = \frac{zp}{2\pi a} \qquad (3\text{-}2)$$

where z is the total number of conductors in the armature winding, p is number of poles and a is number of parallel paths. Magnetic flux itself relates to the field current i_f as in the equation (3-3).

$$\phi = k' i_f \qquad (3\text{-}3)$$

Replacing ϕ in equation (3-1) using equation (3-3) and considering that $i_f = |i_a|$, the following will result:

$$T_e = k k' i_f i_a \xrightarrow{k"=kk'} T_e = k" i_a |i_a| \qquad (3\text{-}4)$$

In the forward operation as shown in the Figure 3-4, ia is positive ($i_a>0$) and equation (3-3) yields $T_e = k" i_a^2$. However, switching to reverse operation (Figure 3-5) ($i_a<0$) will change the sign of electromagnetic torque and it will turn to $T_e = -k" i_a^2$ meaning the negative torque has been generated in the modified bi-directional series wound dc motor.

3.2.2 Characteristic Waveforms and Control Strategy

Due to the fact that the electromagnetic torque T_e has a constant value in the steady-state, a Proportional-Integral (PI) controller perfectly works to implement torque control for the proposed bi-directional series wound DC motor. Figure 3-6 shows the control block diagram along with the power circuit. The characteristic waveforms of the proposed bi-directional series motor with torque control have been shown in Figure 3-7. Reference torque T_e is calculated from i_a based on equation (3-1).

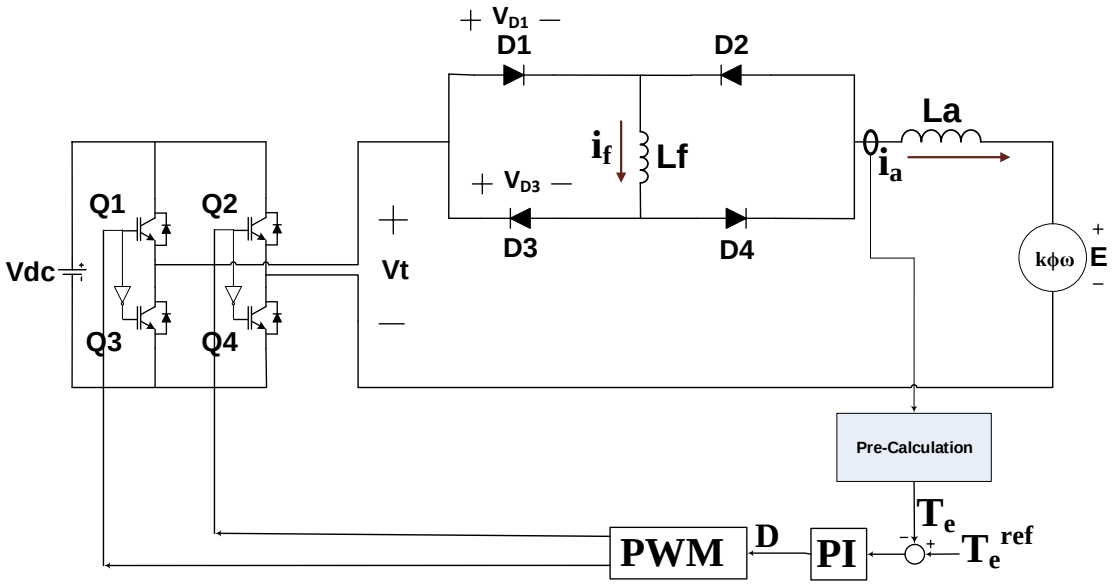

Figure 3-6 PI torque control of the proposed bidirectional motor – Diode method

Following the Figure 3-7, the ON/OFF status of the switches Q1, Q2, Q3 and Q4, and also diodes D1, D2, D3 and D4 within each interval have been explained. In Figure 3-7, $i_{a\,max}$, $i_{f\,max}$, and $i_{D\,max}$ are equal and are related to T^* by equation (3-1). Motor speed ω_m is related to torque T^* through the dynamic equation of rotor ($T^* = \frac{Jd\omega}{dt}$), where J is the inertia of the rotor.

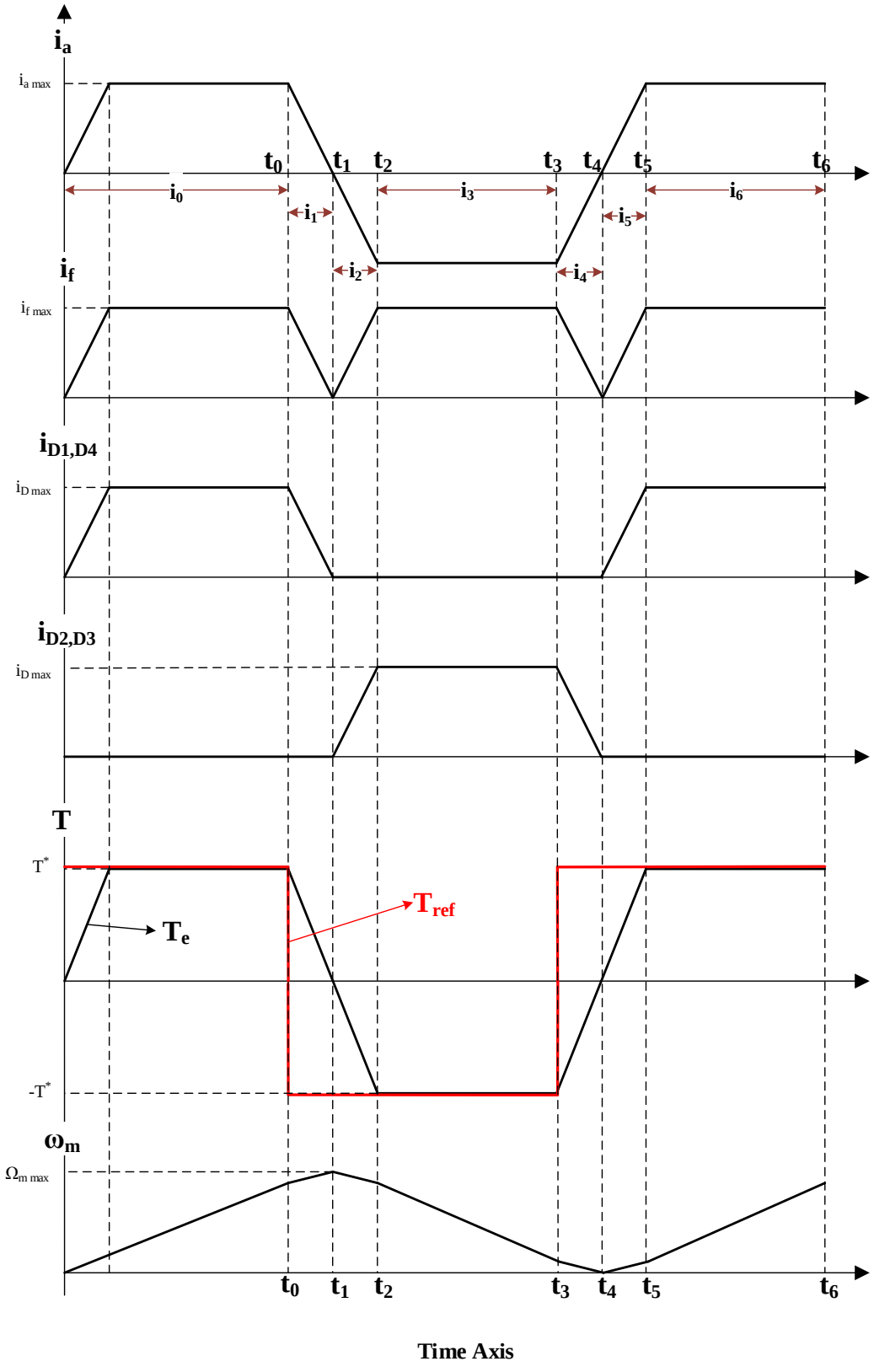

Figure 3-7 Switching waveforms – Diode method with torque control

$$interval\ i_0\ (0 - t_0): \begin{cases} i_a > 0, i_f > 0 \rightarrow T_e > 0 \\ T_{ref} > 0 \\ G1, G2, G3, G4 : PWM\ from\ PI\ Loop \\ D1, D4\ ON, \\ D2, D3\ OFF \end{cases}$$

$$interval\ i_1\ (t_0 - t_1): \begin{cases} i_a > 0, i_f > 0 \rightarrow T_e > 0 \\ T_{ref} < 0 \\ G1, G2, G3, G4 : PWM\ from\ PI\ Loop \\ D1, D4\ ON, \\ D2, D3\ OFF \end{cases}$$

$$interval\ i_2\ (t_1 - t_2): \begin{cases} i_a < 0, i_f > 0 \rightarrow T_e < 0 \\ T_{ref} < 0 \\ G1, G2, G3, G4 : PWM\ from\ PI\ Loop \\ D1, D4\ OFF, \\ D2, D3\ ON \end{cases}$$

$$interval\ i_3\ (t_2 - t_3): \begin{cases} i_a < 0, i_f > 0 \rightarrow T_e < 0 \\ T_{ref} < 0 \\ G1, G2, G3, G4 : PWM\ from\ PI\ Loop \\ D1, D4\ OFF, \\ D2, D3\ ON \end{cases}$$

$$interval\ i_4\ (t_3 - t_4): \begin{cases} i_a < 0, i_f > 0 \rightarrow T_e < 0 \\ T_{ref} > 0 \\ G1, G2, G3, G4 : PWM\ from\ PI\ Loop \\ D1, D4\ OFF, \\ D2, D3\ ON \end{cases}$$

$$interval\ i_5\ (t_4 - t_5): \begin{cases} i_a > 0, i_f > 0 \rightarrow T_e > 0 \\ T_{ref} > 0 \\ G1, G2, G3, G4 : PWM\ from\ PI\ Loop \\ D1, D4\ ON, \\ D2, D3\ OFF \end{cases}$$

$$interval\ i_6\ (t_5 - t_6): \begin{cases} i_a > 0, i_f > 0 \rightarrow T_e > 0 \\ T_{ref} > 0 \\ G1, G2, G3, G4 : PWM\ from\ PI\ Loop \\ D1, D4\ ON, \\ D2, D3\ OFF \end{cases}$$

3.3 Matlab/Simulink Simulations

As there is no torque sensor available in the experimental setup and only the armature current is sensed and fed back to DSP, the circuit of Figure 3-6 has been modified as in Figure 3-8 and have been used in both simulation and experiments. For the series wound motor the internal model available in the Simulink library has been used where 4 diodes have been added to the circuit of the motor. For the DC link a DC battery has been used. Diodes are simulated, taking into account the snubber resistant. Snubber resistors have been shown in parallel with the diodes, see Figure 3-9. The simulation parameters have been listed in Table 3-1. The parameters shown in Table 3-1 are for vacuum cleaner motor that has been used for practical implementation. Further in this chapter, it will be explained that the parameters have been measured experimentally. A 40V DC link has been used as a low DC link voltage in the standard range for haptic devices. Switching frequency was set to 20 kHz. First, it does not generate audible switching noise which is very useful for a desktop haptic device. Second, it provides large enough bandwidth and also smaller current ripple.

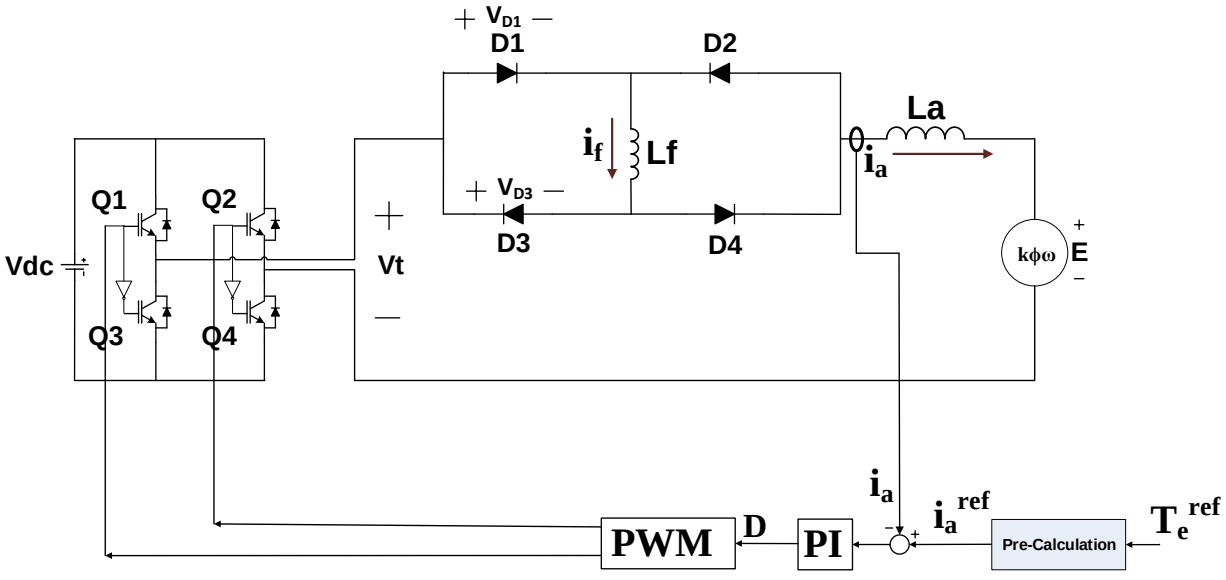

Figure 3-8 Armature current control of proposed bi-directional series motor based on diode-method

Table 3-1 Simulation Parameters

Parameter	Value
Switching Frequency	20 kHz
DC Link	40 V
Armature Resistance	5.45Ω
Field Resistance	1.618Ω
Armature Inductance	3.24mH
Field Inductance	9.33mH
Mutual Inductance	4.39mH
Total Inertia	0.0003 $kg.m^2$
Motor	Vacuum Cleaner

The parameters shown in Table 3-1 are for the vacuum cleaner motor that has been used for practical implementation. Further in this chapter will be explained that the parameters have been measured experimentally. A DC link of 40V has been used as low DC link voltage in the standard range for haptic devices. Switching frequency was set to 20 kHz. First it does not generate audible switching noise which is very useful for a desktop haptic device. Second it provides large enough bandwidth and also smaller current ripple.

Figure 3-9 Diode method with torque control – Matlab/Simulink simulation

3.3.1 Simulation Results

Matlab/Simulink simulations results for diode-method are presented in this section. As shown in Figures 3-10 to 3-17, the proposed method has successfully applied to the series motor and has changed the direction of rotation. Figure 3-10 is a quick capture of main variables all in one figure where the motor speed, armature current, field current, reference and actual torque, and voltage across bridge diodes D1 and D3 have all been depicted. The reference torque signal, the red dashed graph in Figure 3-11, has been used to examine the step response of both diode method and active bridge method. As shown in Figure 3-11, it is composed of three different values as follows:

- **Interval 1: from t=0 sec to t=1 ms:** pulse period: 1 ms, pulse magnitude: 0
- **Interval 2: from t=1 ms to t=3 ms:** pulse period: 2 ms, pulse magnitude: +0.03732 N.m
- **Interval 3: from t=3 ms to t=5 ms:** pulse period: 2 ms, pulse magnitude: -0.03732 N.m
- **Interval 4: from t=5 ms to t=7 ms:** pulse period: 2 ms, pulse magnitude: +0.04665 N.m

During the interval 1, the reference torque equals to zero (Figure 3-11) and the average torque should be controlled at zero, hence, the speed should not change from zero in this interval, see Figure 3-15. At t=1ms, a positive reference torque with the magnitude of 0.03732 N.m is applied. This value corresponds to armature current of 2A which is the nominal current of the vacuum cleaner motor which has been used in experiments. So, the magnitude of the step torque has been calculated based on the current capacity and has been used in simulations. Upon applying the torque step at t=1 ms, proposed diode-method has been able to generate desired torque in less than 800 us, see Figure 3-11. It can be seen from Figure 3-10 and Figure 3-15 that due to the positive torque generated in interval 2, the speed increases through the interval reaching approximately to 0.2 rad/s at t=3 ms.

At t=3ms, a negative reference torque with the magnitude of -0.03732 N.m is applied. Therefore, at this moment, the proposed bidirectional series motor should be able to switch from

a positive torque of +0.03732 N.m in interval 2 to a negative torque of -0.03732 N.m in the interval 3. Figure 3-11 clearly shows the successful negative torque generation of the motor where the motor has tracked the set-point torque in less than 400 us.

At t=5ms, the reference torque jumps from -0.03732 N.m to +0.04665 N.m. Therefore, here the direction change is tested in interval 4, whereas in interval 1 the positive reference torque (+0.03732 N.m) only accelerated the motor from zero speed.

In Figure 3-12 and Figure 3-13, it can be seen that the armature current reverses as fast as less than 400 microseconds. Figure 3-14 illustrates how the utilization of Diode Bridge rectifies the armature current into a unidirectional field current which flows though the field winding only in one direction, from top to the bottom as in Figure 3-6. Figure 3-16 shows the modulating output voltage of the H-bridge. Figures 3-17 and 3-18, show the blocking voltage across diodes D_1 and D_3 and no deteriorating voltage spikes can be seen across the diodes at the transient instants. The voltage across D_4 equals to V_{D1} and also V_{D2} looks exactly the same as V_{D3}. Therefore, only V_{D1} and V_{D3} have been shown.

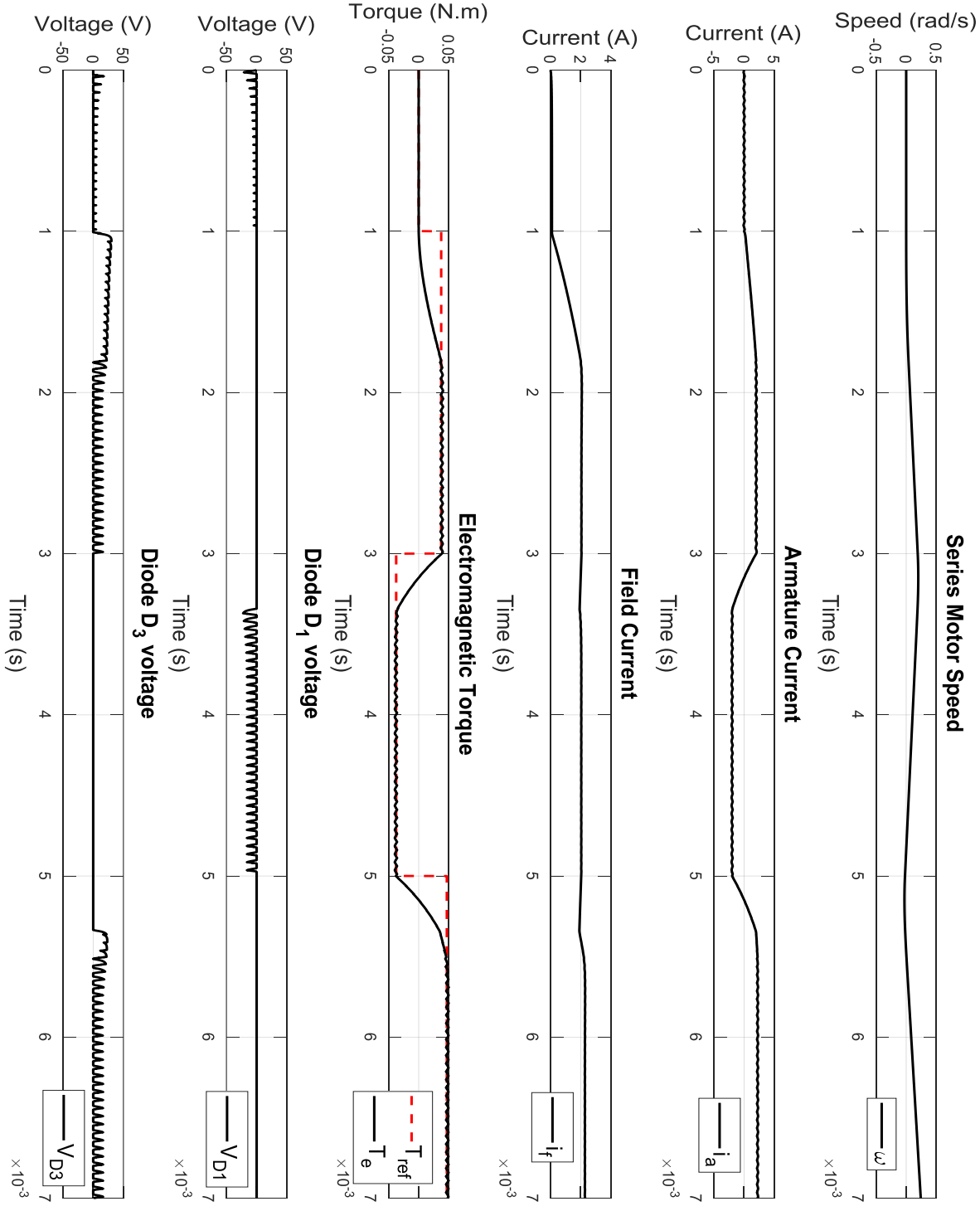

Figure 3-10 Simulation results; Diode method with torque control

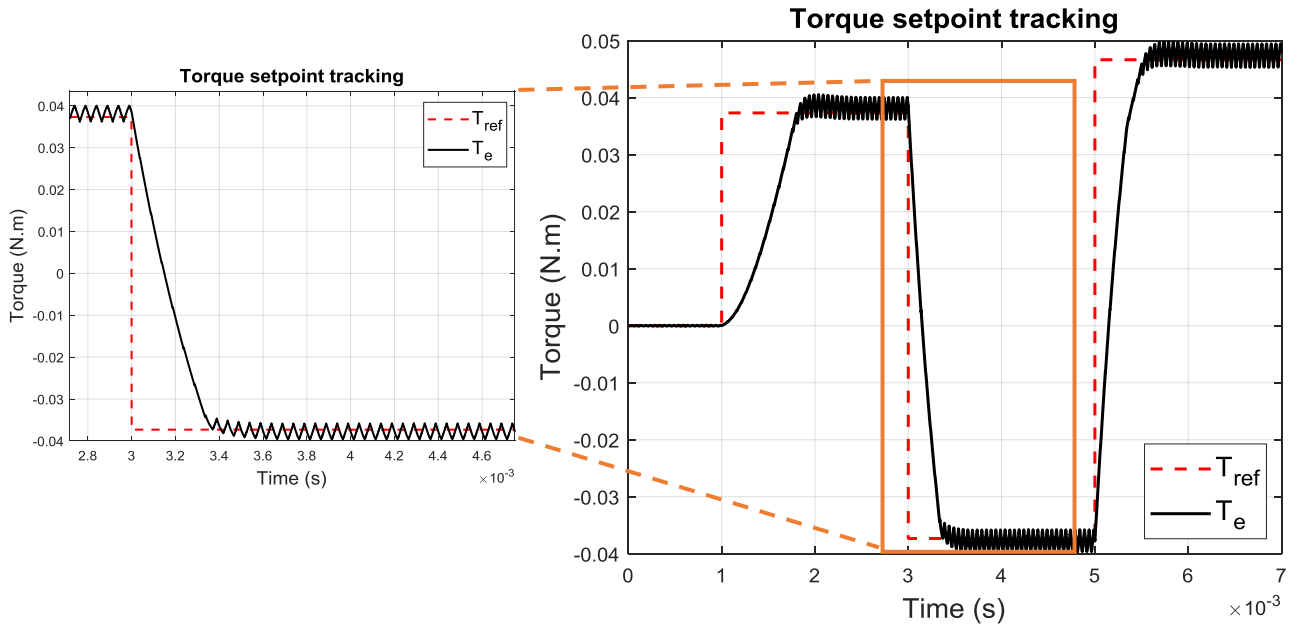

Figure 3-11 Torque setpoint tracking

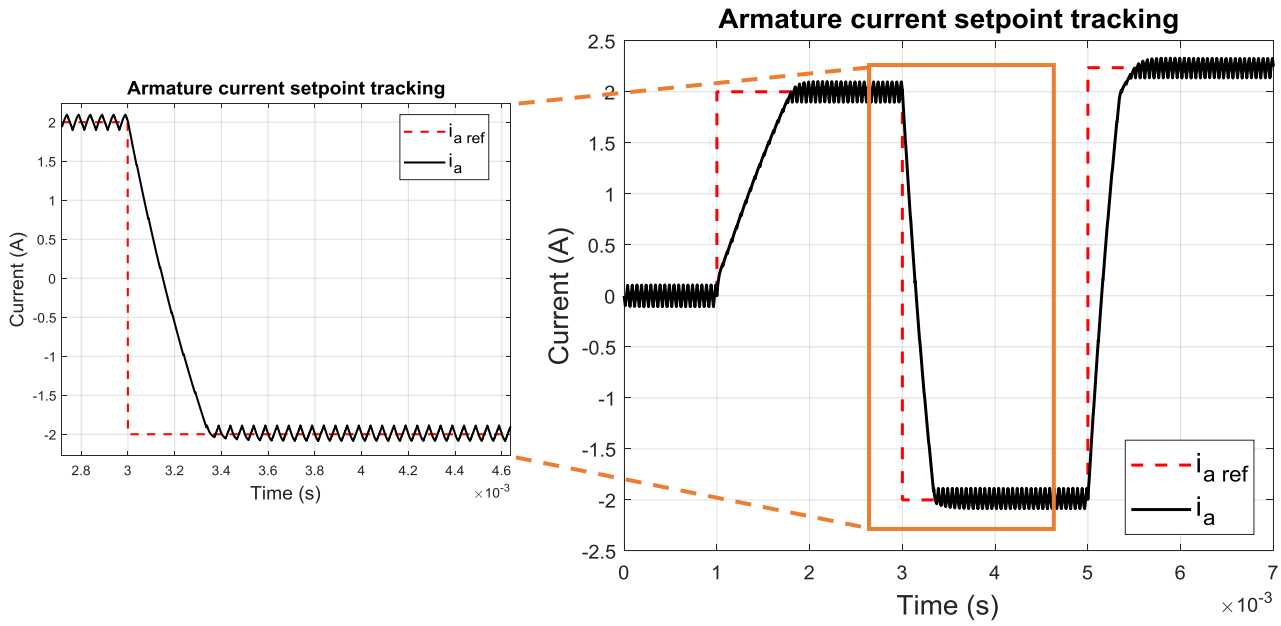

Figure 3-12 Armature current setpoint tracking – Diode method

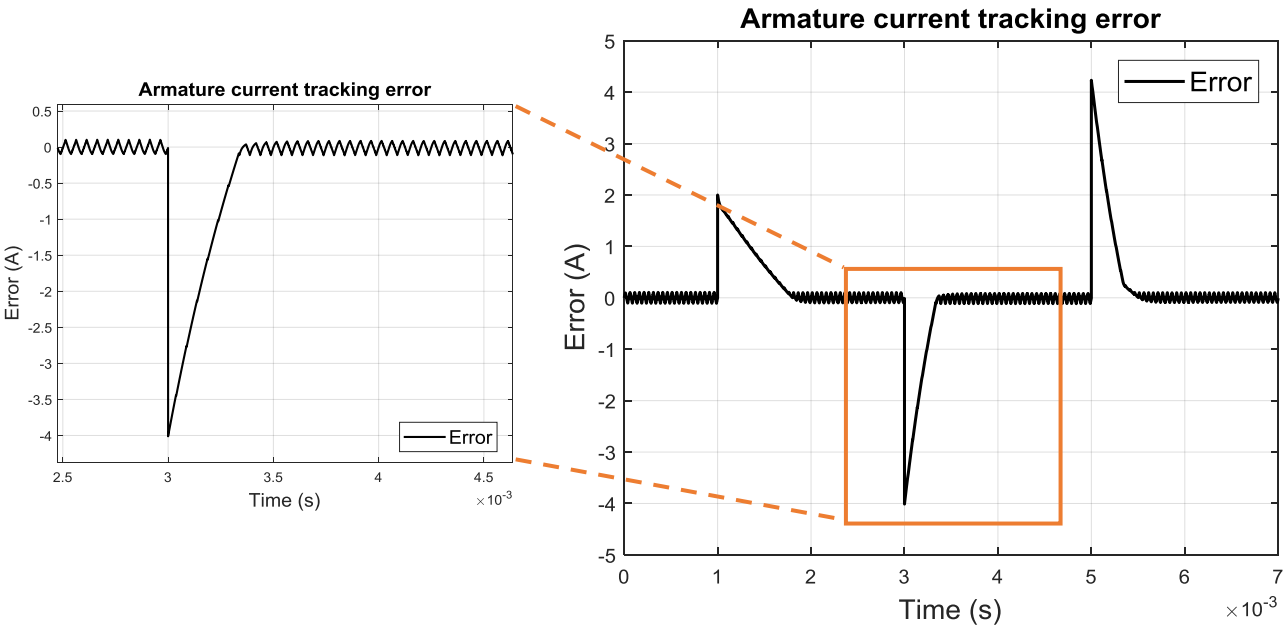

Figure 3-13 Armature current tracking error – Diode method

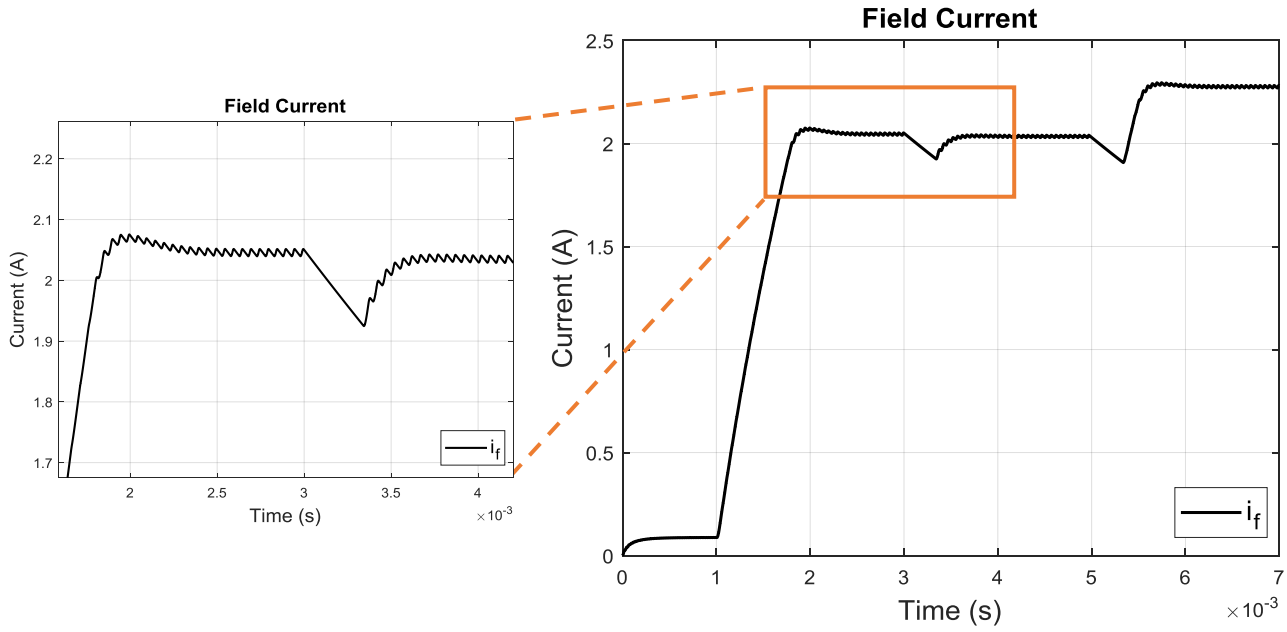

Figure 3-14 Field current – Diode method

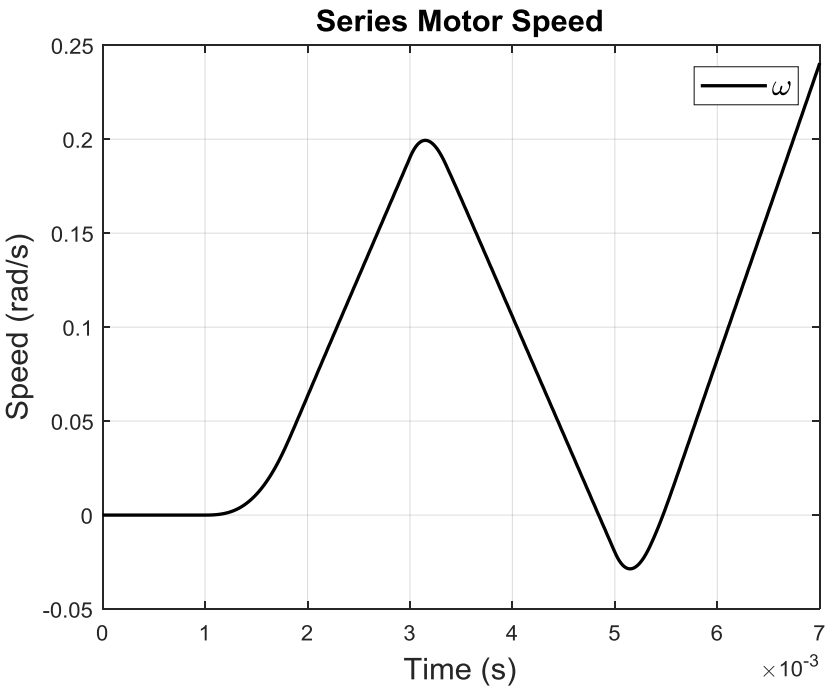

Figure 3-15 Motor speed – Diode method – ω_m

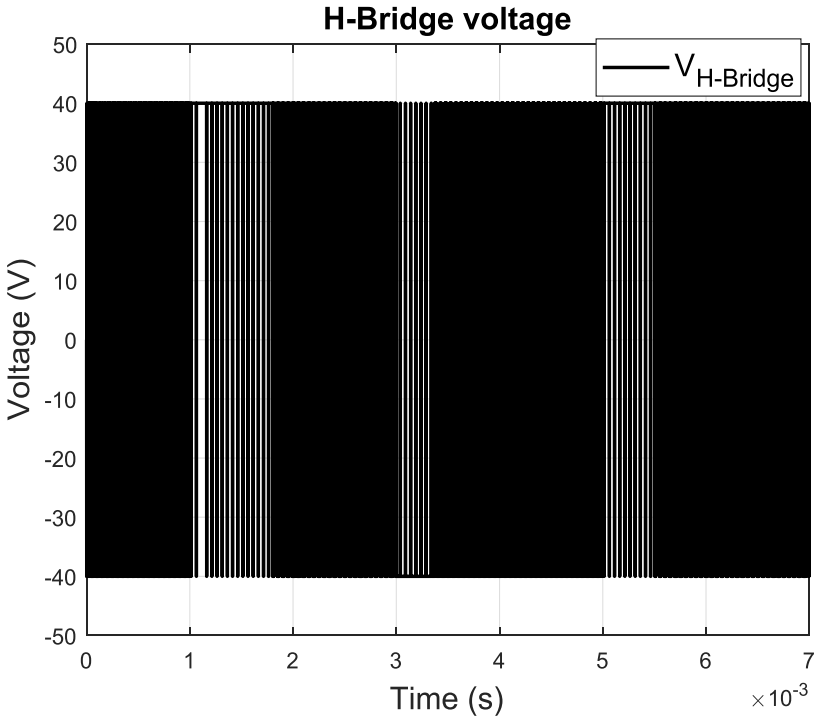

Figure 3-16 Modulating output voltage of H-Bridge

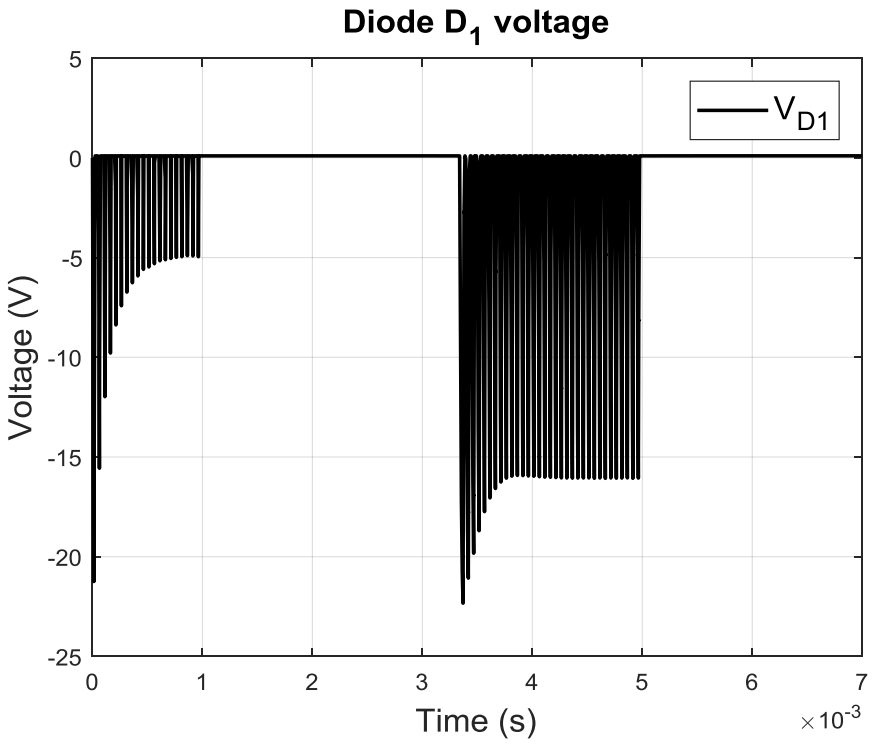

Figure 3-17 Voltage across diode D_1

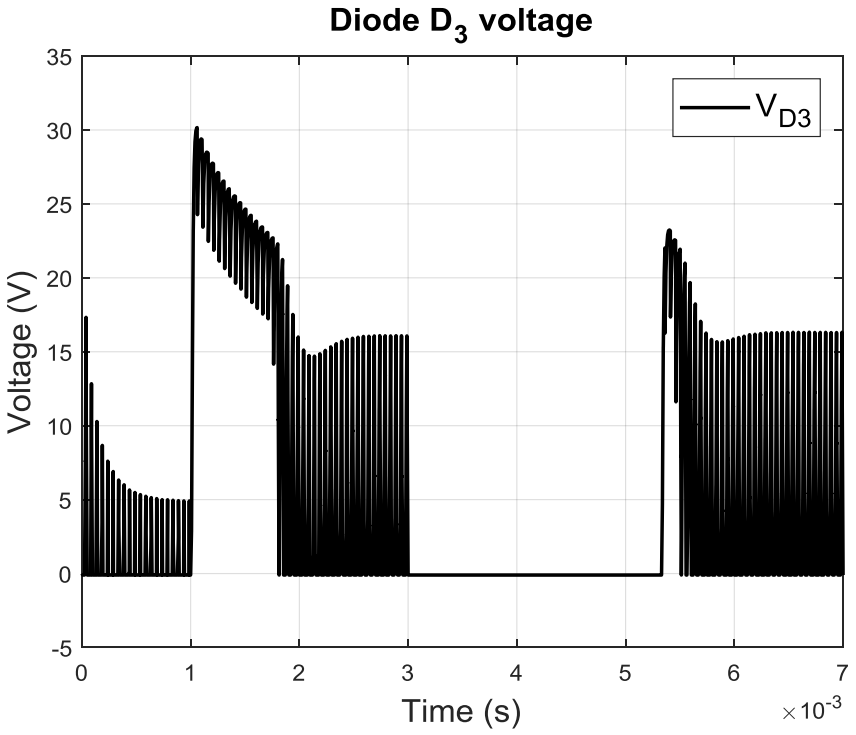

Figure 3-18 Voltage across diode D_3

3.4 Advantages and disadvantages of the diode method

In the diode method, beside 4 active switches in the H-bridge, see Figure 3-3, no more active switches is used in the topology. Compared to the active-bridge which is going to be explained in detail in chapter 4, the diode method uses only 4 diodes in the bridge whereas the active bridge needs 4 AC switches which is composed of 8 discrete active switches. This feature is very interesting and promising in terms of implementation. Less number of switches also leads to less number of isolated gate drivers which decreases the complexity of the design significantly. Hence, clearly the cost of the design in the diode method will be less than that of the active-bridge method. Moreover, no current zero crossing detection is needed for the diode method as opposed to the active-bridge method leading to simpler design and less computational burden. However, there are some applications in which there is a need to generate negative torque such as electrical braking in universal motors. In such applications, the diode-method cannot be applied. The reason is that in those applications where the current is AC, the diode-bridge will periodically generate negative torque in series motor without even braking command from the upper hand controller. This periodic braking will eventually result in a zero average torque on the shaft. In other words, there will be no way to control the average torque of the series motor nor the speed/position. To better illustrate this issue, a Matlab/Simulink simulation was carried out, see Figure 3-19. In this simulation, the series motor with diode-bridge is only supplied with an ideal ac source.

As can be seen in Figure 3-20 , the average electrical torque T_e is zero. In other words, using a diode bridge will uncontrollably reverses the torque every half cycle of the AC source. This will lead to an alternating speed as shown in the Figure 3-20 which is not desirable. Therefore, the diode method cannot be applied for electrical brake applications in universal motors. Later in Chapter 4, it will be shown that to solve the issue of unwanted torque reversals stated above, diodes have to be replaced with controllable active switches where can be gated at a certain time upon the control command to generate negative torque and stay inactive where they are not supposed to change the direction of rotation.

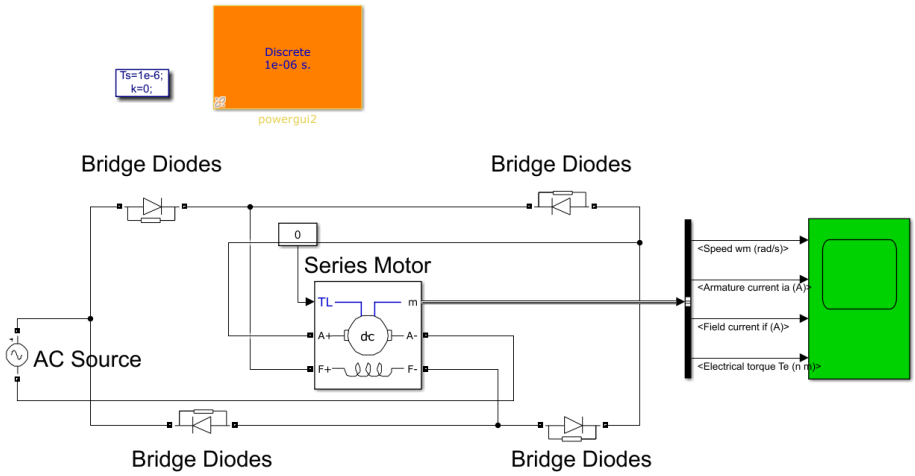

Figure 3-19 Matlab/Simulink simulation

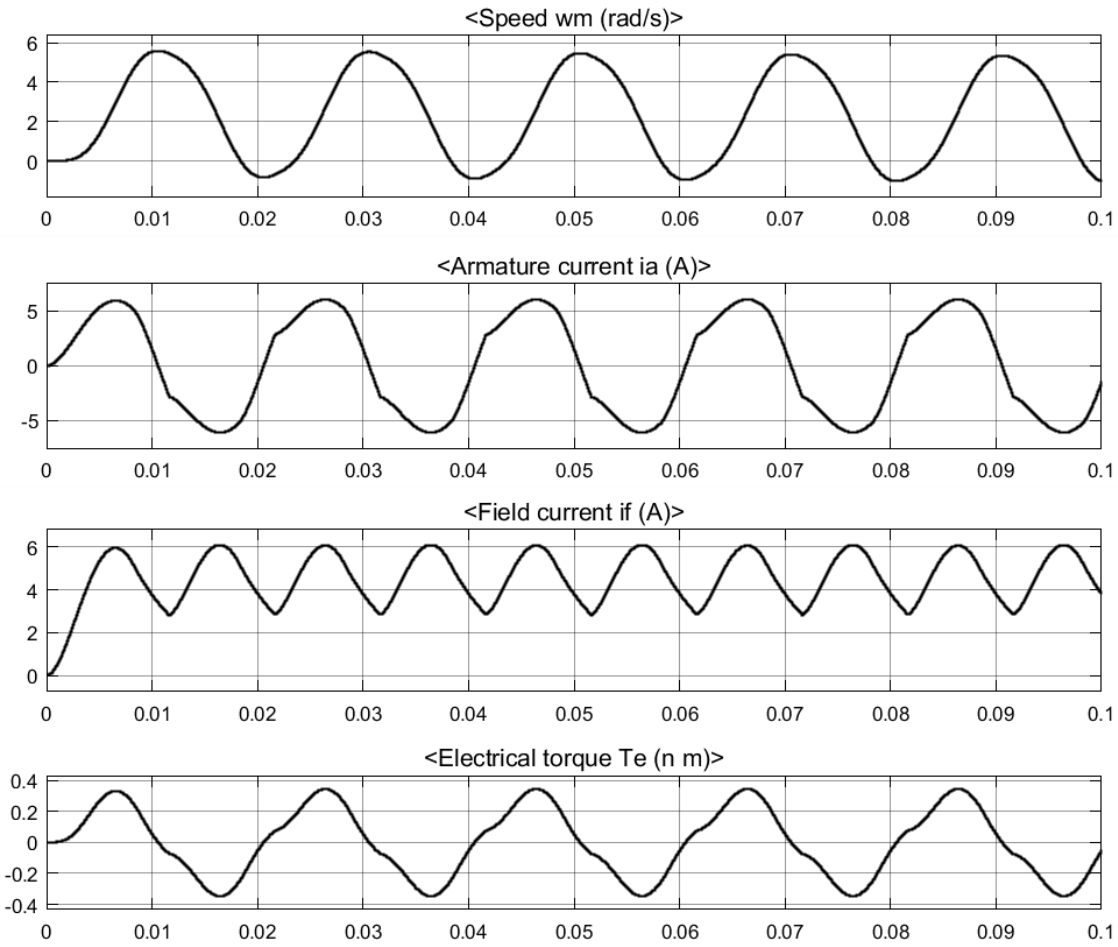

Figure 3-20 AC supply simulation results – from top to bottom – ω_m, i_a, i_f, T_e

3.5 Experimental Work

To verify functionality of the proposed bidirectional series wound motor, I built and developed a prototype experimental setup in ePOWER lab. In this section, different parts of the setup will be explained as follows.

3.5.1 Test Setup

Figure 3-21shows the overall assembly of the setup. The experimental setup consists of a DSP board, H-bridge, diode bridge and a series motor. For measurements and data visualization, a differential voltage meter (ADP305), a current probe (CP015) both from Lecroy, and a digital oscilloscope from Lecroy have been used. For digital implementation of the PI controller a 32-bit floating point TMS320F28335 digital signal processor (DSP) from Texas Instruments has been used, see Figure 3-22.

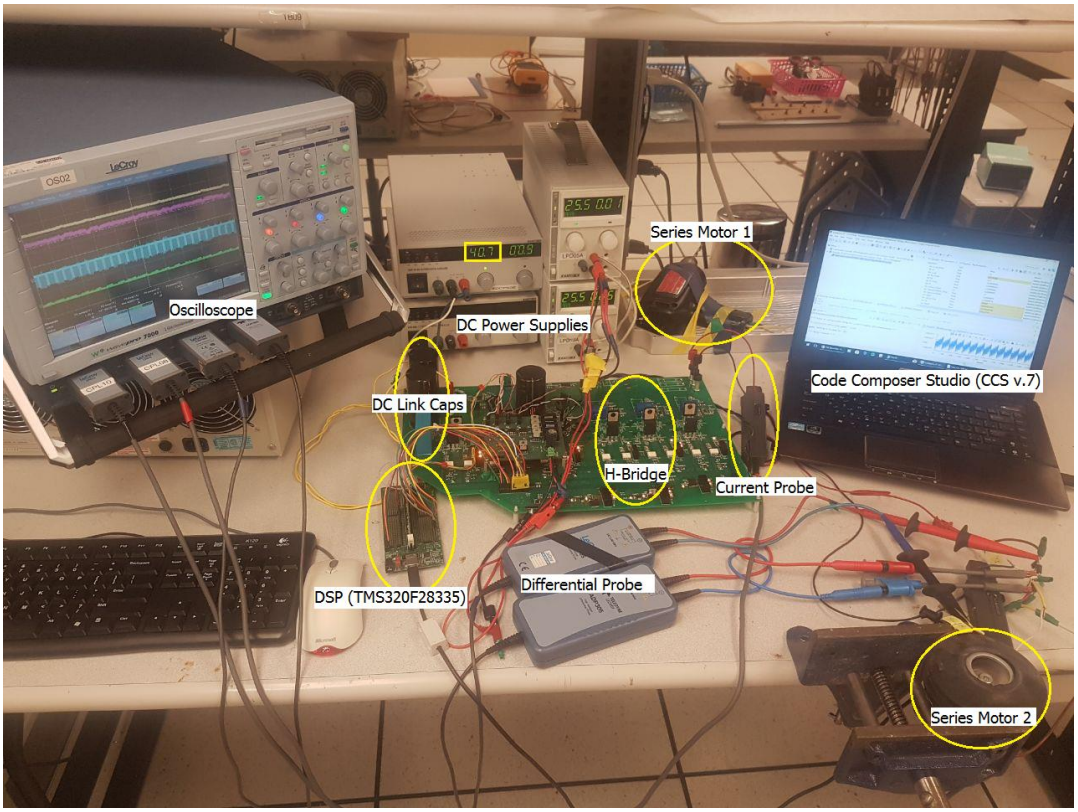

Figure 3-21 Experimental setup

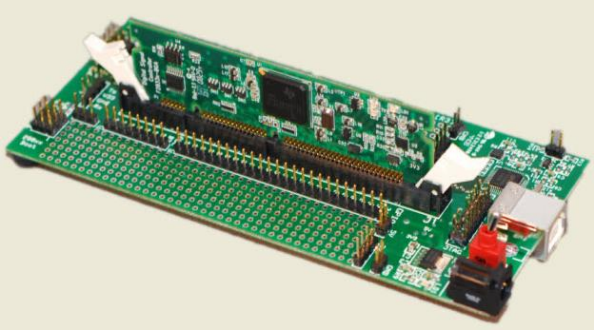

Figure 3-22 Texas Instrument 32-bit DSP – TMS320F28335

Figure 3-23 shows the switching PCB designed for the implementation of the switching H-bridge. This board was designed for multipurpose use, so it could also be used for other projects in the ePOWER lab. The switching PCB, it is a 9-level inverter that I developed in ePOWER and presented at the EPE2017 conference. The inverter can be used as a three-leg three-phase inverter, as a single phase inverter or an H-bridge. All can be used in a grid-tie application as well due to the grid voltage sensing that has been integrated in the design of the PCB. For the grid voltage sensor an ACNT-H790-000E from Avago Technologies was used which is basically an isolated Opto Amplifier Voltage Sensor. This sensor features 1% gain accuracy and its input voltage range can vary from -0.2V to 0.2V.

This board is also equipped with an isolated DC link voltage sensor aimed for grid tie and solar applications. An ACPLC87A000E isolated Opto Amplifier Voltage Sensor which is specifically designed to sense DC Link voltage in different applications. Selected features of this IC (Integrated Circuit) are high input voltage range which can be any value between 0 to 2V, 1% gain accuracy, and a maximum of 0.1% non-linearity. Both grid and DC link voltage sensors along with the signal conditioning circuits have been marked on Figure 3-23. Details of the signal conditioning circuits for these two sensors can be found in [78].

To sense the output current of the H-bridge, a CAS-15NP Hall Effect current sensor from LEM has been used which has been marked on Figure 3-23. The primary nominal current of the

sensors is up to 15A. The output of this sensor is voltage and has a 2.5Voffset at zero current. The output of the current sensor has to go through a signal conditioning circuit that is for scaling and filtering. Figure 3-24 shows the signal conditioning circuit used for current measurements. The output signal of the signal conditioning circuit, V_{out} in Figure 3-24, is then clamped to DSP supply voltage (3.3V) via a Clamp Array IC (TL7726 – Texas Instruments). The clamped voltage is connected to the ADC (Analog to Digital Converter) pins of the DSP via Connector 1 shown on Figure 3-23.

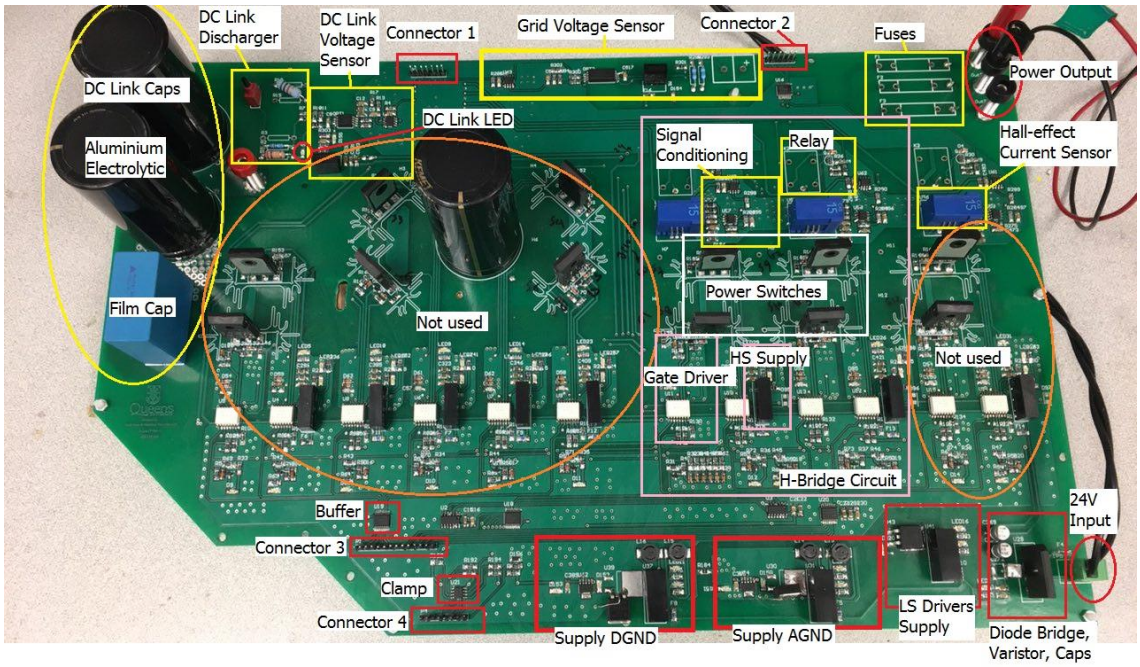

Figure 3-23 Switching PCB, H-bridge

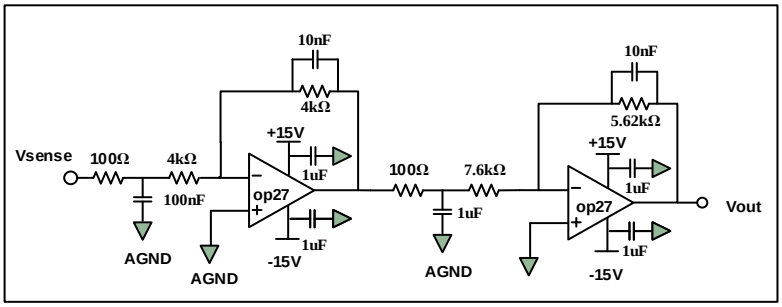

Figure 3-24 Current signal conditioning circuit

Power switches are 15A IGBTs from Infenion (IKW15N120H3 – high speed switching series third generation). Features include very low V_{CEsat}, low EMI, and very soft, fast recovery anti-parallel diode. The Input capacitance (C_{iss}) of only 875 pF makes the switching of these IGBTs faster with less gate drive current for the gate charge. To drive the IGBTs, isolated drivers have been designed for high-side (HS) and low-side (LS) complementary switches in each leg of the H-bridge. Therefore, four 2.5 Amp gate drive optocoupler from Avago Technologies (ACPL-336J) have been used. This fast driver features rail-to-rail output voltage, 250 ns propagation delay, and 30 kV/us CMRR. On top of all, it comes with the integrated fail-safe IGBT protection both for Desaturation Detection and Under Voltage Lockout (UVLO) protection. These protection signals have been fedback to DSP and the fault detection submodule of the microcontroller (Trip-Zone) have been programmed to shut the gates off in case of fault occurrence.

Two supply voltages have been used to turn IGBTs on and off that are +15V and -5V, respectively. High side (HS) switches in the leg need to be supplied with isolated voltage supplies, whereas the low side (LS) switches can share a common supply voltage as they share a common emitter. Thus, a 1 Watt isolated DC/DC converter from XPPOWER (IA2415S) has been used to drive each of the HS switches, shown as HS Supply in Figure 3-23. In addition a 3 Watt isolated DC/DC converter from XPPOWER (IP2415S) has been used to drive the LS switches.

All of the supply voltages are generated from a common standard 24V DC that is generated by the DC power supply available in the ePOWER Lab. The circuit, shown in Figure 3-25, has been designed to protect all the power supplies and parts that are fed by +24 V DC. This circuit includes overcurrent protection (via Fuse), overvoltage protection (via Varistor), and polarity protection (via Diode Bridge).

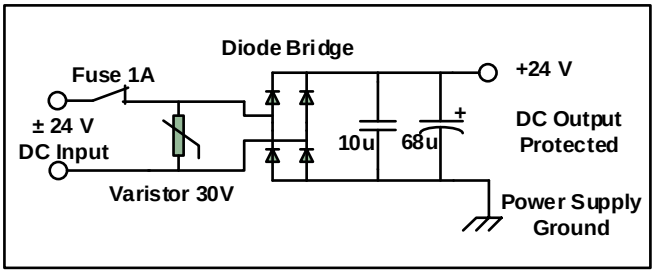

Figure 3-25 Input voltage protection circuit

The board also comes with the option of DC Link discharger, composed of a push-button switch and a power dissipating resistor (3W carbon wire resistor). An LED is used to show if the DC Link capacitors are charged. Pushing the button will discharge the capacitors in the order of seconds, when the main DC supply to the DC link is disconnected. This option will is very useful in the test and debug stage especially when the DC link capacitors frequently need to be charged and discharged. Four ultra-fast 25 ns reverse recovery diodes (MUR460) from ON Semiconductor have been used for the diode bridge.

In the design of PCB layout, several practical considerations have been applied. Placement of the components especially the switching parts have been carried out with minimal coupling. Isolated ground planes and clearances have all been strictly considered to minimize switching noise, EMI, cross-talk and maximize the clean performance of the switching PCB in a wide range of operating points in terms of Voltage, Current, Frequency. Figure 3-26 and Figure 3-27 illustrate the top and bottom sides of the two-layer PCB.

As it can be seen analog and digital grounds (AGND and DGND) do not have overlaps and DGND polygon is spread over the bottom of the PCB whereas the AGND lays on the top. DC Link is composed of two parallel 820uF 350V Aluminum Electrolyte capacitors from KEMET (ALC10A821EH350) which are low ESR (Equivalent Series Resistor) with very long life capable of high ripple currents. A 10uF film capacitor is also in parallel with electrolyte capacitors to filter high frequency ripples across the DC Bus and hence the H-Bridge.

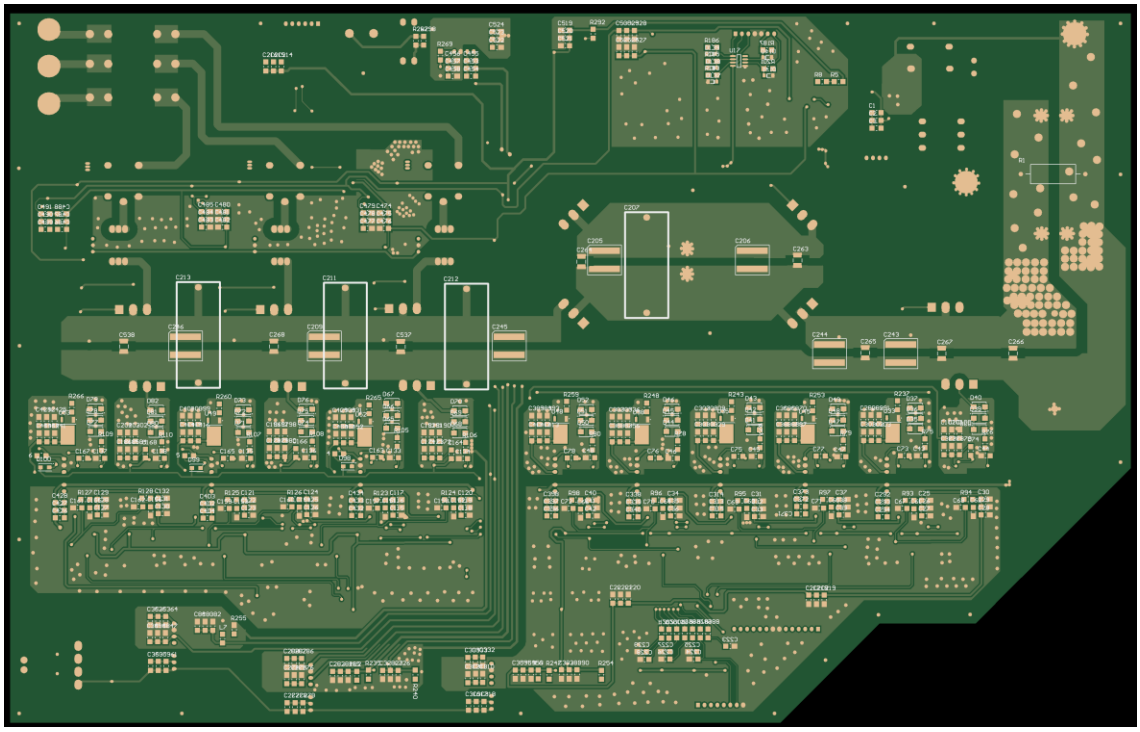

Figure 3-26 Top side

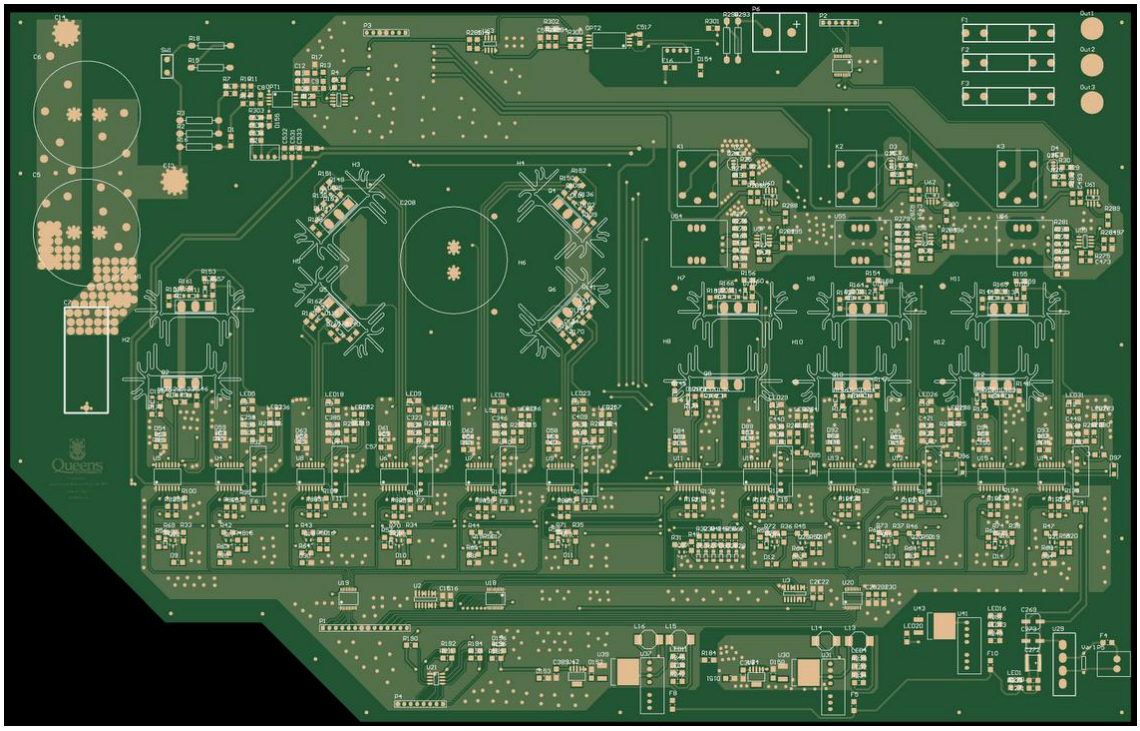

Figure 3-27 Bottom side

3.5.2 Experimental Test

As the setup was explained in the previous section, there is no torque sensor available in the experimental prototype setup. In fact, torque sensors are not common in practical implementations for torque control applications. Therefore instead, a related variable, typically current, is measured for torque control, as in FOC (Field Oriented Control) and DTC (Direct Torque Control) methods that are widely used in drive applications [71, 73]. As shown earlier, Figure 3-8 presents the armature current control of motor.

Two test motors were used to carry on the experiments both dismantled from a drill and a vacuum cleaner, respectively. Table 3-2 summarizes the motor parameters. As mentioned earlier, the parameters of Series motor 2 have been used in simulations. Field and armature resistance and inductance was measured by an Agilent 4294 Precision Impedance Analyzer, see Figure 3-28. However, no data is available for the armature constant so to precisely convert the reference torque into its equivalent reference armature current. Thus, to carry out this experiment, the armature current is directly controlled. Also, no speed sensor (encoder, resolver, tacho-generator) is integrated into the setup.

With the equipment and options available in the setup, it is only possible to verify functionality of the proposed method through measurement of armature and field current and analysis. As shown in simulation Figures 3-10 and 3-11, armature current changes polarity at the instant of torque reversal while the field current remains positive and does not change polarity the entire time but it goes to zero and rises again to its previous value before the torque reversal command. In other words, based on equation (3-4) ($T_e = kk'i_f i_a$), having measured i_f and i_a we can prove that whether torque T_e changes sign after torque reversal command or not. In the following the results of the armature current control (torque control) is reported.

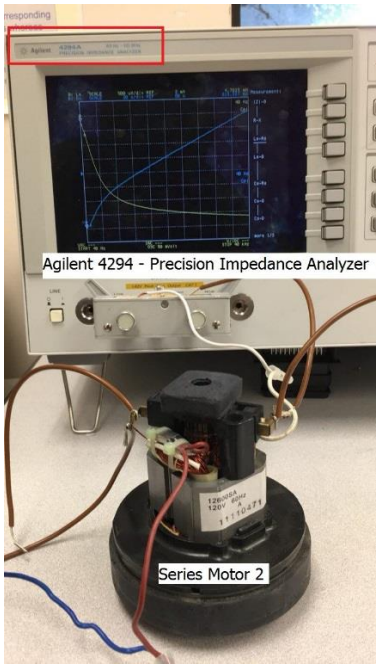

Figure 3-28 Precision Impedance Analyzer used to measure motor parameters

Table 3-2 Test motor parameters

Test Motors	Application	Voltage, Current	R_a	L_a	R_f	L_f	L_M
Series Motor 1	Drill	120V/60Hz, 2.5A	11Ω	28mH	5.72Ω	28mH	22.4mH
Series Motor 2	Vacuum Cleaner	120V/60Hz, 2A	5.45Ω	3.24mH	1.618Ω	9.33mH	4.39mH

3.5.3 Experimental Results

3.5.3.1 Step Change In Reference Current from -1.7A (Reverse) to +2A (Forward) – Series Motor 1

Using Series Motor 1 as the test motor, a step change in armature current is commanded (-1.7A → +2A). DC link voltage is set to 70V when using series motor 1. Figure 3-29 shows the experimental results. Prior to the instant of the torque reversal command, motor is in backward rotation and a negative (reverse) current is flowing into the armature winding equal to -1.7A (Red/Second graph). At the same time the field current is equal to armature current but with the opposite sign, i.e., +1.7A (Orange/First graph). Therefore, according to equation (3-4), T_e is negative prior to reversal command. But after the torque reversal command marked on the figure, armature current changes sign while the filed current sign remained unchanged. After the transient state, i_a and i_f are equally settled into the new set-point value that is +2A. Again, according to equation (3-4), after the transient, T_e is positive.

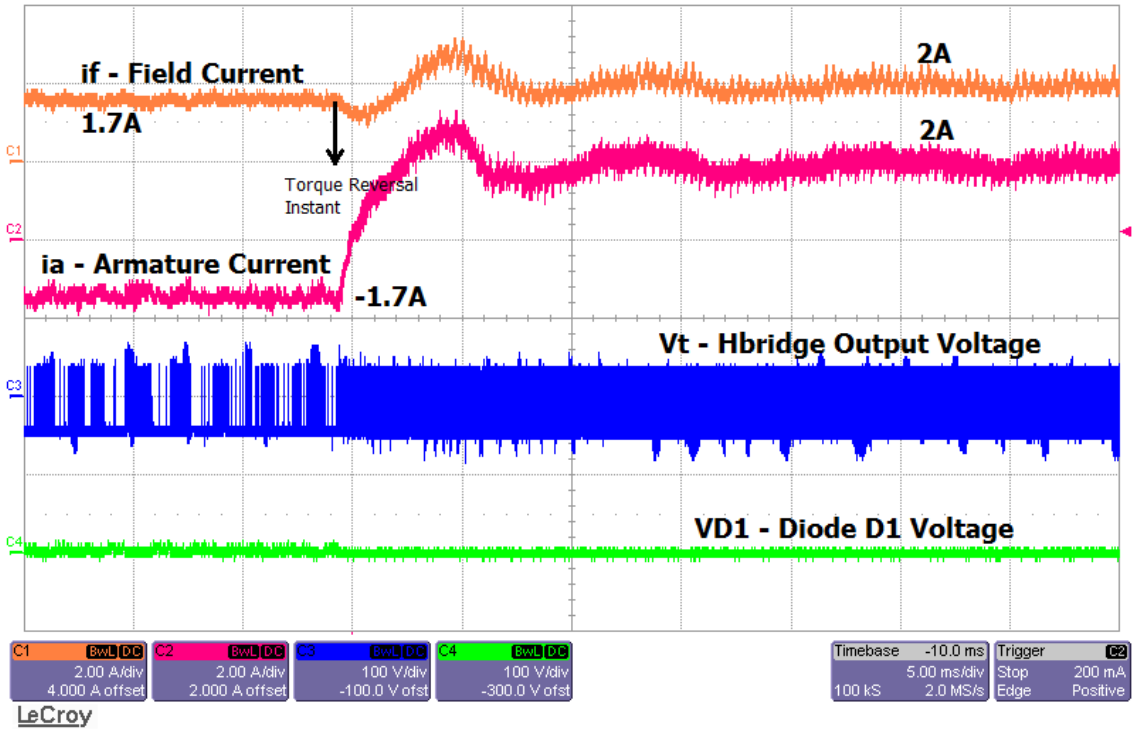

Figure 3-29 Experimental results – armature current step response – Drill Motor

3.5.3.2 Step Change In Reference Current from -1.3A (Reverse) to +2A (Forward) – Series Motor 2

In another test using Series Motor 2 as the test motor, a step change in armature current is commanded (-1.3A → +2A). DC link voltage is set to 40V when using series motor 2. It can be seen from Figure 3-30 that the diode-method has been successfully worked out in practice. The first graph from top on Figure 3-30 shows the field current which has remained positive before and after transient step change in armature current. The second graph from top on Figure 3-30 shows the armature current which is controlled to reverse the electromagnetic torque generated by the motor. The armature current has been settled to the new set-point (+2A) in less than 7 milliseconds with an overshoot of less than 30%. No deteriorating spikes can be seen in the voltage across the bridge diode as well.

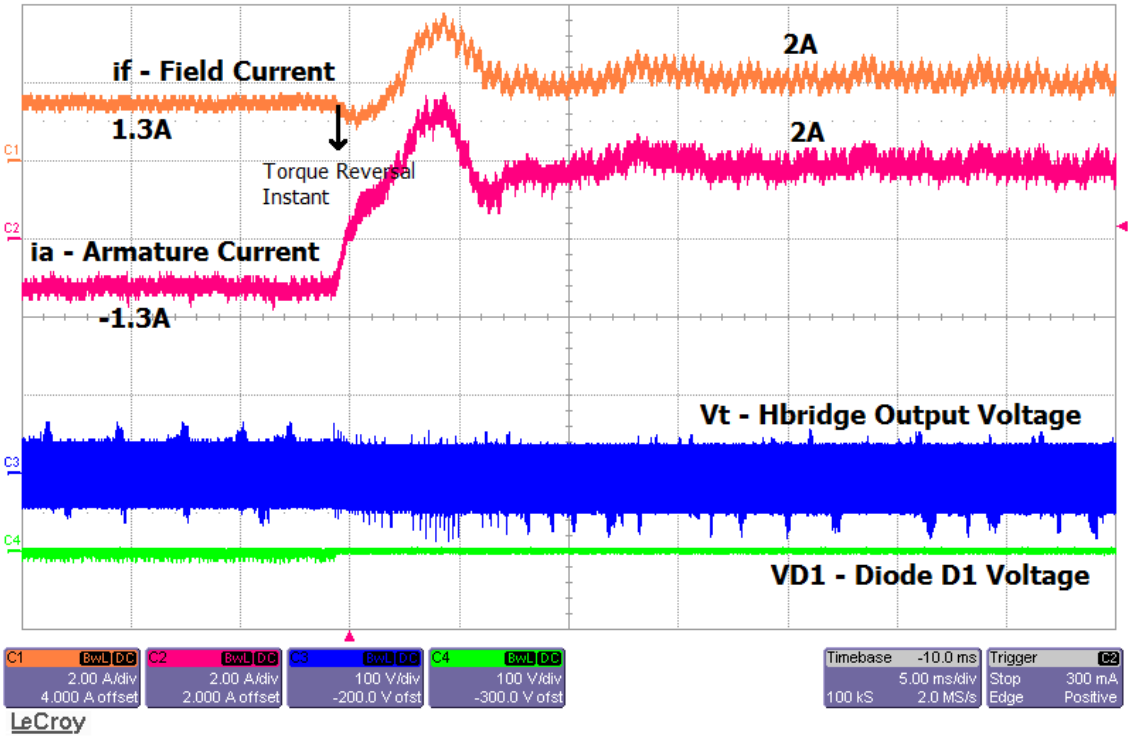

Figure 3-30 Experimental results – armature current step response – Vacuum Cleaner Motor

3.5.3.3 Step Change In Reference Current from +1.7A (Forward) to -1.3A (Reverse) – Series Motor 2

Using Series Motor 2 as the test motor, a step change in armature current is commanded this time from +1.7A to -1.3A (+1.7A → -1.3A). DC link voltage is set to 40V. Figure 3-31 shows the experimental results for this test. Likewise the previous test, the functionality of the diode-method in reversing the torque (armature current) has been tested and verified but this time from a positive current (forward) to a negative current (reverse). As seen in Figure 3-31, armature current has been controlled to track the new set-point (-1.3A) in less than 5 milliseconds with an overshoot of less than 10%. No damaging voltage spikes are generated across the diode, and the field current preserves the positive sign before and after transient state.

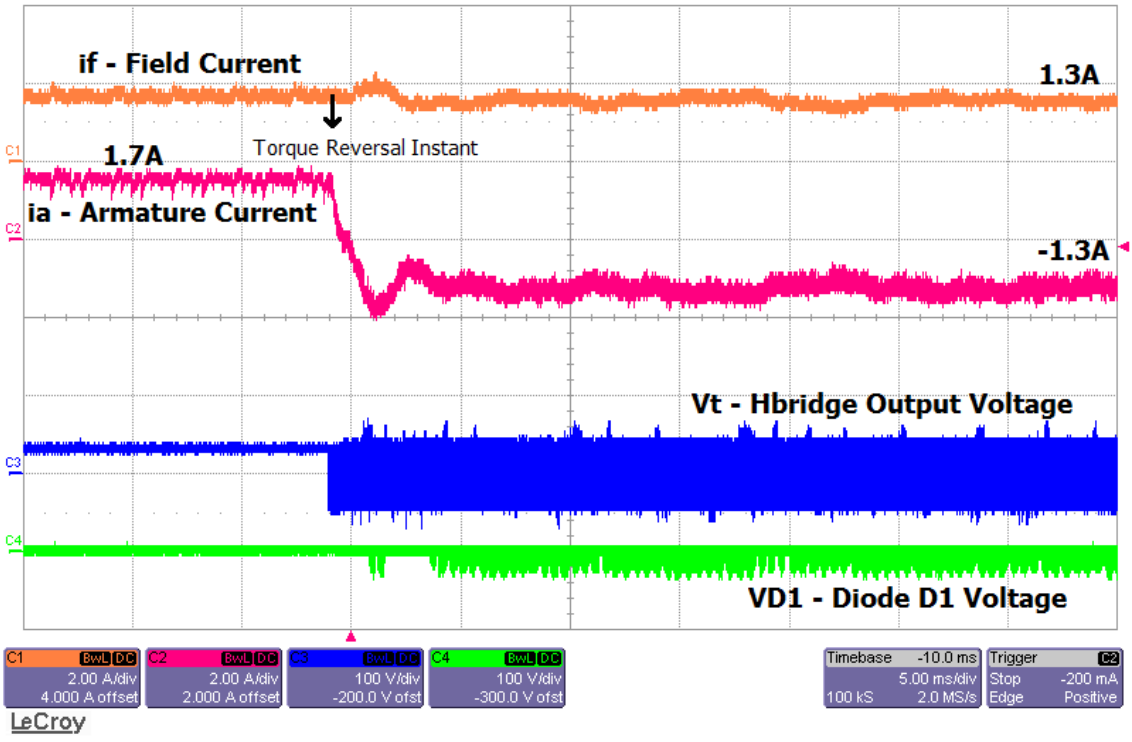

Figure 3-31 Experimental results – armature current step response – Vacuum Cleaner Motor

3.5.3.4 Steady State Waveforms for Armature Reference Current +2A

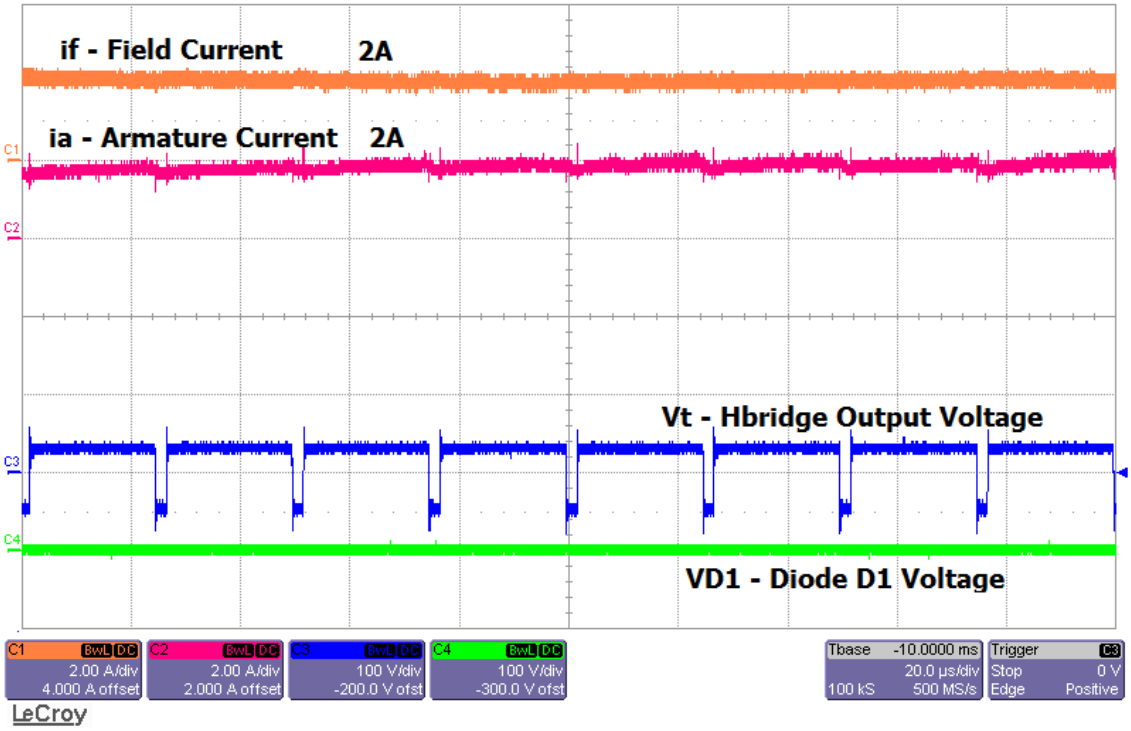

Figure 3-32 Experimental results – steady state – Vacuum Cleaner Motor

3.5.3.5 Steady State Waveforms for Armature Reference Current -1.6A

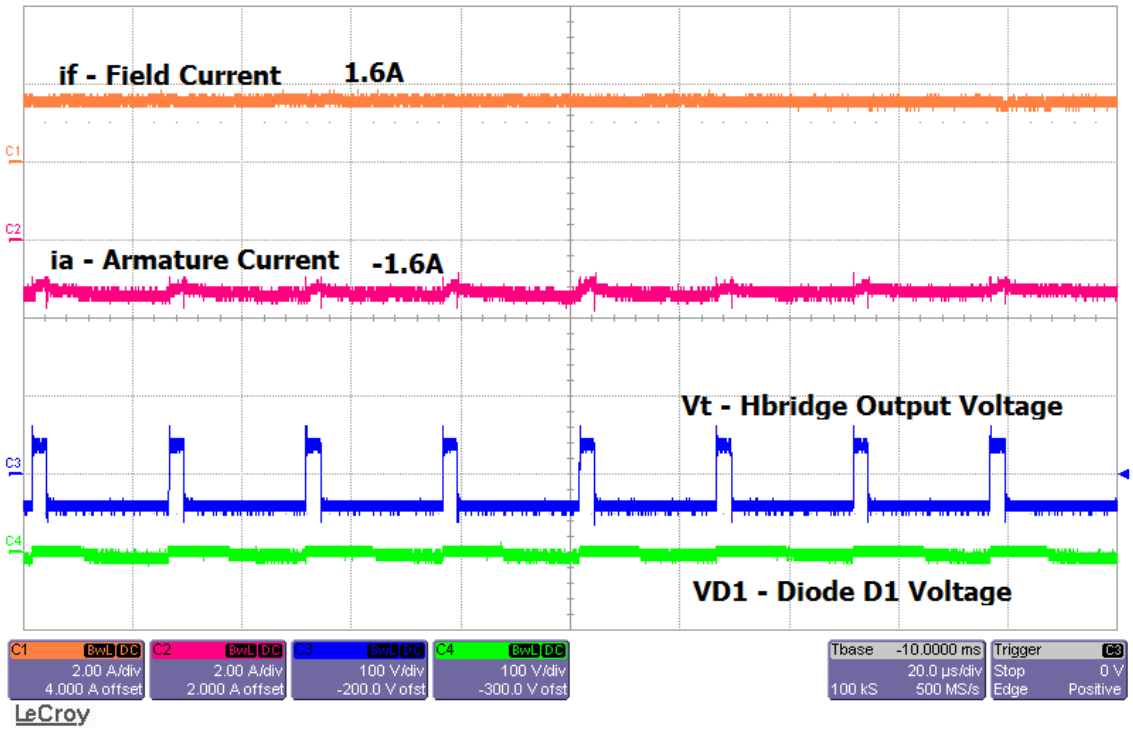

Figure 3-33 Experimental results – steady state – Vacuum Cleaner Motor

Figure 3-32 shows a smaller window (zoomed version) of the measured variables (field current, armature current, H-bridge output voltage, and diode D1 voltage) in the steady-state where the set-point armature current is at +1A. The field current is also at +1A that together with a +1A controlled armature current generates a positive torque leading to forward rotation of the rotor. However, in an opposite situation in Figure 3-33 the armature current is controlled at -1A and together with a +1A field current generates a negative torque leading to backward (reverse) rotation of the rotor.

Chapter 4

Generalized Torque Reversal Method:

Active Bridge Method

4.1 Proposed active-bridge method

Despite the fact that the diode method is very promising for a DC motor but it cannot change the direction of an AC supplied series wound motor such as universal motor. Therefore, we developed another digital method to safely change the direction of series motor referred to as active-bridge method. It is computationally more intense than the diode-method and requires more components; thus higher cost. However, it is a generalized approach that can fully work on any supply voltage either DC or AC. Hence, we explain this method after the diode method. Needless to say, for DC motor with a DC supply Diode method is recommended and for an AC-fed universal motor the Active-bridge method should be applied.

The main idea behind this method is to reverse the connection of field winding upon the need for reverse rotation/torque. Therefore, we realized that to reverse the field winding actively without any voltage spikes and damage to the circuit, it has to occur at the zero crossing of the field current. In this way, soft switching will occur and no inductive spikes will be produced. But to do this, field current which is equal to the armature current has to cross zero. For AC series motor the current is sinusoidal, thus inherently there are frequent zero crossings occurring for the motor current. This makes this approach easily applicable to universal motors which the diode method cannot address for this type of motor. However, the current never goes zero in a DC series motor unless the motor is off. Therefore, we developed a novel approach to make current zero crossing occur momentarily which will be explained in the following.

As mentioned before, in order to reverse the connection of the field winding without any spikes, the switching has to occur at the zero crossing of the field current right away. Therefore, a 4-switch topology based on power electronics switches is proposed which is illustrated in Figure 4-1. AC switches are necessary to let the current flow in both directions before and after field reversal. When the motor is in forward direction, current flows into the armature as shown

by $i_{a\text{-forward}}$ in Figure 4-1 and when the motor is in reverse mode the current will go out of the armature as shown by $i_{a\text{-reverse}}$.

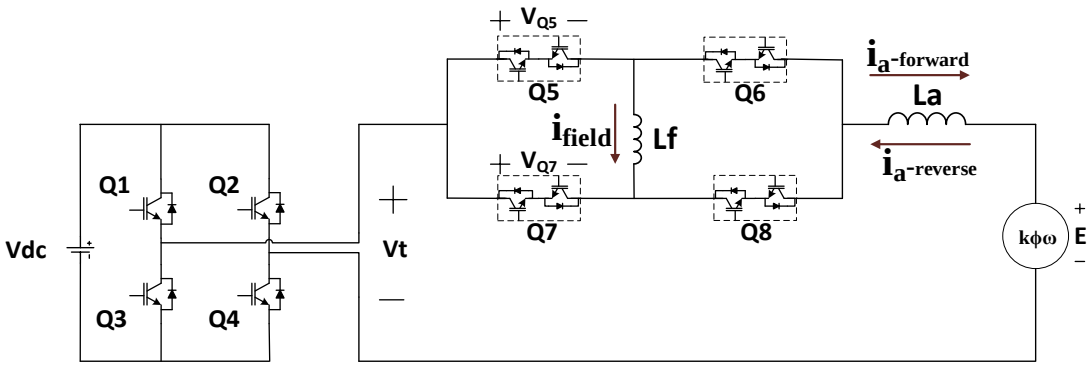

Figure 4-1 Proposed Topology – Active-bridge method

As an inherent characteristic of series motor, we know that it does not change rotation if the polarity of the supply voltage is reversed. This is why the series motor is unidirectional. However, by changing the polarity of the supply the field and armature currents equally reverse, hence the torque will remain constant, see equation (3-3). Therefore, the algorithm to reverse the field would be as follows: a) Reverse the supply voltage b) Track the field current as it dies out to zero c) reverse the field winding at zero crossing of the field current. The flowchart of the above algorithm is shown in Figure 4-2.

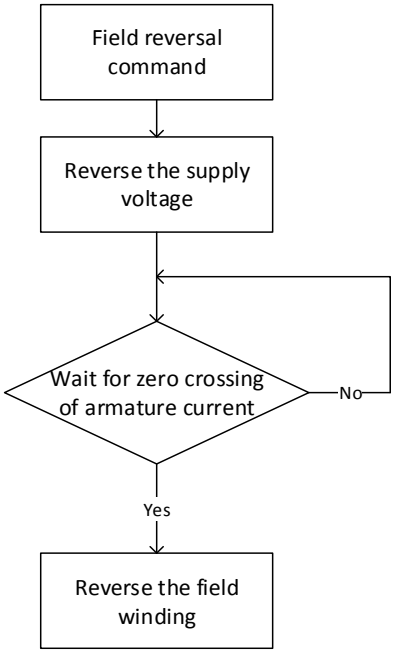

Figure 4-2 Flowchart of the negative torque generation in the active-bridge bi-directional series wound motor

Figure 4-3 shows how the response of a series motor when the supply voltage is reversed. Figure 4-3(a) shows the step change in supply voltage which is a step from $+V_{bus}$ to $-V_{bus}$ (V_{bus}=48V). By applying this voltage step the armature current will change polarity as well, see Figure 4-3(b). Zero crossing of armature current occurs 1 ms after step change in supply voltage. This time may vary depending on armature and field inductance of motor and the supply voltage. It should be noted that the difference between transient response of diode-method and active-bridge method stems from this this time interval.

In fact, the active-bridge method generates a zero crossing following the torque reversal command by applying a reverse supply voltage and waits for armature current to cross zero and at the zero-crossing instant connection of field winding is reversed. Whereas in diode-method there is no waiting time for zero-crossing which makes diode-method faster than active-bridge method.

Without applying the reversal algorithm motor torque will remain positive (Figure 4-3(c)), hence the speed (Figure 4-3(b)). Results of torque reversal simulations will be covered later in the chapter. It will be shown in the simulations that the reversing the field winding will occur smoothly without inflicting damages.

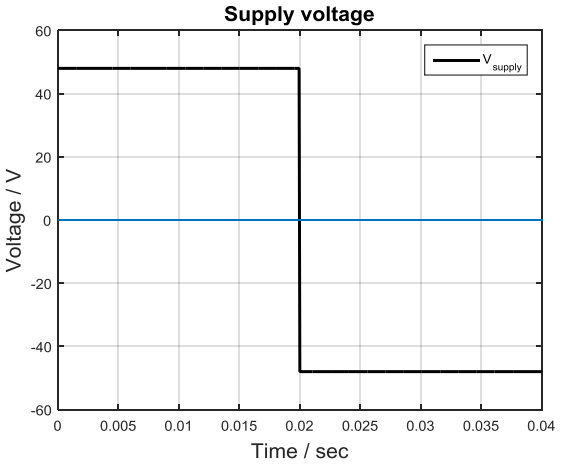

(a) Supply voltage

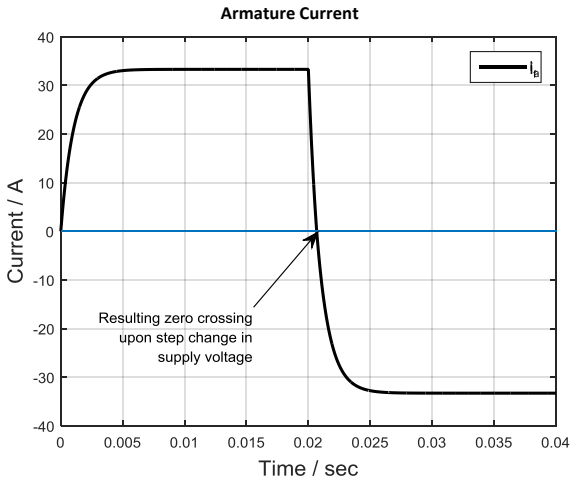

(b) Armature current

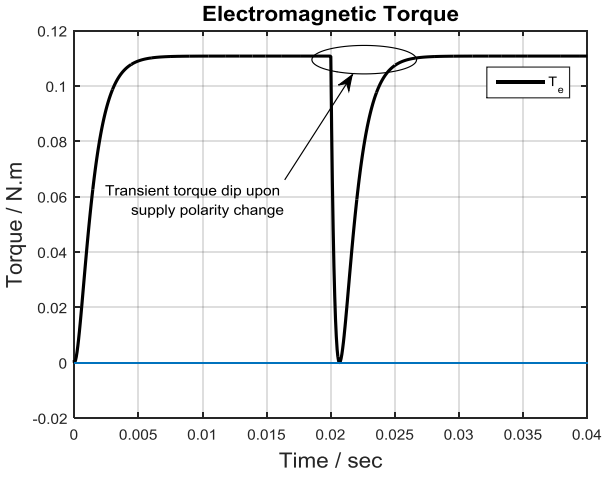

(c) Torque - T_e

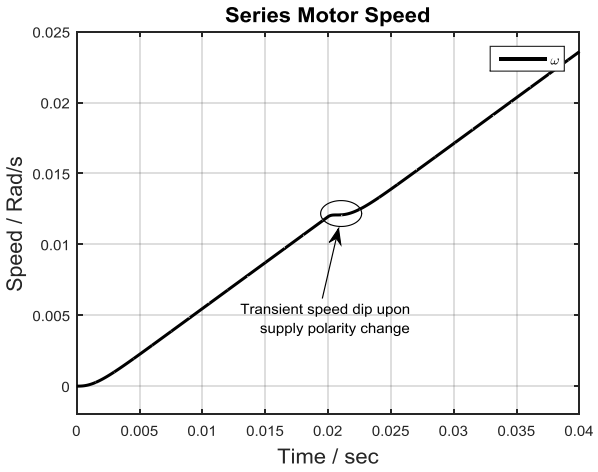

(d) Motor speed – ω_m

Figure 4-3 Series motor response to a reversed supply voltage

4.2 Proposed Switching and Control Strategy

In the diode-method a simple PI closed loop could control the torque (see Figure 3-6). In the active-bridge, however, the same control loop will not work. There is a need for an added digital block to control H-bridge and active-bridge switches simultaneously. Figure 4-4 shows the proposed torque control block that can be used for the torque control of the proposed active-bridge topology. As can be seen in the block diagram, a similar PI control loop exists for the control of the active-bridge topology but another decision making digital block has been added to the control to generate desired pulses to gate the switches of the H-bridge and also the four AC switches of the active-bridge. The proposed switching algorithm can be explained by characteristic waveforms of the proposed torque control system of Figure 4-4. Pre-calculation of the reference current based on the reference torque is done by using equation (3-1). The characteristic waveforms are shown in Figure 4-5. The desired status of all of the switches in each interval (i_0 – i_6 in Figure 4-5) have been determined following the waveforms. Table 4-1 summarizes the key parameters that can be used to determine the status of the switches in the active-bridge topology. The parameters "a" and "b" are the gate pulses that are generated by PWM block in Figure 4-4. Under certain conditions shown in Table 4-1, pulse "a" gates switches Q_1 and Q_4 whereas pulse "b" gates switches Q_3 and Q_4.

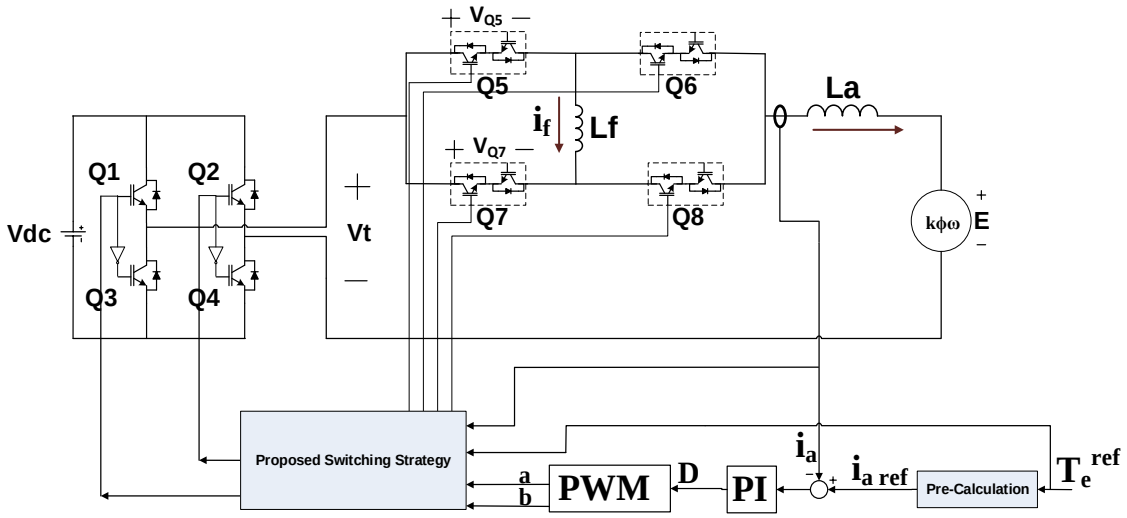

Figure 4-4 Proposed control and topology – Active bridge method

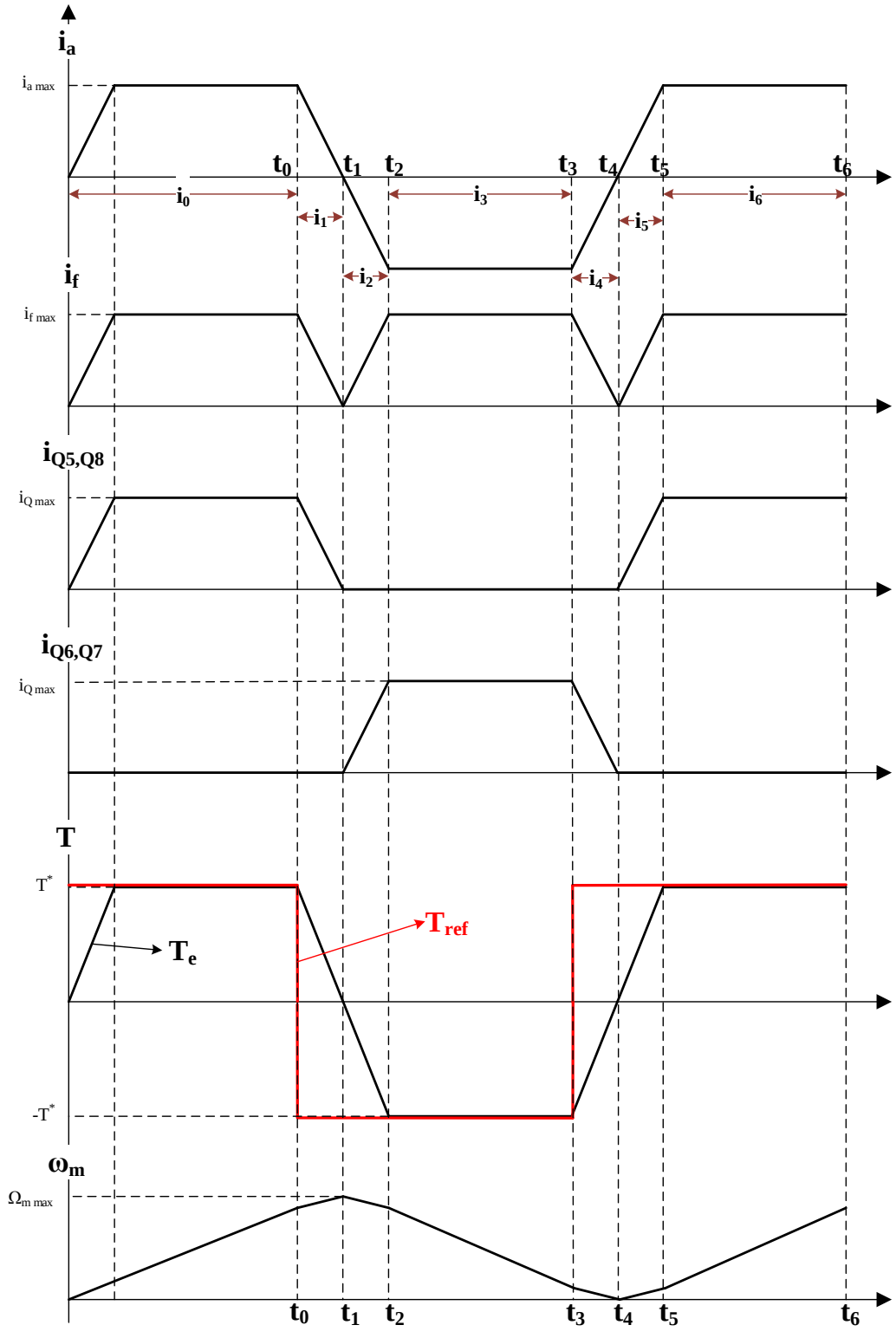

Figure 4-5 Switching waveforms – active-bridge method with torque control

In Figure 4-5, $i_{a\,max}$, $i_{f\,max}$, and $i_{Q\,max}$ are equal and are related to T^* by equation (3-1). Motor speed ω_m is related to torque T^* through the dynamic equation of rotor ($T^* = \frac{Jd\omega}{dt}$), where J is the inertia of the rotor.

$$interval\ i_0\ (0 - t_0): \begin{cases} i_a > 0, i_f > 0 \rightarrow T_e > 0 \\ T_{ref} > 0 \\ Q1, Q2, Q3, Q4 : PWM\ from\ PI\ Loop \\ Q5, Q8\ ON, \\ Q6, Q7\ OFF \end{cases}$$

$$interval\ i_1\ (t_0 - t_1): \begin{cases} i_a > 0, i_f > 0 \rightarrow T_e > 0 \\ T_{ref} < 0 \\ Q1, Q4\ OFF, \\ Q2, Q3\ ON, \\ Q5, Q8\ ON, \\ Q6, Q7\ OFF \end{cases}$$

$$interval\ i_2\ (t_1 - t_2): \begin{cases} i_a < 0, i_f > 0 \rightarrow T_e < 0 \\ T_{ref} < 0 \\ at\ t_1\ i_f\ and\ i_a\ cross\ zero\ thus\ Q5, Q8\ and\ Q6, Q7\ change\ state \rightarrow \\ Q1, Q2, Q3, Q4 : PWM\ from\ PI\ Loop \\ Q5, Q8\ OFF, \\ Q6, Q7\ ON \end{cases}$$

$$interval\ i_3\ (t_2 - t_3): \begin{cases} i_a < 0, i_f > 0 \rightarrow T_e < 0 \\ T_{ref} < 0 \\ Q1, Q2, Q3, Q4 : PWM\ from\ PI\ Loop \\ Q5, Q8\ OFF, \\ Q6, Q7\ ON \end{cases}$$

$$interval\ i_4\ (t_3 - t_4): \begin{cases} i_a < 0, i_f > 0 \rightarrow T_e < 0 \\ T_{ref} > 0 \\ Q1, Q4\ ON, \\ Q2, Q3\ OFF, \\ Q5, Q8\ OFF, \\ Q6, Q7\ ON \end{cases}$$

$$interval\ i_5\ (t_4 - t_5): \begin{cases} i_a > 0, i_f > 0 \rightarrow T_e > 0 \\ T_{ref} > 0 \\ at\ t_4\ i_f\ and\ i_a\ cross\ zero\ thus\ Q5, Q8\ and\ Q6, Q7\ change\ state \rightarrow \\ Q1, Q2, Q3, Q4 : PWM\ from\ PI\ Loop \\ Q5, Q8\ ON, \\ Q6, Q7\ OFF \end{cases}$$

$$interval\ i_6\ (t_5 - t_6): \begin{cases} i_a > 0, i_f > 0 \rightarrow T_e > 0 \\ T_{ref} > 0 \\ Q1, Q2, Q3, Q4 : PWM\ from\ PI\ Loop \\ Q5, Q8\ ON, \\ Q6, Q7\ OFF \end{cases}$$

Table 4-1 Switching Table – Active-bridge method with torque control

i_a	T_{ref}	Zero-cross	Q1,Q4	Q2,Q3	Q5,Q8	Q6,Q7	Interval
0	0	1	a	b	1	0	-
0	> 0	1	a	b	1	0	-
0	< 0	1	a	b	0	1	-
> 0	0	x	a	b	1	0	-
> 0	> 0	x	a	b	1	0	i_0,i_5,i_6
> 0	< 0	x	0	1	1	0	i_1
< 0	0	x	a	b	0	1	-
< 0	> 0	x	1	0	0	1	i_4
< 0	< 0	x	a	b	0	1	i_2,i_3

Using Table 4-1 a digital code has to be developed. The following code has been developed to implement the switching strategy for bidirectional torque control of the proposed active-bridge bidirectional series wound motor:

("a" and "b" are indices that are PWM pulses generated by the PI torque control loop, see Figure 4-4)

```
if (ia == 0)
    if(Tref == 0)
        Q1=a;Q4=a;Q2=b;Q3=b;
        Q5=1;Q8=1;Q6=0;Q7=0;
    elseif(Tref > 0)
        Q1=a;Q4=a;Q2=b;Q3=b;
        Q5=1;Q8=1;Q6=0;Q7=0;
    elseif(Tref < 0)
        Q1=a;Q4=a;Q2=b;Q3=b;
        Q5=0;Q8=0;Q6=1;Q7=1;
    end
elseif(ia > 0)
    if(Tref == 0)
        Q1=a;Q4=a;Q2=b,Q3=b;
        Q5=1;Q8=1;Q6=0;Q7=0;
    elseif(Tref > 0)
        Q1=a;Q4=a;Q2=b,Q3=b;
        Q5=1;Q8=1;Q6=0;Q7=0;
    elseif(Tref < 0)
        Q1=a;Q4=0;Q2=1;Q3=1;
        Q5=1;Q8=1;Q6=0;Q7=0;
    end
elseif(ia < 0)
    if(Tref == 0)
        Q1=a;Q4=a;Q2=b;Q3=b;
        Q5=0;Q8=0;Q6=1;Q7=1;
    elseif(Tref > 0)
        Q1=a;Q4=1;Q2=0;Q3=0;
        Q5=0;Q8=0;Q6=1;Q7=1;
    elseif(Tref < 0)
        Q1=a;Q4=a;Q2=b;Q3=b;
        Q5=0;Q8=0;Q6=Q7=1;
    end

end
```

4.3 Matlab/Simulink Simulations

In order to verify the validity of proposed active-bridge method and proposed digital switching strategy, the circuit of Figure 4-6 was simulated in Matlab/Simulink environment. The reference signal for the torque reference used for the simulation is exactly the same as the one used for the simulation of the diode-method so as to make the results comparable.

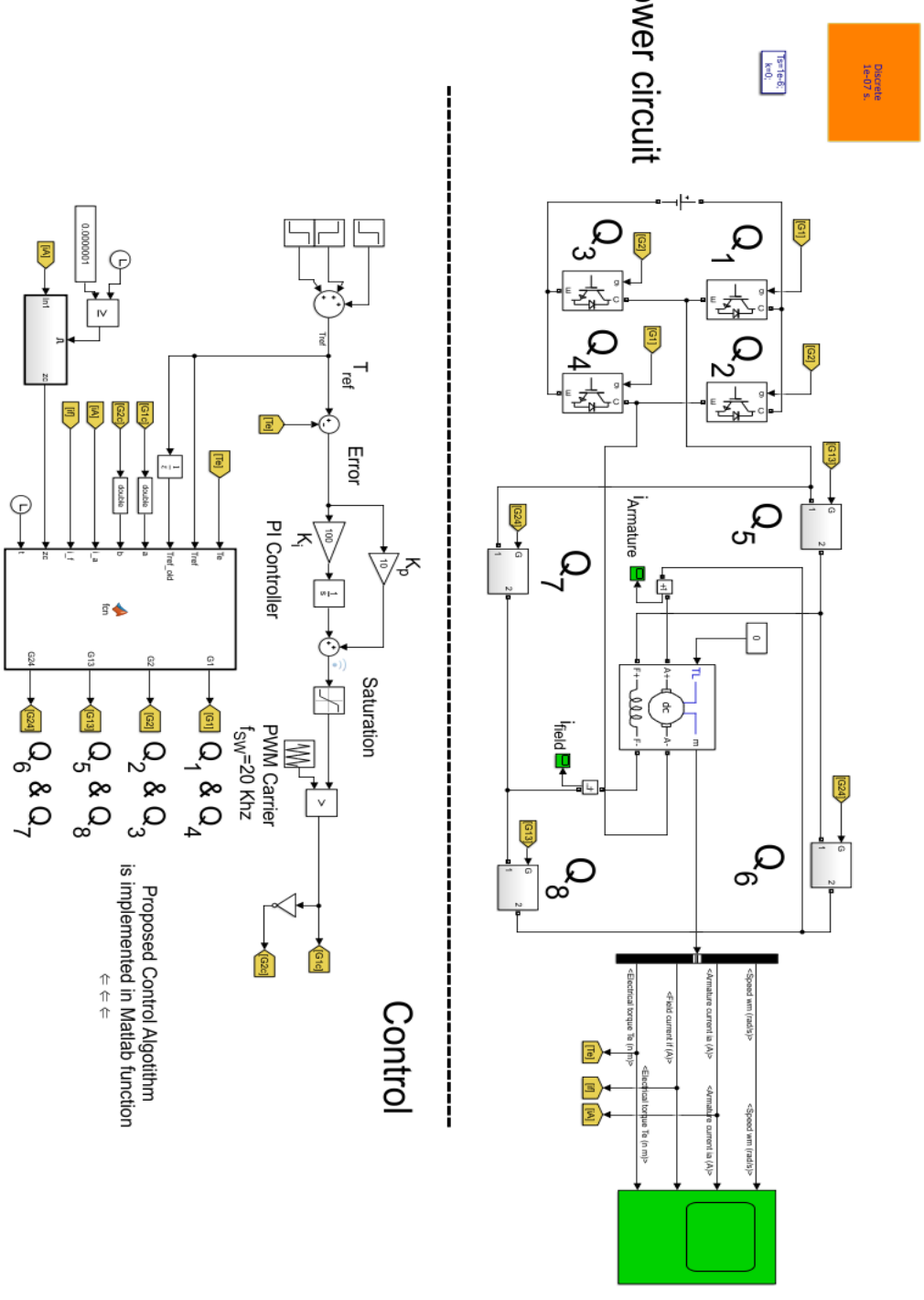

Figure 4-6 Active-bridge method with torque control – Matlab/Simulink simulation

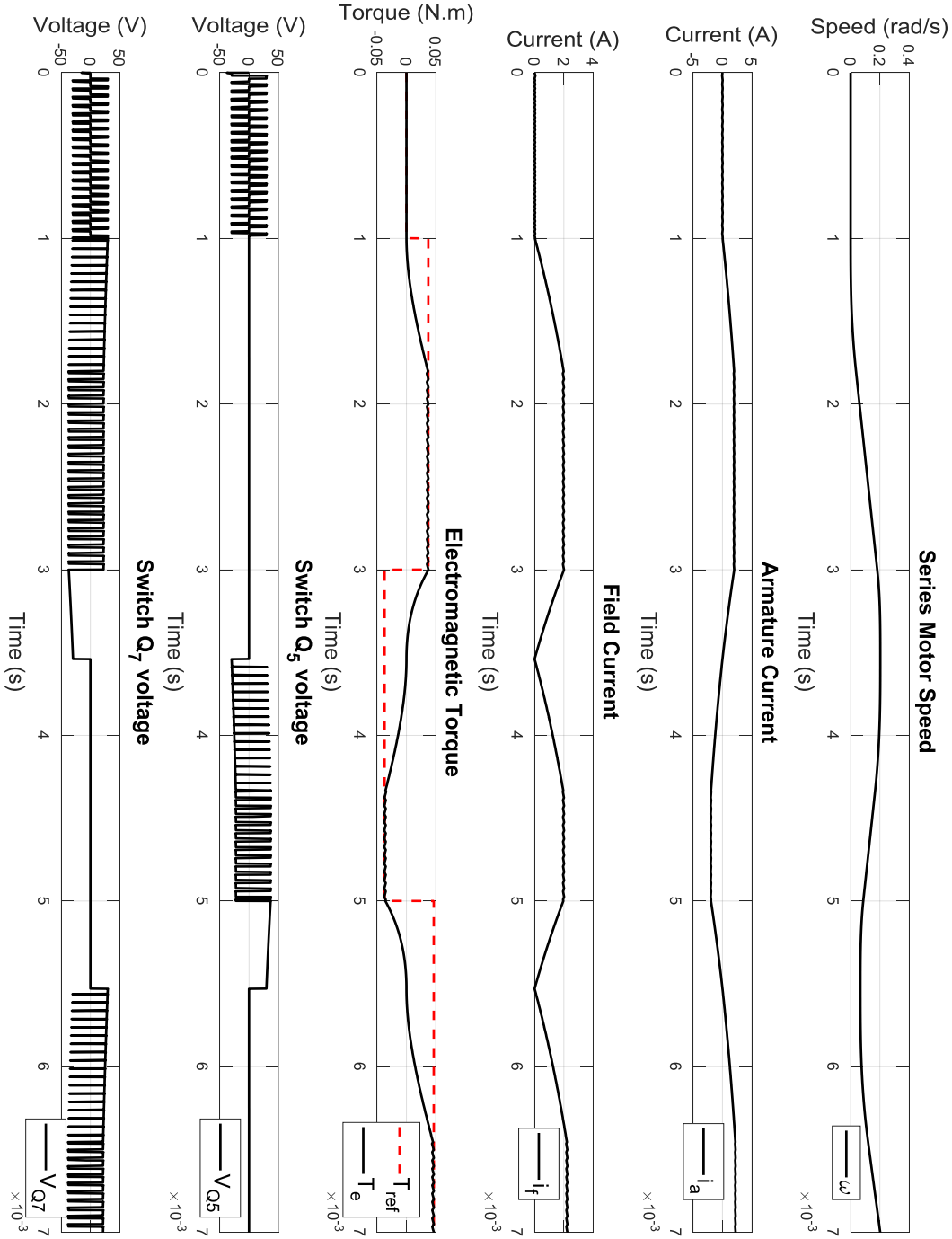

Figure 4-7 Simulation results; Active-bridge method with torque control

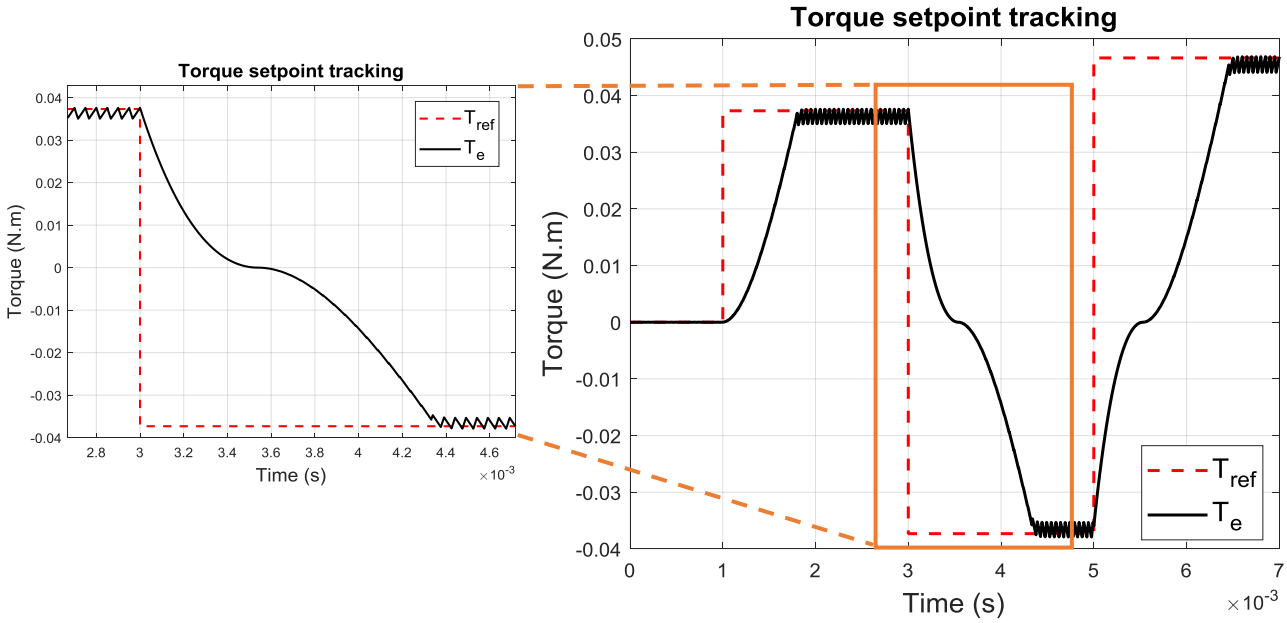

Figure 4-8 Torque setpoint tracking

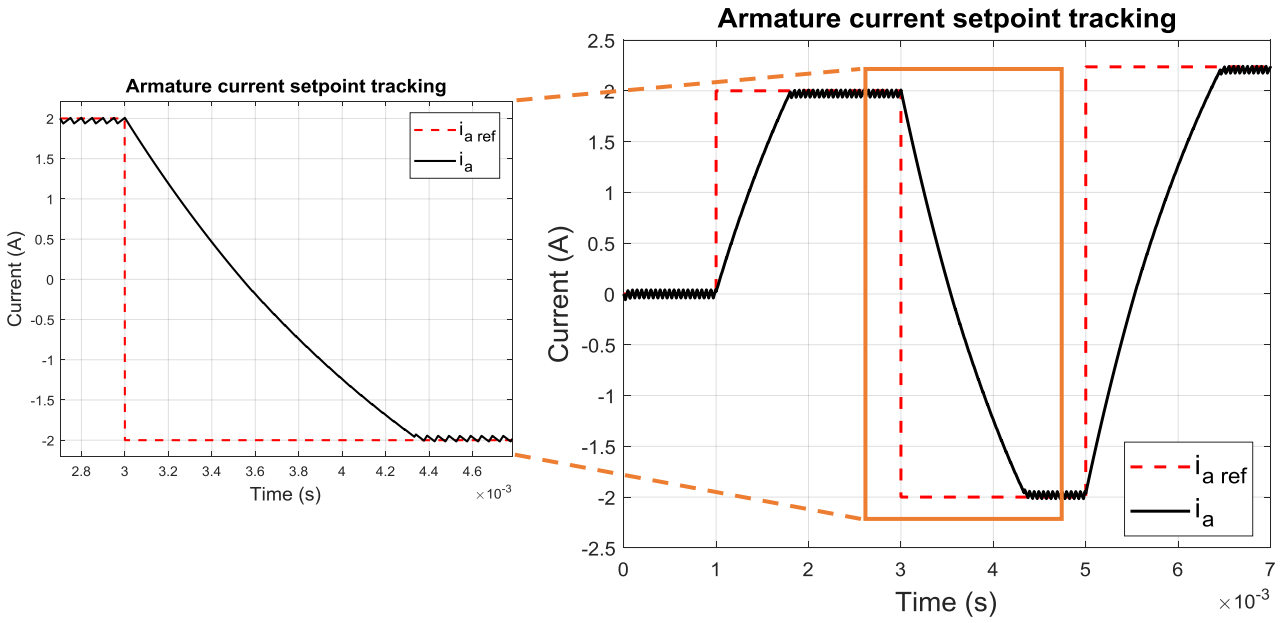

Figure 4-9 Armature current setpoint tracking – Active bridge method

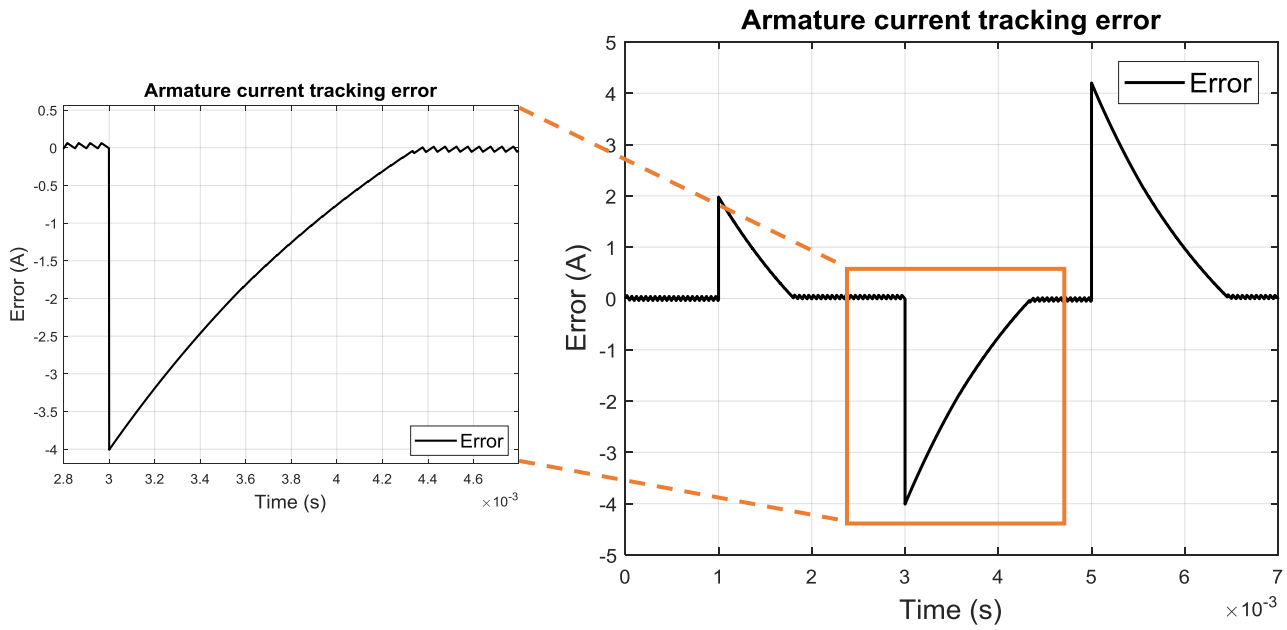

Figure 4-10 Armature current tracking error – Active bridge method

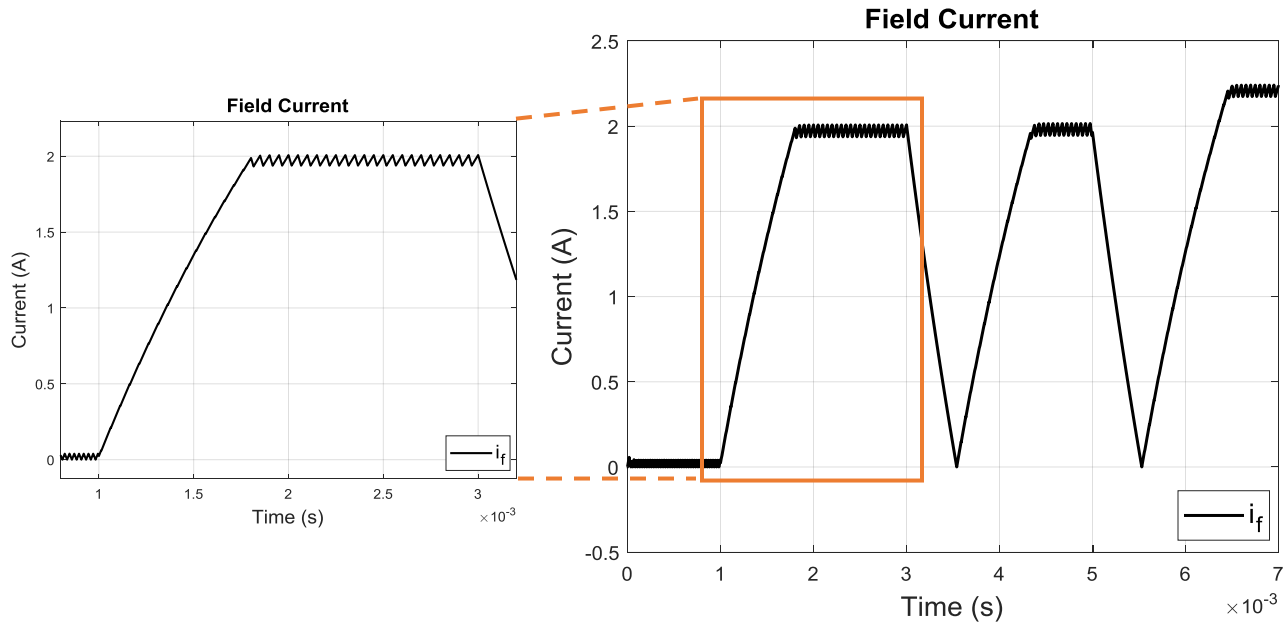

Figure 4-11 Field current – Active bridge method

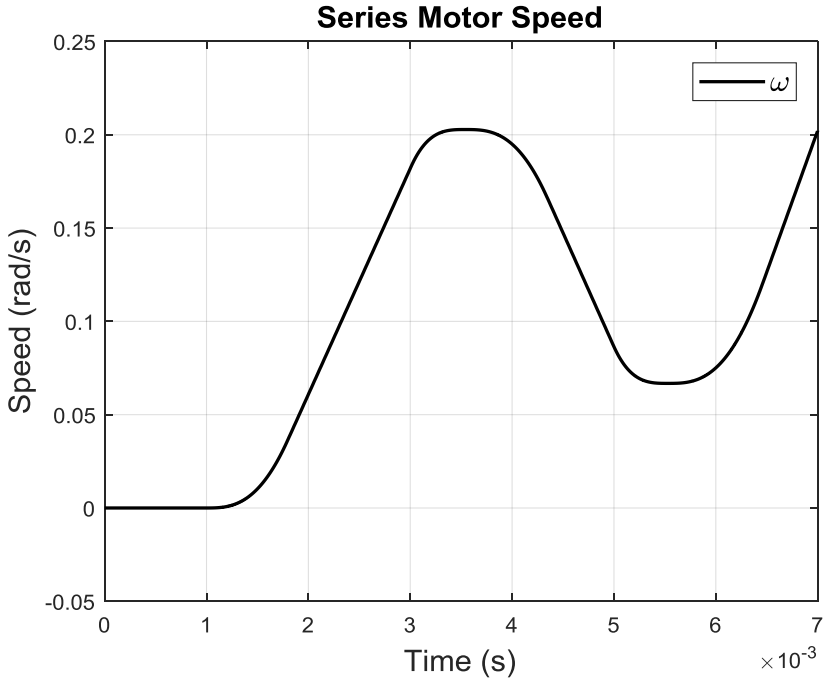

Figure 4-12 Motor speed – Active bridge method - ω_m

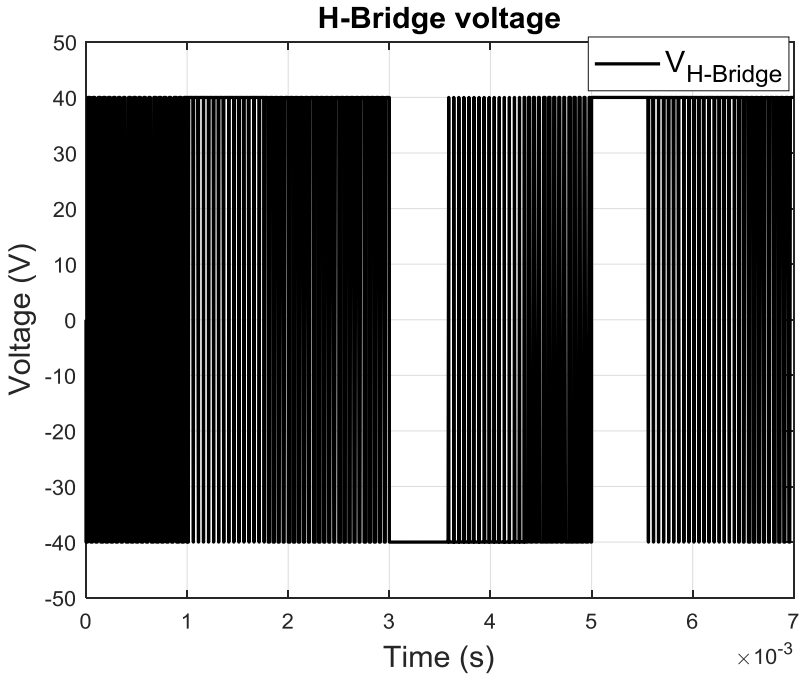

Figure 4-13 Modulating output voltage of H-Bridge

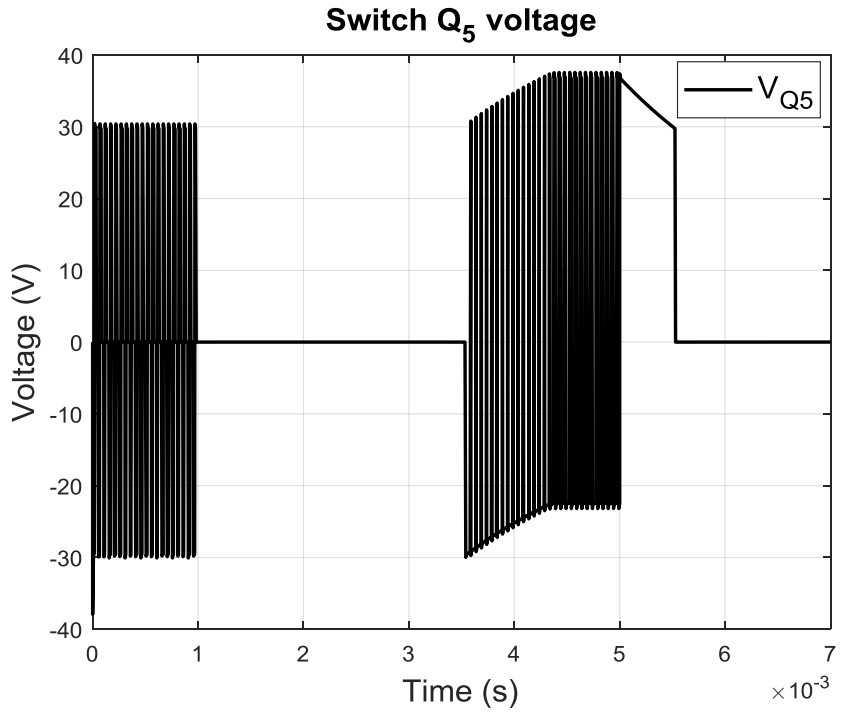

Figure 4-14 Voltage across switch Q_5

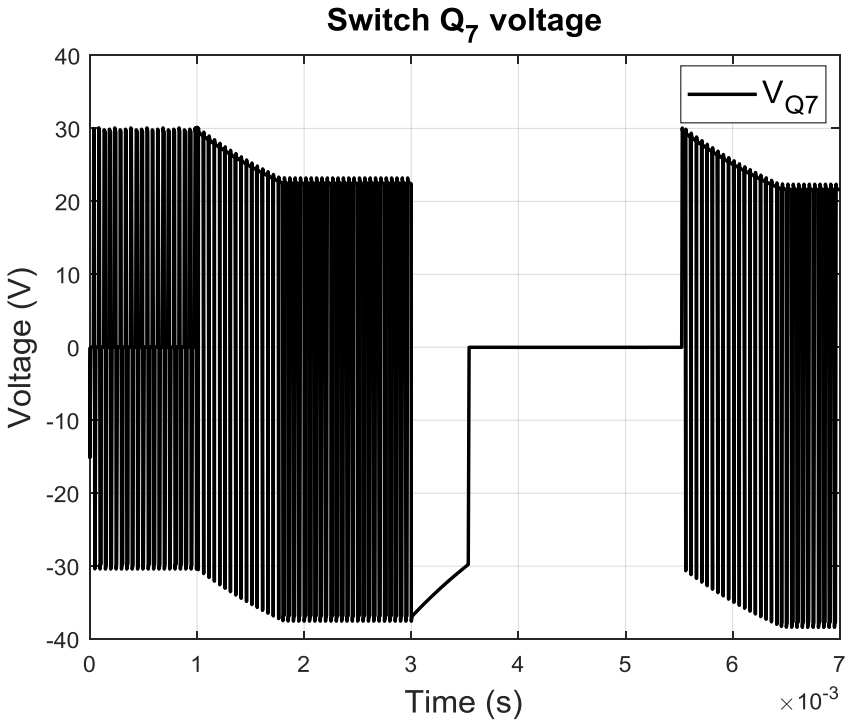

Figure 4-15 Voltage across switch Q_7

Simulation results of the active-bridge method have been shown in Figures 4-7 to 4-15. As stated earlier in Chapter 3, the same reference signal used in the simulation of diode-method was also utilized for the simulation of the active bridge method. Figure 4-7 shows all the variables at one glance. Torque dynamic response can be seen in Figure 4-8 where the active bridge method has been able to track the torque set-point in less than 1.5 milliseconds. In Figure 4-9 and Figure 4-10, the dynamic response of the armature current and error has been shown. The current tracking error after applying a step change at t=3ms has become zero in around 1.4 milliseconds. Figure 4-11 shows the field current with the active bridge method applied. It can be seen that in this method the control algorithm brings both currents (field and armature) equally to zero and negative torque is generated right after the zero crossing of the current(s).

Figure 4-12 shows that the speed of the motor has less sharp changes compared to that of diode method (see Figure 3-15). Figure 4-13 shows the modulating voltage across the output of the H-bridge whereas Figures 4-14 and 4-15 show the voltage active-bridge switches Q_5 and Q_7, respectively. The voltage across Q_8 equals to V_{Q5} and also V_{Q6} looks exactly the same as V_{Q7}. Therefore, only V_{Q5} and V_{Q7} have been shown. It can be seen that no deteriorating voltage spikes are generated across the switches verifying the feasibility of the active-bridge method.

4.3.1 Comparison of Simulation Results Diode-Method and Active Bridge Method

As mentioned earlier, the same reference torque signal was used to simulate responses of both diode-method and active bridge-method to make the results comparable. In order to better compare the results, torque and armature current dynamic responses for both methods have been put into one graph as shown in Figure 4-16. As can be seen in Figure 4-16, settling time for tracking a positive (+2A) to negative (-2A) step change for the diode-method is around 0.4 milliseconds whereas for the active-bridge method it is 1.4 milliseconds. Therefore, the

dynamic response of the diode-method is faster than that of the active-bridge method. However, for the active bridge the ripple current/torque is smaller than the ripple when the diode method is applied.

This dynamic response gap between the two methods stems from the fact that in the active-bridge method we need to apply a reverse voltage first and wait for the resulting zero crossing of the field/armature current which adds to the dynamic response of the system. However, in the diode method no zero crossing generation of the field/armature current is needed upon the reverse torque command therefore it is comparatively faster. Nonetheless, the advantage of the active-bridge method is where an AC series wound motor (Universal Motor) is required to be torque controlled in 4 quadrants. In that case, as mentioned earlier, bridge method will not function and the only way would be active-bridge method.

4.3.2 Simulation of the Active-bridge Method for AC-fed universal motor

As stated before, the diode-method cannot be used when a universal motor is fed by an AC supply. However, the active-bridge method can work under both DC and AC supply conditions. Circuit of Figure 4-17 was simulated in Matlab/Simulink environment. At t=0.039s, a command is sent to the proposed active bridge to generate negative (brake) torque. At t=0.039s armature and field current are not zero (see Figure 4-18). Therefore, the active bridge method waits till next zero crossing of the armature current and reverses the armature circuit right at zero crossing (at t=0.0432s). The time delay to capture the zero-crossing in this case is 0.0042s. Figure 4-18 shows that the active bridge has been able to generate negative torque whereas the diode-method cannot operate if supplied with an AC source (Figure 3-20).

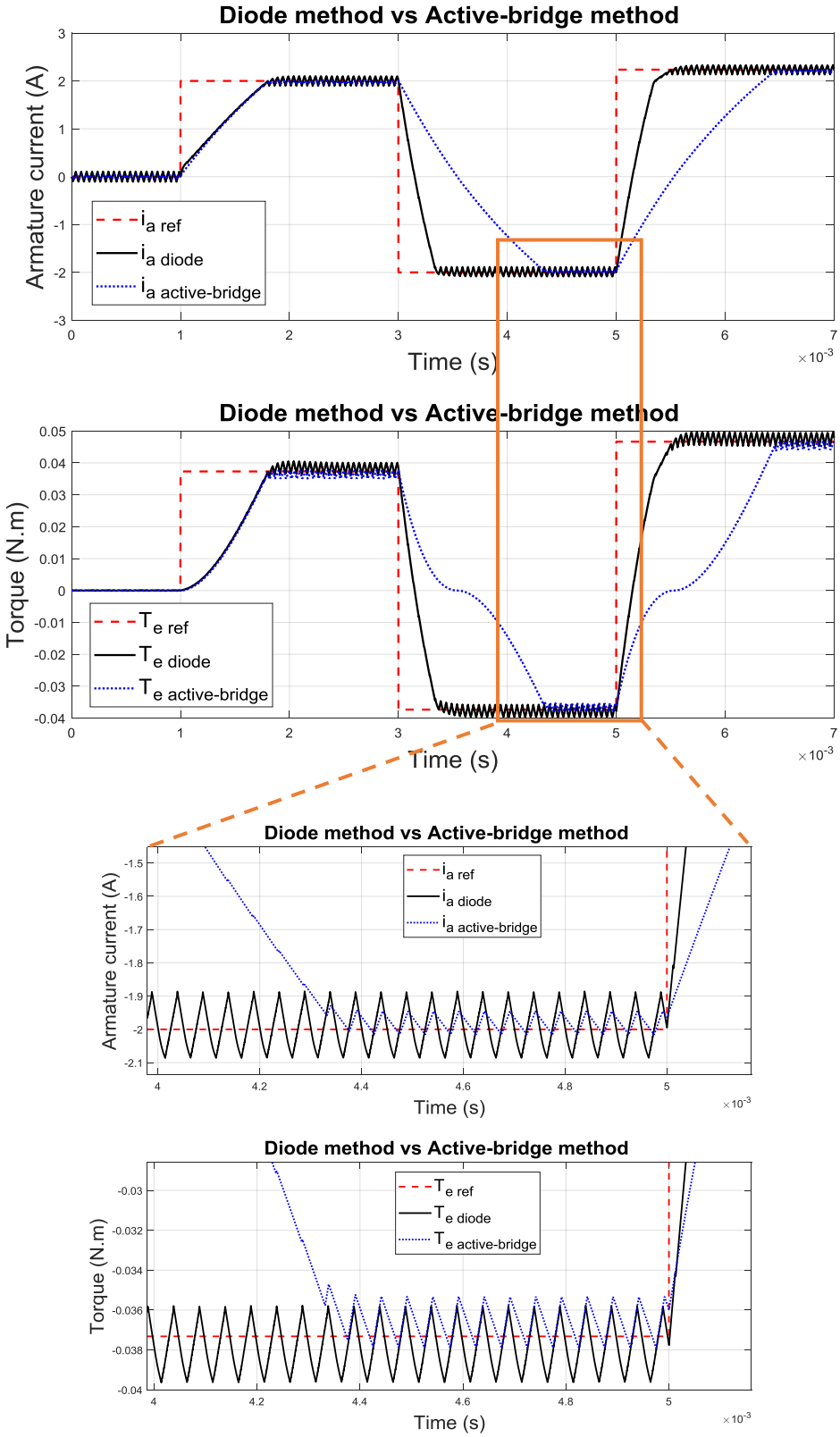

Figure 4-16 Comparison of transient response Diode-method vs Active Bridge-method

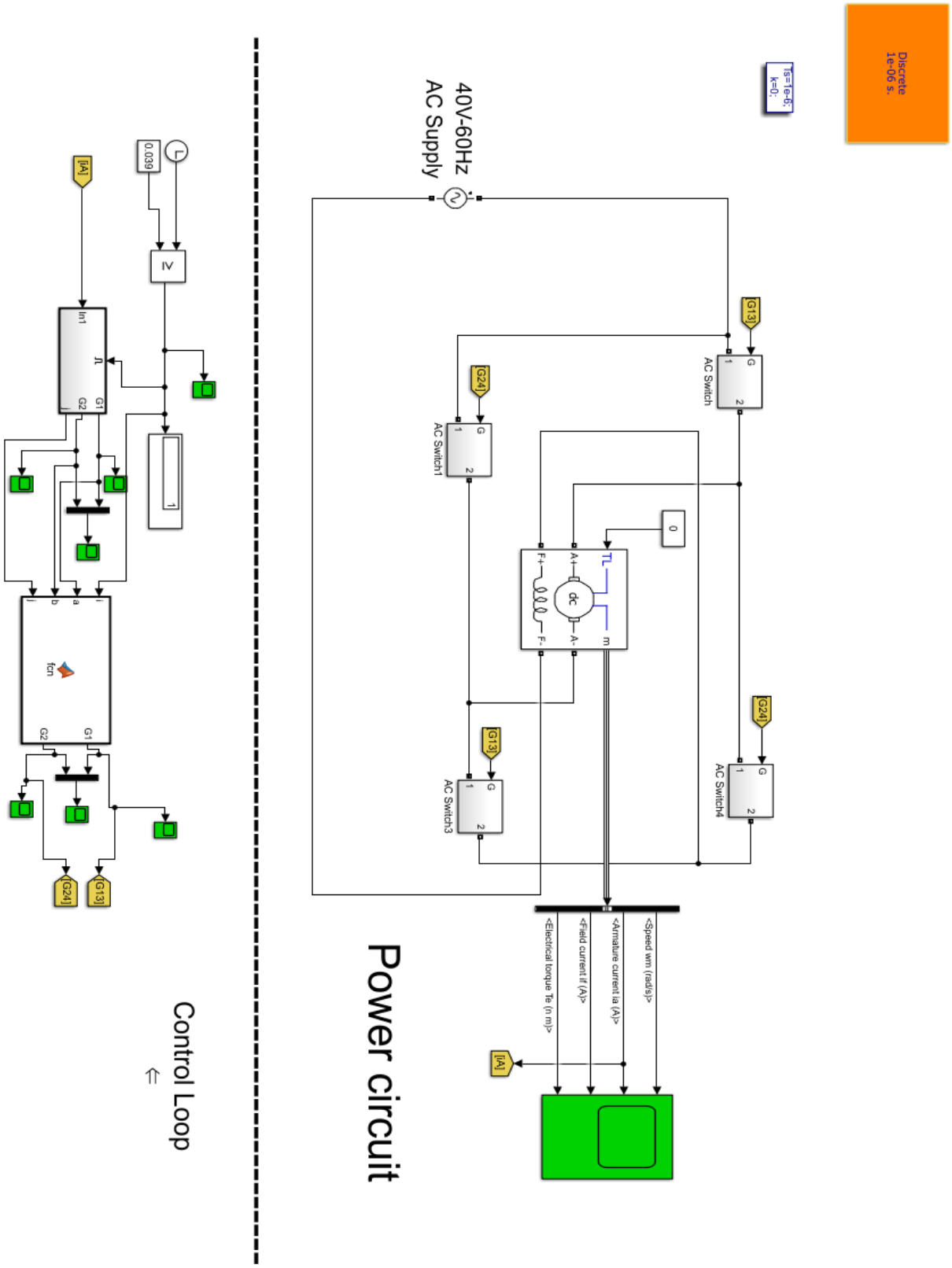

Figure 4-17 Active-bridge method with AC supply – Matlab/Simulink simulation

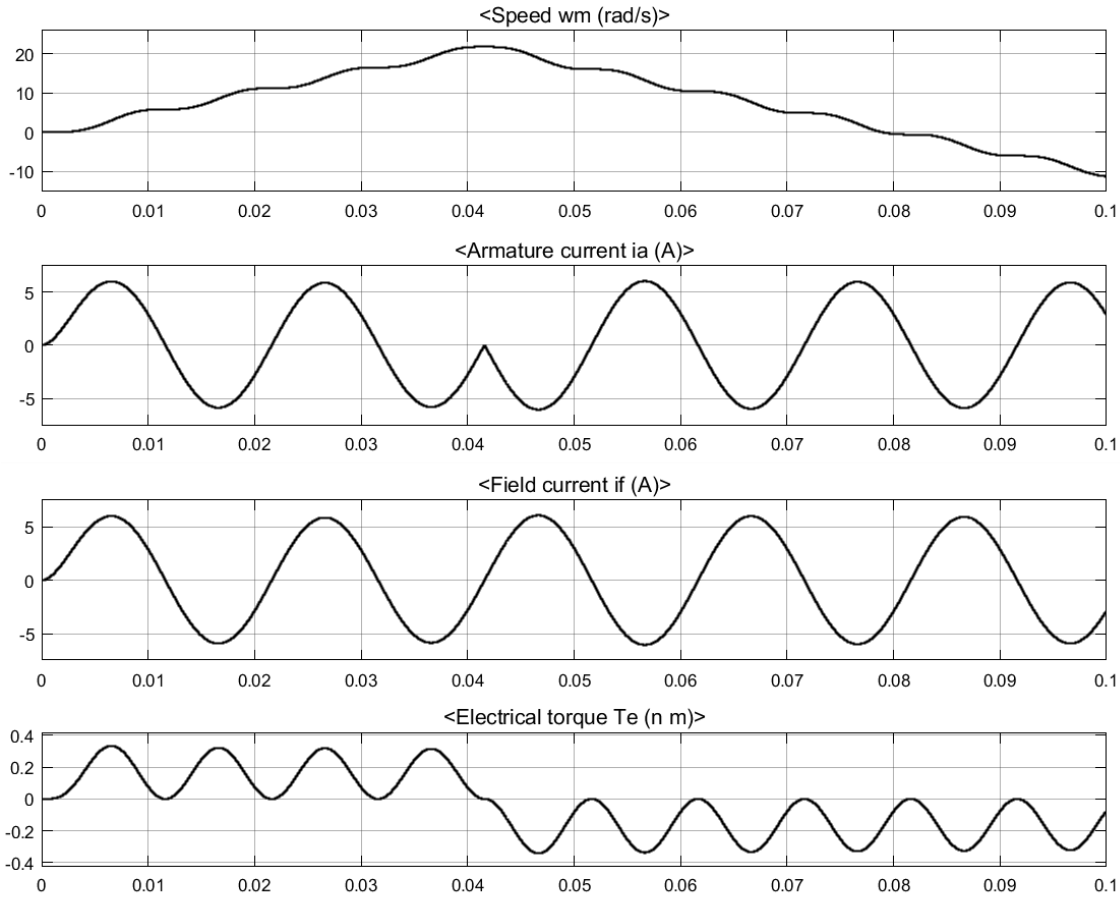

Figure 4-18 Simulation results - Active-bridge method with AC supply

Chapter 5

Conclusion and future work

5.1 Conclusion

Haptic technology will significantly benefit from a direct drive actuation mechanism due the problems that geared solutions can cause, such as increased friction, backlash, cost, and inertia, decreased backdrivability. There are many different types of motors already available in the market and some of them can be candidate for haptic device application; specifically those with high torque at low speed (~ zero). Inherently high torque series motor (universal motor), however, has not been counted as a candidate for use in all four T-ω quadrants. The reason is that series motors can only rotate in one direction. In other words they can only generate torque in one direction. If by any means a series motor could generate torque in both directions, then it could be a strong candidate motor in applications requiring high torque at very low speed (~ zero). Moreover, the reverse torque generation capability could also be used in electrical braking of the universal motors.

In this thesis, by means of power electronics, a standard series motor (universal motor) is converted to a bidirectional series motor that could be used in any four-quadrant applications, especially those requiring high torque at low speed. The proposed bidirectional series motor works based on two different approaches referred to as the "diode-method" and the "active-bridge method", each addressing a targeted set of applications. For the DC drive applications diode-method is the preferred method due its faster response and design simplicity. For AC drive and also electrical braking of universal motors the active-bridge method is suggested. Both methods were presented in detail in Chapters three and four, and were compared using MATLAB/SIMULINK simulations. Preliminary experimental results were presented. Simulation and experiments, clearly verify the feasibility of the proposed methods and to operate the series motor in two directions.

5.2 Future work

The major contribution of this thesis, is the development of a hardware/software technology that converts a series motor into a bidirectional actuator with no to minimal change to the motor integrity. With this new high torque bidirectional motor, one major application that can highly benefit is haptic device. Another interesting application for the proposed active-bridge method is to use the approach in dynamic electrical braking of universal motors. Therefore future suggested works include:

- Test the bidirectional actuator under various loads in a haptic simulation system
- Evaluate the specifications of the actuator
- Benchmark the actuator against currently available actuators such as coreless DC motor
- Hardware implementation of active-bridge method for dynamic electrical braking of a universal motor
- Use of PID controller for faster torque reversal of the actuator
- Using unipolar PWM to decrease EMI noise and vibrational torque on the shaft of the motor in idle mode (zero reference torque)

Bibliography

[1]. V. Hayward and K. E. Maclean, "Do it yourself haptics: part I," *in IEEE Robotics & Automation Magazine*, vol. 14, no. 4, pp. 88-104, Dec. 2007.

[2]. K. E. Maclean and V. Hayward, "Do It Yourself Haptics: Part II [Tutorial]," *in IEEE Robotics & Automation Magazine*, vol. 15, no. 1, pp. 104-119, March 2008.

[3]. P. Fischer, R. Daniel and K. V. Siva, "Specification and design of input devices for teleoperation," *Proc. of IEEE Robotics and Automation Conf.*, pp. 540-545 OH, 1990.

[4]. https://realtimecities.wikispaces.com/Medical+Training+Haptic+Device

[5]. R. L. Hollis and S. E. Salcudean, "Lorentz Levitation Technology: a New Approach to Fine Motion Robotics, Teleoperation, Haptic Interfaces, and Vibration Isolation," *Int. Symp. for Robotics Research*, 1993.

[6]. R. L. Hollis, S. E. Salcudean and A. P. Allan, "A six-degree-of-freedom magnetically levitated variable compliance fine-motion wrist: design, modeling, and control," *in IEEE Trans. on Robotics and Automation*, vol. 7, no. 3, pp. 320-332, Jun 1991.

[7]. J. Perret, P. Vercruysse, "Advantages of mechanical backdrivability for medical applications of force control," researchgate.net.

[8]. http://www.forcedimension.com/

[9]. L. Zeng and G. Weber, "Audio-Haptic browser for a geographical information system," *Proc. of Int. Conf. Computers Helping People*, pp. 466-473, 2010.

[10]. C. Chandrabalan, "Design and Construction of 1 D.O.F Haptic Interface," M.Sc thesis, The Florida State University, Fall 2004.

[11]. K.E. MacLean, "Haptic Interaction Design for Everyday Interfaces," Reviews of Human Factors and Ergonomics, in press, M. Carswell, ed., *Human Factors and Ergonomics Soc.*, 2008.

[12]. V. Hayward, O. R. Astley, M. Cruz-Hernandez, D. Grant, and G. Robles-De-La-Torre, "Haptic interfaces and devices," Sens. Rev., vol. 24, no. 1, pp. 16–29, 2004.

[13]. S. Grange, F. Conti, P. Helmer, P. Rouiller. and C. Baur, "Overview of the Delta Haptic Device," *Eurohaptics '01*, Birmingham, England, July 2001.

[14]. Hayward, V. and Astley, "Performance Measures for Haptic Interfaces," *7th Int. Symp.*, Springer Verlag, 195-207.

[15]. P. J. Berkelman, R. L. Hollis and S. E. Salcudean, "Interacting with virtual environments using a magnetic levitation haptic interface," *Proc. of IEEE Human Robot Interaction and Cooperative Robots Conf.*, pp. 117-122, Pittsburgh, PA, 1995.

[16]. S. E. Salcudean and L. Stocco, "Isotropy and actuator optimization in haptic interface design," *Proc. of IEEE Robotics and Automation Conf.*, pp. 763-769, San Francisco, CA, 2000.

[17]. T. Fong, F. Conti, S. Grange, and C. Baur, "Novel interfaces for remote driving: Gesture, haptic and PDA," *in Int. society for optics and photonics*, Boston, MA, 2000.

[18]. V. Hayward and O. Astley, "Performance Measures for Haptic Interfaces," Proc. of Robotics Research, *Springer-Verlag*,
pp. 195-207, 1996.

[19]. P. Fischer, R. Daniel and K. V. Siva, "Specification and design of input devices for teleoperation," *Proc. of IEEE Robotics and Automation Conf.*, pp. 540-545, Cincinnati, OH, 1990.

[20]. V. Hayward, "Toward a seven axis haptic device," *Proc. of IEEE Robotics and Automation Conf.*, pp. 133-139, Pittsburgh, PA, 1995.

[21]. Srinivasan, M. A., "What is Haptics?", *The Touch lab, Massachusetts Institute of Technology*, 2004.

[22]. R. L. Hollis, S. E. Salcudean and A. P. Allan, "A six-degree-of-freedom magnetically levitated variable compliance fine-motion wrist: design, modeling, and control," *in IEEE Trans. on Robotics and Automation*, vol. 7, no. 3, pp. 320-332, Jun 1991.

[23]. K. M. Stanney,Handbook of Virtual Environments. London, U.K.: Lawrence Erlbaum, 2002.

[24]. W. Leonhard, "Control of Electrical Drives", *Springer-Verlag*, 1985

[25]. M. G. Simoes and P. Vieira, "A high-torque low-speed multiphase brushless machine-a perspective application for electric vehicles," *in IEEE Trans. on Ind. Elect.*, vol. 49, no. 5, pp. 1154-1164, Oct 2002.

[26]. Jinyun Gan, K. T. Chau, C. C. Chan and J. Z. Jiang, "A new surface-inset, permanent-magnet, brushless DC motor drive for electric vehicles," *in IEEE Trans. on Magnetics*, vol. 36, no. 5, pp. 3810-3818, Sep 2000.

[27]. Lixin Tang, Limin Zhong, M. F. Rahman and Yuwen Hu, "A novel direct torque control for interior permanent-magnet synchronous machine drive with low ripple in torque and flux-a speed-sensorless approach," *in IEEE Trans. on Ind. App.*, vol. 39, no. 6, pp. 1748-1756, Nov.-Dec. 2003.

[28]. P. Pillay and R. Krishnan, "Application characteristics of permanent magnet synchronous and brushless DC motors for servo drives," *in IEEE Trans. on Ind. App.*, vol. 27, no. 5, pp. 986-996, Sep/Oct 1991.

[29]. M. Zeraoulia, M. E. H. Benbouzid and D. Diallo, "Electric Motor Drive Selection Issues for HEV Propulsion Systems: A Comparative Study," *in IEEE Trans. on Veh. Tech.*, vol. 55, no. 6, pp. 1756-1764, Nov. 2006.

[30]. P. Pillay and R. Krishnan, "Modeling, simulation, and analysis of permanent-magnet motor drives. II. The brushless DC motor drive," *in IEEE Trans. on Ind. App.*, vol. 25, no. 2, pp. 274-279, Mar/Apr 1989.

[31]. T. M. Jahns and W. L. Soong, "Pulsating torque minimization techniques for permanent magnet AC motor drives-a review," *in IEEE Trans. on Ind. Elect.*, vol. 43, no. 2, pp. 321-330, Apr 1996.

[32]. G. S. Buja and M. P. Kazmierkowski, "Direct torque control of PWM inverter-fed AC motors - a survey," *in IEEE Trans. on Ind. Elect.*, vol. 51, no. 4, pp. 744-757, Aug. 2004.

[33]. Simone Buso; Paolo Mattavelli, "Digital Control in Power Electronics," *in Digital Control in Power Electronics* , 1, Morgan & Claypool, pp.158-, 2006.

[34]. Yong Liu, Z. Q. Zhu and D. Howe, "Direct torque control of brushless DC drives with reduced torque ripple," *in IEEE Trans. on Ind. App.*, vol. 41, no. 2, pp. 599-608, March-April 2005.

[35]. M. George, "Speed control of separately excited dc motor", *American Journal of Applied Science 5*, pp. 227-233, 2008.

[36]. Sung Jun Park, Han Woong Park, Man Hyung Lee and F. Harashima, "A new approach for minimum-torque-ripple maximum-efficiency control of BLDC motor," *in IEEE Trans. on Ind. Elect.*, vol. 47, no. 1, pp. 109-114, Feb 2000.

[37]. F. Aghili, "Fault-Tolerant Torque Control of BLDC Motors," *in IEEE Trans. on Power Elect.*, vol. 26, no. 2, pp. 355-363, Feb. 2011.

[38]. S. B. Ozturk and H. A. Toliyat, "Direct Torque Control of Brushless DC Motor with Non-sinusoidal Back-EMF," *Proc. Of IEEE Int. Electric Machines & Drives Conf.*, pp. 165-171, Antalya, 2007.

[39]. T. S. Low, K. J. Tseng, T. H. Lee and K. S. Lock, "Servo performance of a BLDC drive with instantaneous torque control," *Proc. Of IEEE Ind. App. Society Annu. Meeting Conf.*, pp. 454-459, Seattle, WA, USA, 1990.

[40]. T. S. Low, K. J. Tseng, T. H. Lee, K. W. Lim and K. S. Lock, "Strategy for the instantaneous torque control of permanent-magnet brushless DC drives," *Proc. of IEEE Electric Power App. Conf.*, pp. 355-363 , no. 6, Nov. 1990.

[41]. Y. Liu, Z. Q. Zhu and D. Howe, "Commutation-Torque-Ripple Minimization in Direct-Torque-Controlled PM Brushless DC Drives," *in IEEE Trans. on Ind. App.*, vol. 43, no. 4, pp. 1012-1021, July-aug. 2007.

[42]. Z. Q. Zhu, Y. Liu and D. Howe, "Comparison of Performance of Brushless DC Drives under Direct Torque Control and PWM Current Control," *Proc. Of IEEE Electrical Machines and Systems Int Conf.*, pp. 1486-1491, Nanjing, 2005.

[43]. J. Fang, X. Zhou and G. Liu, "Instantaneous Torque Control of Small Inductance Brushless DC Motor," *in IEEE Trans. on Power Elect.*, vol. 27, no. 12, pp. 4952-4964, Dec. 2012.

[44]. J. Gao and Y. Hu, "Direct Self-Control for BLDC Motor Drives Based on Three-Dimensional Coordinate System," *in IEEE Trans. on Ind. Elect.*, vol. 57, no. 8, pp. 2836-2844, Aug. 2010.

[45]. E. Cerruto, A. Consoli, A. Raciti and A. Testa, "A robust adaptive controller for PM motor drives in robotic applications,*" in IEEE Trans. on Power Elect.*, vol. 10, no. 1, pp. 62-71, Jan 1995.

[46]. W. Xu, J. Zhu, Y. Guo, S. Wang, Y. Wang and Z. Shi, "Survey on electrical machines in electrical vehicles," *Proc. Of IEEE Applied Superconductivity and Electromagnetic Devices Conf.*, pp. 167-170, Chengdu, 2009.

[47]. G. H. Jang, J. H. Park and J. H. Chang, "Position detection and start-up algorithm of a rotor in a sensorless BLDC motor utilising inductance variation," *Proc. IEEE Electric Power Applications Conf.*, pp. 137-142, no. 2, Mar 2002.

[48]. B. Akin, and M. Bhardwaj, Sensorless Field Oriented Control of 3-Phase Parmanent Magnet Synchronous Motors, *Texas Instruments, Application Notes*.

[49]. A. Boglietti, M. Pastorelli, and F. Profumo, "A conduction angle control strategy for high speed brushless motors for spindle drives", *Archiv für Elektrotechnik*, Springer, 1993.

[50]. Z. Li, Y. Li, P. Wang, H. Zhu, C. Liu and F. Gao, "Single-Loop Digital Control of High-Power 400-Hz Ground Power Unit for Airplanes," *in IEEE Trans. on Ind. Elect.*, vol. 57, no. 2, pp. 532-543, Feb. 2010.

[51]. A. G. Yepes, F. D. Freijedo, J. Doval-Gandoy, Ó Lopez, J. Malvar and P. Fernandez-Comesaña, "Correction to "Effects of Discretization Methods on the Performance of Resonant Controllers," *in IEEE Trans. on Power Elect.*, vol. 27, no. 12, pp. 4976-4976, Dec. 2012.

[52]. C. Buccella, C. Cecati and H. Latafat, "Digital Control of Power Converters—A Survey," *in IEEE Trans. on Ind. Inform.*, vol. 8, no. 3, pp. 437-447, Aug. 2012.

[53]. C. C. Chan, J. Z. Jiang, W. Xia and K. T. Chau, "Novel wide range speed control of permanent magnet brushless motor drives," *Proc. of IEEE Power Elect. and Drive Systems Int. Conf.*, pp. 780-785, 1995.

[54]. R. Jarman, B. Janko and W. S. Harwin, "Current over-stressing small DC motors to evaluate performance limits of electromechanical actuators for haptic applications," *Proc. Of Int. Conf. on Haptics*, pp. 171-176, Evanston, IL, 2015.

[55]. A. Ortega, A. Weill-Duflos, S. Haliyo, S. Régnier and V. Hayward, "Linear induction actuators for a haptic interface: A quasi-perfect transparent mechanism," *Proc. Of Int. Conf. on Haptics*, pp. 575-580, Munich, 2017.

[56]. J. M. Hollerbach, "Some current issues in haptics research," *Proc. Of Robotics and Automation, Int. Conf.*, vol. 1, pp. 757-762, San Francisco, CA, 2000.

[57]. O. Selvi, T. Bilgincan, Y. Kant and M. I. Can Dede, "Novel structural design of a haptic device for medical applications," *14th National Biomedical Engineering Meeting*, pp. 1-4, Balcova, Izmir, 2009.

[58]. L. Barbe, B. Bayle, J. Gangloff, M. de Mathelin and O. Piccin, "Design and Evaluation of a Linear Haptic Device," *Proc. Of Robotics and Automation, Proc. Of Int. Conf.*, pp. 485-490, Roma, 2007.

[59]. M. Yasukawa, K. Hirata and M. Kato, "Novel oscillatory actuator for haptic device using principle of stepper motor," *Proc. Of Linear Drives for Industry Applications* (LDIA), pp. 1-4, Osaka, Japan, 2017.

[60]. R. Shanmugasundram, K. M. Zakariah and N. Yadaiah, "Implementation and Performance Analysis of Digital Controllers for Brushless DC Motor Drives," *in IEEE Trans. on Mechatronics*, vol. 19, no. 1, pp. 213-224, Feb. 2014.

[61]. M. S. Merzoug and F. Naceri, ”Comparison of Field-Oriented Control and Direct Torque Control for Permanent Magnet Synchronous Motor (PMSM),” *World Academy of Science, Engineering and Technology 45*, 2008.

[62]. A. R. Paul and M. George, "Brushless DC motor control using digital PWM techniques," *Proc. of Signal Processing, Communication, Computing and Networking Technologies (ICSCCN) Int. Conf.*, pp. 733-738, Thackeray, 2011.

[63]. P. C. Sen, "Principles of electric machines and power electronics, " *John Wiley & Sons*, New York , 2013.

[64]. H. A. Toliyat and G. B. Kliman, “Handbook of Electric Motors,” New York: Marcel Dekker, 2004.

[65]. X. D. Xue, K. W. E. Cheng and N. C. Cheung, "Selection of Electric Motor Drives for Electric Vehicles," (AUPEC) *Proc. Of Australasian Universities Power Eng. Conf.*, pp. 1-6, Sydney, NSW, 2008.

[66]. K. T. Chau, C. C. Chan and C. Liu, "Overview of Permanent-Magnet Brushless Drives for Electric and Hybrid Electric Vehicles," *in IEEE Trans. on Ind. Elect.*, vol. 55, no. 6, pp. 2246-2257, June 2008.

[67]. T. Shi, Y. Guo, P. Song and C. Xia, "A New Approach of Minimizing Commutation Torque Ripple for Brushless DC Motor Based on DC–DC Converter," *in IEEE Trans. on Ind. Elect.*, vol. 57, no. 10, pp. 3483-3490, Oct. 2010.

[68]. http://rcadvisor.com/inrunner-vs-outrunner-motors

[69]. http://www.rcuniverse.com/magazine/article_display.cfm?article_id=1344

[70]. http://adamone.rchomepage.com/guide5.htm

[71]. D. Casadei, F. Profumo, G. Serra and A. Tani, "FOC and DTC: two viable schemes for induction motors torque control," *in IEEE Trans. on Power Elect.*, vol. 17, no. 5, pp. 779-787, Sep 2002.

[72]. http://woodgears.ca/motors/dc.html

[73]. Hoang Le-Huy, "Comparison of field-oriented control and direct torque control for induction motor drives," *Proc. of Ind. App. Conf.*, pp. 1245-1252, Phoenix, AZ, 1999.

[74]. A. Emadi, "Energy-Efficient Electric Motors,"3rd ed. Boca Raton, FL: CRC, Aug. 2004.

[75]. Kollmorgen, "SERVODIS™ CATALOG, " *Kollmorgen Motion Technologies Group*, Commack, New York

[76]. Hardin, "Dynamic braking for universal motors," *US Patent US3673481A*, Jun. 1972.

[77]. T. A. O. Gross, "Dynamic braking of universal motors," *US Patent US3548276*, Dec. 1970.

[78]. H. H. Rottmerhusen, "Electrodynamic braking device for a universal motor," *US Patent US8704468*, Apr. 2014.

[79]. D. Muzar, E. Lanteigne, "Experimental Characterization Of Brushless DC Motors and Propellers for Flight Application,", *Proc. Of Mech. Eng. Int. Congr.*, pp 1-11, Canada, Jun 2016

[80]. O. Salari, M. Nouri, K. Hashtrudi-Zaad, A. Bakhshai and P. Jain, "A novel nine-level boost inverter with reduced structure and simple DC link capacitor control," *Proc. Of European Conf. on. Power. Elect.*, pp. 1-10, Warsaw, 2017.

[81]. M. Yasukawa, K. Hirata and M. Kato, "Novel oscillatory actuator for haptic device using principle of stepper motor," *Proc. Int. Symp. on. Linear Drives for Industry Applications (LDIA)*, pp. 1-4, Osaka, 2017.

[82]. K. Jin, S. Kim and I. Lee, "A hand-held controller with haptic feedback for virtual reality," *Proc. Of Int. Conf. on. Intelligent Informatics and Biomedical Sciences (ICIIBMS)*, pp. 129-132, Okinawa, 2017.

[83]. A. Ortega, A. Weill-Duflos, S. Haliyo, S. Régnier and V. Hayward, "Linear induction actuators for a haptic interface: A quasi-perfect transparent mechanism," *Proc. Of. Int. Conf. on. IEEE World Haptics (WHC)*, pp. 575-580, Munich, 2017.

[84]. F. Tian, Z. Chen and Y. Yu, "Design of control load system of flight simulator based on torque motor," *Proc. Of. Int. Conf. on Control Science and Systems Engineering (ICCSSE)*, pp. 106-109, Beijing, 2017.

[85]. J. Shi, F. Chai, X. Li and S. Cheng, "Study of the number of slots/pole combinations for low speed high torque permanent magnet synchronous motors," *Proc. Of. Int. Conf. on. Electrical Machines and Systems*, pp. 1-3, Beijing, 2011.

[86]. X. Li and Y. Zhao, "Design of high energy density permanent magnet synchronous motor," *Chinese Control Conference (CCC)*, pp. 10232-10235, Chengdu, 2016.

[87]. K. S. Devi, R. Dhanasekaran and S. Muthulakshmi, "Improvement of speed control performance in BLDC motor using fuzzy PID controller," *Proc. Of. Int. Conf. on. Advanced Communication Control and Computing Technologies (ICACCCT)*, pp. 380-384, Ramanathapuram, 2016.